INSTITUTE
FOR
AEROSPACE STUDIES
UNIVERSITY OF TORONTO

FINAL REPORT

EXPERIMENTAL EVALUATION OF THE TENSOR POLYNOMIAL FAILURE CRITERION FOR DESIGNING COMPOSITE STRUCTURES

by

R. C. Tennyson

Submitted to the

NATIONAL AERONAUTICS AND SPACE ADMINISTRATION
LANGLEY RESEARCH CENTER

Under Grant No. NSG-7219

October 1977

UNIVERSITY OF TORONTO
INSTITUTE FOR AEROSPACE STUDIES
4925 DUFFERIN ST
DOWNSVIEW, ONTARIO, CANADA, M3H 5T6
TEL 667-7700

November 7, 1977

667-7710

NASA Scientific and Technical
Information Facility
P.O. Box 8757
Baltimore/Washington International Airport
Baltimore, Maryland 21240
U.S.A.

Dear Sir:

I have enclosed two copies of my final report under NASA Grant NSG 7219 entitled "Experimental Evaluation of the Tensor Polynomial Failure Criterion for Designing Composite Materials". Three copies have also been sent to the Technical Officer, Dr. Don Baker (replacing Dr. R. L. Foye), at NASA Langley Research Center.

Many thanks for NASA's continued financial support of our research programme. This particular report will be published in an abbreviated form in the J. of Composites. Copies of the paper will also be forwarded to you.

Sincerely,

R. C. Tennyson

RCT/df
Enc.

R. C. Tennyson
Professor

FINAL REPORT

EXPERIMENTAL EVALUATION OF THE TENSOR POLYNOMIAL FAILURE CRITERION FOR DESIGNING COMPOSITE STRUCTURES

by

R. C. Tennyson

Submitted to the

National Aeronautics and Space Administration
Langley Research Center

Under Grant No. NSG-7219

October 1977

Abstract

A comprehensive experimental and analytical evaluation of the tensor polynomial failure criterion was undertaken to determine its capability for predicting the ultimate strength of a composite limina subject to a plane stress state. Results are presented demonstrating that a quadratic formulation is too conservative and a cubic representation is required Strength comparisons with test data derived from glass/epoxy and graphite/epoxy tubular specimens are also provided to validate the cubic strength criterion.

Environmental effects including ambient temperature, exposure to vacuum ($\sim 10^{-7}$ torr), length of post-cure time and rate of cool down have also been investigated. Behaviour changes associated with polymer (epoxy) matrix composites have been determined in terms of variations in stiffness (E_{22}) and tensile strength.

Acknowledgement

The author would like to acknowledge the contributions made to this research program by his Research Engineers: Mr. D. MacDonald, Mr. G Mabson, Mr. P. Nanyaro and Mr. R Holzer. In addition, the financial aid of the National Research Council of Canada (Grant No. A-2783) has provided a valuable supplement to the support given by the National Aeronautics and Space Administration under Grant No. NSG-7219. We are also particularly appreciative to Dr. R. L. Foye (NASA) for his continued interest in our work.

CONTENTS

Notation

B_{ij}	Biaxial stress ratio σ_i/σ_j
E_{11}, E_{22}	Orthotropic elastic moduli of the lamina measured in the fiber and transverse directions, respectively
F_i, F_{ij}, F_{ijk}	Strength tensors
F_1, F_2, F_6	$\frac{1}{X} - \frac{1}{X'}$, $\frac{1}{Y} - \frac{1}{Y'}$, $\frac{1}{S} - \frac{1}{S'}$, respectively
F_{11}, F_{22}, F_{66}	$\frac{1}{XX'}$, $\frac{1}{YY'}$, $\frac{1}{SS'}$, respectively
F_{12}	Quadratic interaction strength parameter
F_{112}, F_{122} F_{166}, F_{266}	Cubic interaction strength parameters
G_{12}	Orthotropic elastic shear modulus
ksi	1000 lbs/in^2
p	Internal pressure
$\bar{R}$	Average tube radius measured to median surface
S, S'	Positive and negative lamina shear failure stresses, respectively
$\bar{t}$	Average lamina thickness
T	Temperature
torr	mm of Hg at 0°C
X, X'	Uniaxial lamina strength in fiber direction, tensile and compressive, respectively
Y, Y'	Uniaxial lamina strength transverse to fibers, tensile and compressive, respectively
β	$(1 - \nu_{12}\nu_{21})$
θ	Fiber orientation relative to longitudinal (x) structural axis

ν_{12}, ν_{21}	Major and minor orthotropic Poisson ratios, respectively
σ	Normal stress

Subscripts

i, j, k	Integers, 1, 2, 6
x, y	Structural axes, axial and circumferential, respectively
1, 2	Principal lamina axes corresponding to the fiber and transverse directions, respectively
6	In-plane shear

1. INTRODUCTION

One of the major difficulties associated with the design and use of composite materials for load-bearing structural applications is the current lack of a suitable failure criterion for both the individual laminae and the laminated structure as a whole. Although many lamina failure criteria have been proposed (see Refs. 1, 2 and 3, for example), insufficient experimental data particularly under combined states of stress have been accumulated to indicate which criterion is best able to predict the failure stresses. The difficulty is of course that each strength criterion has been developed empirically with certain interaction parameters being neglected and they are all phenomenological in nature. In other words, they can predict the occurrence of failure but they do not describe the physics or mode of failure.

It would appear that the most general failure criterion proposed up to the present is that given by Wu (Refs. 4, 5, 6) in the form of a tensor polynomial

$$f(\sigma_i) = F_i\sigma_i + F_{ij}\sigma_{i\,j} + F_{ijk}\sigma_i\sigma_j\sigma_k + \ldots = 1 \qquad (1)$$

(where i, j, k = 1, 2, 3, ...6) which can be shown to encompass all other failure criteria which are currently available. The simplest form of Eq. (1) which retains the interaction tensor strength components is (Refs. 7, 8),

$$F_i\sigma_i + F_{ij}\sigma_i\sigma_j = 1 \qquad (2)$$

This quadratic tensor polynomial defines a failure surface in stress space in terms of two strength tensors F_i and F_{ij} of the second and

fourth ranks, respectively. Of particular interest in this formulation is the existence of the linear terms in σ_i which can account for the observed differences between positive and negative stress induced failures. However, in order to employ the stress tensor polynomial strength equation, one is faced with the difficulty of evaluating not only the standard principal strength parameters as defined by the (F_i, F_{ii}) relations, but also determining the interaction terms (F_{ij}, F_{ijk}, etc.) which are regarded as independent material properties. Since the failure surface may not be ellipsoidal in shape (i.e., the principal directions of strength may not always be orthogonal), it is necessary to include higher order terms in the tensor polynomial equation (such as the sixth-order failure tensor F_{ijk}). Thus the number of independent strength parameters that have to be determined experimentally can become inordinately large.

Except for the tensor polynomial formulation, all of the other criteria are quadratic. This report will demonstrate the analytical and experimental methods employed to evaluate both the quadratic and cubic strength equations. Biaxial stress tests utilizing glass/epoxy and graphite/epoxy tubes will also be presented for comparative purposes. It should be emphasized that the main intent of this program was to arrive at a reasonably accurate lamina failure criterion based on a plane stress state.

In addition, results will also be presented showing the effect of various environmental conditions on the change in strength parameters. The factors considered include ambient temperature, high vacuum ($\sim 10^{-7}$ torr), length of post-cure time and rate of post-cure cool down of the specimen. It might be noted that some of this data pertaining to the glass/epoxy material has been presented in a previous report to NASA by the author (Ref. 9). However, all

of the graphite/epoxy data are new and the derivation of the cubic strength criterion with validation tests represents a major improvement. Both material systems have been included for completeness.

2. EVALUATION OF STRENGTH TENSORS

The general form of the tensor polynomial failure criterion proposed by Wu is

$$F_i\sigma_i + F_{ij}\sigma_i\sigma_j + F_{ijk}\sigma_i\sigma_j\sigma_k + \cdots$$

$$= f(\sigma) \begin{cases} < 1 & \text{no failure} \\ = 1 & \text{failure} \\ > 1 & \text{exceeded failure} \end{cases} \qquad (3)$$

for i, j, k = 1, 2, 3, ...6. F_i, F_{ij} and F_{ijk} are strength tensors of the 2nd, 4th and 6th rank, respectively. If one restricts the analysis to a plane stress state and considers only a cubic formulation as being a reasonable representation of the failure surface, then Eq. (3) reduces to

$$F_1\sigma_1 + F_2\sigma_2 + F_6\sigma_6 + F_{11}\sigma_1^2 + F_{22}\sigma_2^2 + F_{66}\sigma_6^2$$
$$+ 2F_{12}\sigma_1\sigma_2 + 2F_{16}\sigma_1\sigma_6 + 2F_{26}\sigma_2\sigma_6 + 3F_{116}\sigma_1^2\sigma_6$$
$$+ 3F_{126}\sigma_1\sigma_2\sigma_6 + 3F_{112}\sigma_1^2\sigma_2 + 3F_{221}\sigma_1\sigma_2^2 + 3F_{166}\sigma_1\sigma_6^2$$
$$+ 3F_{226}\sigma_2^2\sigma_6 + 3F_{266}\sigma_2\sigma_6^2 + F_{111}\sigma_1^3 + F_{222}\sigma_2^3 + F_{666}\sigma_6^3 = 1 \qquad (4)$$

if it is further assumed that the material has some form of symmetry (Ref. 6) such that $F_{ij} = F_{ji}$ for $i \neq j$ and $F_{ijk} = F_{ikj} = F_{jik} = F_{jki} = F_{kij} = F_{kji}$. Since it has also been shown (Ref. 6) that inclusion of the cubic terms F_{iii} (for i = 1, 2 and 6) is redundant, therefore they can be omitted. One other important simplification of

Eq. (4) can also result if it can be experimentally determined that a lamina exhibits identical strength for both positive and negative shear. If this condition is satisfied, then all odd-order terms in σ_6 can be set to zero to remove the shear stress "sign" dependence. Hence Eq. (4) reduces to

$$F_1\sigma_1 + F_2\sigma_2 + F_{11}\sigma_1^2 + F_{22}\sigma_2^2 + F_{66}\sigma_6^2$$
$$+ 2F_{12}\sigma_1\sigma_2 + 3F_{112}\sigma_1^2\sigma_2 + 3F_{221}\sigma_2^2\sigma_1$$
$$+ 3F_{166}\sigma_1\sigma_6^2 + 3F_{266}\sigma_2\sigma_6^2 = 1 \qquad (5)$$

2.1 Principal Strength Terms (F_i, F_{ii})

From the analysis by Wu (Ref. 8), it was shown that the principal strength tensor components (F_i and F_{ii}) can be readily calculated from the experimentally determined values of the uniaxial tensile and compressive failure stresses in the fiber direction (X and X'), perpendicular to the fibers (Y and Y') and from positive and negative pure shear failure stresses (S and S', respectively). The appropriate relations are given by:

$$F_1 = \frac{1}{X} - \frac{1}{X'} \qquad F_2 = \frac{1}{Y} - \frac{1}{Y'}$$
$$F_6 = \frac{1}{S} - \frac{1}{S'} \qquad F_{11} = \frac{1}{XX'} \qquad (6)$$
$$F_{22} = \frac{1}{YY'} \qquad F_{66} = \frac{1}{SS'}$$

2.2 Quadratic Interaction (F_{ij})

If one assumes that a quadratic strength formulation is adequate, then the interaction terms F_{ij} can be determined from biaxial stress experiments if sufficient control over the biaxial

stress ratio $B_{ij} = \sigma_i/\sigma_j$ is maintained. In Ref. 8, Wu has shown that the best resolution of the interaction tensors is obtained by using an optimal value of B_{ij} together with the most suitable stress state since the resolution of F_{ij} is dependent on both of these variables.

Considering now only the F_{12} interaction parameter, "best" estimates of its value can only be obtained by performing a set of experiments and iterating since it can be shown (Ref. 8) that the optimal value for B_{12} depends on F_{12}, assuming the other strength components are known. However, analysis must be done prior to testing to ascertain the "best" stress state to achieve the most accurate resolution in the measurement of F_{12}. Graphs illustrating the optimal biaxial stress ratios (B_{12}) and attainable resolution for estimating F_{12} are shown in Figs. 1-4 for the glass/epoxy and graphite/epoxy materials studied in this program. Based on this analysis, experiments were undertaken using combined internal pressure with axial compression loading such that the specimen stress state was defined by $\sigma_1 > 0$, $\sigma_2 < 0$.

2.3 Cubic Interaction Terms (F_{ijk})

In order to derive an appropriate cubic formulation one must not only solve for the cubic strength parameters but re-calculate the quadratic interaction terms as well. This can be seen by examining the solution for F_{12} which is given by

$$F_{12} = \frac{1}{2\sigma_1\sigma_2}\left[1 - (F_1\sigma_1 + F_2\sigma_2 + F_{11}\sigma_1^2 + F_{22}\sigma_2^2 + 3F_{112}\sigma_1^2\sigma_2 + 3F_{221}\sigma_2^2\sigma_1)\right] \quad (7)$$

for the case of biaxial loading in which $\sigma_6 = 0$.

Because of the inordinate amount and complexity of experiments required to accurately evaluate the F_{ij} and F_{ijk} terms, a hybrid method was employed. This approach was based on determining F_{12} and four cubic parameters utilizing a biaxial strength test (i.e., Eq. (7)) and four constraint equations. The latter conditions were derived by setting the discriminant of the cubic polynomial coefficients to zero, thus requiring the failure equation to yield three real roots, two of which must be equal. This satisfies the physical consideration of having only two distinct roots for two colinear loading paths (Ref. 4).

Assume that the plane stress state can be described by some load parameter λ such that,

$$\begin{aligned} \sigma_1 &= k_1\lambda \\ \sigma_2 &= k_2\lambda \\ \sigma_6 &= k_6\lambda \end{aligned} \tag{8}$$

where k_1, k_2 and k_6 are constants for a given material and lamina ply angle relative to some arbitrary set of structural axes. Hence the cubic strength equation (5) can be rewritten in the form,

$$a\lambda^3 + b\lambda^2 + c\lambda + d = 0 \tag{9}$$

where $a = 3(F_{112}k_1^2k_2 + F_{221}k_1k_2^2 + F_{166}k_1k_6^2 + F_{266}k_2k_6^2)$

$b = F_{11}k_1^2 + F_{22}k_2^2 + F_{66}k_6^2 + 2F_{12}k_1k_2$

$c = F_1k_1 + F_2k_2$

$d = -1$

If the discriminant of Eq. (9) is set to zero and $d = -1$ substituted, one obtains the following constraint equation,

$$27a^2 + a(4c^3 + 18bc) - 4b^3 - b^2c^2 = 0 \qquad (10)$$

Equation (10) can now be solved for varying lamina configurations as described previously.

2.4 Experimental Evaluation of Strength Parameters

Details of the fabrication process using the belt-wrapper apparatus and the various test methods for evaluating the strength parameters are contained in Appendix A and B, respectively. The two material systems investigated include glass/epoxy (Scotchply* Type 1002) and graphite/epoxy (Scotchply* Type SP-288T300). Where possible, circular cylindrical tubes were utilized to obtain the strength data. However, for the 0° compression tests on SP-288T300, solid bars of rectangular cross-section were employed to avoid wall buckling problems.

In Tables 1 and 2, the principal strength test data are presented for the glass/epoxy and graphite/epoxy materials, respectively. A summary of the average failure loads used to evaluate the principal strength parameters is contained in Table 3. During the strength tests, stress-strain plots were obtained to allow the calculation of the orthotropic elastic constants and, at the same time, determine the range of linear elastic behaviour. Tables 4 and 5 give the values of E_{11}, E_{22}, ν_{12} and G_{12} for both glass/epoxy and graphite/epoxy, respectively. The actual stress-strain curves are shown in Figs. 5-10.

From the failure loads listed in Table 3, the principal strength tensor components (F_i, F_{ii}) were calculated using Eqs. (6). These results are presented in Table 6.

---

* Products of 3M Co.

A series of biaxial stress tests were undertaken using the optimal stress state (see Figs. 1-4; $\sigma_1 > 0$, $\sigma_2 < 0$, $\sigma_6 = 0$) to evaluate the quadratic interaction strength term F_{12}. This stress condition was achieved by combined internal pressure/axial compression loading for fixed ratios of B_{12} ($\equiv \sigma_1/\sigma_2$) (see Appendix B for details). Repeat tests for varying B_{12} leading to convergence between estimated and measured values of F_{12} were performed based on a quadratic failure model (i.e., Eq. (2)). Tables 7 and 8 summarize the series of biaxial interaction stress tests undertaken to arrive at an estimated value of F_{12}. It must be emphasized that F_{12} in this particular phase of the study was calculated using only a quadratic failure model since the cubic terms were unknown.

2.5 Solution for Cubic Model

If one now requires a higher order theory than the quadratic, recourse to the hybrid method of solution can be made. In this case, solutions for F_{12}, F_{112}, F_{221}, F_{166} and F_{266} were obtained for each material using the 'optimal' biaxial test result, Eq. (7) and Eq. (10) (assuming internal pressure loading, i.e., $\lambda = p$) and four angle ply ($\pm \theta$) laminations (45°, 50°, 55°, 60°). Note that no experimental data were used in this solution except for the one biaxial stress test performed at the optimal (quadratic) B_{12} ratio. Hence, the four interaction strength parameters were determined from solving five nonlinear simultaneous algebraic equations of third power. The results of this analysis are given in Table 9 for both materials.

3. COMPARISON OF STRENGTH PREDICTIONS WITH EXPERIMENTS

An extensive series of tests were undertaken on four-ply, symmetric balanced $\pm \theta$ laminated tubes subjected to internal pressure

loading over the range $0 \leq \theta \leq 90°$. It is important to note that none of these test results were used in the evaluation of any of the strength components. A description of the geometry of the glass and graphite tubes is presented in Tables 10 and 11. The corresponding failure pressures for each test specimen are listed in Tables 12 and 13.

Figures 11 and 12 compare the experimental data and calculated failure pressures for both glass/epoxy and graphite/epoxy materials, respectively. Plotted on each graph are the cubic and quadratic predictions. Clearly one can see that the quadratic model is far too conservative in the range where high failure loads occur. On the other hand, the cubic form of the strength criterion is quite accurate by comparison. It would appear that for the glass/epoxy tests, the data and predicted results are somewhat offset. One can readily see that a small variance in fiber orientation can lead to substantial differences in failure loads when one designs in the region of optimum fiber angle.

It is of interest to calculate the principal stresses (σ_1, σ_2 and σ_6) corresponding to the failure pressure as a function of fiber angle θ. Although the results obtained for the graphite/epoxy (see Fig. 13) are based on a linear elastic model, one can use them in conjunction with the observed failure modes of the test samples (Figs. 14-17) to define various regions of structural behaviour. From such a comparative study, the following failure zones for pressure tubes ($\pm \theta$) can be described:

Estimated Range	Material Behaviour		Structural Behaviour
$0° \leq \theta < 45°$	matrix failure fibers intact	→	Weeping Mode Structure Intact

Continued...

Estimated Range	Material Behaviour		Structural Behaviour
$45° \leq \theta < 60°$	matrix and fiber failure	→	Open Fracture
$60° \leq \theta < 70°$	matrix failure fibers intact	→	Weeping Mode Structure Intact
$70° \leq \theta < 90°$	matrix failure leading to fiber failure	→	Open Fracture
$\theta = 90°$	matrix failure fibers intact	→	Open Fracture

4. ENVIRONMENTAL EFFECTS ON STRENGTH PARAMETERS

The various environmental conditions investigated in this program include - ambient temperature, high vacuum, length of post-cure time and rate of cool down. The first two parameters relate directly to the performance characteristics of the material for space applications. In the latter two cases, they have a bearing on manufacturing variables which could affect the mechanical behaviour of the composite structure. It is to be expected that these particular environmental factors would influence the epoxy matrix material far more than the glass or graphite fibers. Hence the test data were obtained from specimens designed to exhibit the largest matrix response changes (i.e., $\theta = 90°$). As far as the strength tensors are concerned, one can examine the effect of varying F_2 and F_{22} on the overall lamina failure loads. For example, using the cubic strength criterion, the failure pressure as a function of fiber orientation was calculated based on a 50% reduction in matrix tensile/compression strength for the graphite/epoxy tubes. These results are shown in Fig. 18 where they can be compared to the ambient predicted values (Fig. 12). Clearly one can see that substantial degradation occurs over the full range of fiber angles even though the fiber strength and interaction terms remain unchanged.

4.1 Ambient Temperature

The effect of ambient temperature over the range $-150°F \leq T \leq 250°F$ was investigated to provide strength data that could be used in the design of polymer matrix composites subjected to thermal loading. As noted at the outset, the major temperature effects should occur in the properties associated with the polymer matrix. In this case, since we are primarily concerned with strength, we shall limit our attention to variations in F_2 and F_{22} with temperature.

For the initial test series with glass/epoxy tubular specimens, internal pressure loading up to failure was employed. In Ref. 9, it is shown that for $\theta = 90°$, the quadratic formulation is quite accurate. This then permitted the solving for F_2 and F_{22} provided one assumed that the changes in matrix tensile and compressive strengths were proportionately the same at a given temperature, i.e.,

$$F_2(T) = \frac{F_{2_{RT}}}{(1 \pm k)}$$

$$F_{22}(T) = \frac{F_{22_{RT}}}{(1 \pm k)^2}$$

where k denotes the change in strength with temperature and RT refers to the room temperature values. A summary of the specimens tested together with the variation in orthotropic elastic constants and failure stresses is contained in Table 14. The corresponding calculated values for F_2 and F_{22} as a function of temperature are shown in Fig. 19.

For the graphite/epoxy tests, tubular samples ($\bar{R} = 2.0"$, $\bar{t} = 0.015"$, $\theta = 90°$) were loaded directly in axial tension to failure. Again, the assumption was made that the change in compressive matrix strength was proportionally the same as that found in tension at a

given temperature. Table 15 presents a summary of the specimens tested and the measured (matrix) modulus (E_{22}) and failure strengths. Using this data, the variation in F_2 and F_{22} with temperature was calculated and plotted in Figs. 20 and 21. One can see that for both material systems, the qualitative trends are the same. Essentially one must only be concerned with temperature effects beyond 150°F for this class of epoxy matrix composites. Note that the interaction strength parameters in the cubic model can be re-calculated based on new values obtained for F_2 and F_{22}. This would of course necessitate an elevated temperature biaxial test.

4.2 Vacuum Environment

Because of the existence of substantial outgassing of polymer materials in a hard vacuum such as exists in space, a preliminary set of tests was undertaken to evaluate the performance of graphite/epoxy subjected to $\sim 10^{-7}$ torr at room temperature. It is recognized that the addition of thermal loading can also affect the outgassing of the polymer matrix material. However, this particular phase of our study has not been completed and will be the subject of another report at a later date.

Extensive effort has been devoted to the development of a thermal-vacuum test facility having the unique capability of in-situ loading of structural specimens up to failure. This is accomplished by applying and monitoring the loads externally through movable leak-proof, accordion-type bellows constructed from thin-walled stainless steel tubing. For a detailed description of the facility, designed and constructed at UTIAS, the reader is referred to Appendix C.

Table 16 presents a summary of the specimens tested, time in vacuum, change in (matrix) modulus (E_{22}) and tensile strength.

It should be noted that the two specimens representing the ambient reference state failed about 14% ~ 26% higher than their counterparts listed in Table 3. The reason for this increase in performance lies in the universal gimbals used to support the tubes and apply the load (see Appendix C). There was no possibility of any eccentric loading and thus the apparent strength of the samples increased.

Figures 22 and 23 illustrate the change in E_{22} and axial failure stress (Y) with exposure time in vacuum. As far as stiffness is concerned, no appreciable difference can be discerned, although there is some consistent trend in the data for longer duration exposures where a nominal 10% increase might be attributable to vacuum.

Of some concern is the strength data. At first glance it would appear that no vacuum effect is present, except for two abnormally low test values. However, it must be pointed out that throughout the whole of the test program involving graphite/epoxy specimens which were all manufactured from the same material batch, never have we encountered two such low test points. They fall totally out of the range of strength "scatter". Thus it is felt that there might exist a particular specimen flaw size that can be encountered during fabrication which, when subject to vacuum and associated outgassing, is of a critical nature that can lead to catastrophic failure of the structure under load. Based on the data obtained up to present, probability of occurrence is estimated at 20%. From a design viewpoint, 50% or more strength reductions (admittedly in the matrix parameter) cannot be tolerated and recourse to more vacuum strength testing with and without thermal loading should be undertaken to clarify this anomolous behaviour. Particular emphasis should also be directed towards examining the fracture

surfaces of the "low" and "high" test specimens to determine if such a flaw exists. Much more load testing of composite structures in-situ (i.e., in vacuum) should be stressed.

4.3 Length of Post-Cure Time

Various lengths of post-cure time were investigated to determine the variation in matrix strength. In this phase of the program, only the glass/epoxy material was studied, the results of which are summarized in Table 17. Using the analysis described previously in which "burst" strength data were converted to estimated parameter changes in F_2 and F_{22}, Fig. 24 was constructed showing the variations found over the time range from zero (i.e., no additional post-cure beyond manufacturer's specifications) to 24 hours.

4.4 Rate of Post-Cure Cool Down

An interesting parameter from a manufacturing point of view is the rate at which the composite structure is cooled down after the required cure cycle time in the autoclave. Consequently a test program was initiated to study the effects of varying the post-cure cool down rate in terms of measuring the changes in the matrix modulus (E_{22}) and tensile strength (Y). Varying rates of cool down were achieved and recorded by thermocouples mounted on the specimens. Typical rates of temperature reduction are shown in Fig. 25 where it is indicated how the values of (dT/dt) were estimated. Table 18 presents a summary of the corresponding values of modulus (E_{22}) and tensile strength (Y) as a function of cool down rate. The actual graphical representation of strength changes is given in Fig. 26 where it can be seen that little variation was found in the range of $27 \leq dT/dt \leq 343$ (F°/hr), although a slight trend towards strength reduction was observed.

5. CONCLUSIONS

Based on the test results obtained in this program, it would appear that the cubic form of the tensor polynomial strength criterion is well suited for analysing a composite lamina under plane stress conditions. There is little doubt that the general application of a quadratic formulation is not accurate over the full range of lamina orientations and can yield far too conservative failure loads. Although one cannot guarantee that a particular failure model will always provide good results, it is recommended that further complex structural configurations and load cases be studied to test the capabilities of the cubic equation proposed. Further work should also be directed towards the validation of the hybrid method used in this report for evaluating the interaction strength parameters.

As far as environmental effects on the strength of (epoxy) polymer matrix composites are concerned, large changes were found at the high end of the temperature scale, as expected, with only nominal variations extending down to temperatures as low as -150°F. Varying the length of post-cure time and the rate of cool down produced significant changes only in the former case. By far the most intriguing behaviour was the occurrence of sporadic anomolous catastrophic strength reductions for graphite/epoxy material when subjected to hard vacuum conditions ($\sim 10^{-7}$ torr). No explanation for this effect has yet been determined, except to note that the variance in strength far exceeded any nominal scatter found with the same batch of material used throughout the test program. This particular phenomenon deserves more attention to assess the possibility of any existing mechanism that could account for such behaviour.

REFERENCES

1. "Strength Theories of Failure for Anisotropic Materials" by B. E. Kaminski and R. B. Lantz, Composite Materials: Testing and Design, ASTM STP 460, 1969.
2. "A Survey of Failure Theories of Isotropic and Anisotropic Materials" by R. S. Sandhu, AFFDL Tech. Rept. AFFDL-TR-72-71.
3. "A Brief Survey of Empirical Multiaxial Strength for Composites" by G. P. Sendeckyj, Composite Materials: Testing and Design, ASTM STP 497, 1972.
4. "Phenomenological Anisotropic Failure Criterion" by E. M. Wu, Treatise on Composite Materials, Broutman, Krock and Sendeckyj, Eds., Academic Press, 1973.
5. "Failure Criteria to Fracture Mode Analysis of Composite Laminates" by E. M. Wu, 39th Meeting, AGARD Structures & Materials Panel (Failure Modes of Composite Materials), Munich, Germany, October 1974.
6. "Laminate Strength - A Direct Characterization Procedure" by E. M. Wu and J. K. Scheublein, Composite Materials: Testing and Design, (Third Conference), ASTM STP 546, June 1974.
7. "A General Theory of Strength for Anisotropic Materials" by S. W. Tsai and E. M. Wu, J. Composite Materials, Vol. 5, Jan. 1971.
8. "Optimal Experimental Measurements of Anisotropic Failure Tensors" by E. M. Wu, J. Composite Materials, Vol. 6, Oct. 1972.
9. "Experimental Evaluation of the Tensor Polynomial Failure Criterion for the Design of Composite Structures" by R. C. Tennyson, NASA-CR-142701, March 1975.

TABLE I

TENSILE, COMPRESSIVE, AND SHEAR FRACTURE DATA

(GLASS/EPOXY)

SPECIMEN NO.		ULTIMATE STRENGTH (P.S.I.)
Longitudinal Tensile Strength Tests		
2a	0°	131,158
2b	0°	111,004
3a	0°	119,735
3b	0°	121,336
Mean Value		120,808
Longitudinal Compressive Strength Tests		
7a	0°	83,784
7b	0°	89,491
8a	0°	86,013
9a	0°	86,885
9b	0°	91,629
18a	0°	88,676
19a	0°	87,091
Mean Value		88,081
Transverse Tensile Strength Tests		
1a	90° (I)	2,980
1a	90° (II)	3,520
3a	90°	3,204
5a	90° (I)	3,150
5a	90° (II)	3,338
6b	90°	3,418
8b	90°	3,109
Mean Value		3,246

TABLE 1 (cont'd.)

TENSILE, COMPRESSIVE AND SHEAR FRACTURE DATA

SPECIMEN NO.		ULTIMATE STRENGTH (P.S.I.)
Transverse Compressive Strength Tests		
2a	90°	13,158
3b	90°	14,035
4b	90°	14,246
7b	90°	12,218
8c	90°	13,819
16b	90°	13,431
17a	90°	14,114
Mean Value		13,574
Shear Strength Tests		
2b	90°	6,737
4a	90°(I)	6,777
4a	90°(II)	6,851
5b	90°	6,864
6a	90°	6,765
7a	90°	6,497
17b	90°	7,336
Mean Value		6,832

TABLE 2

TENSILE, COMPRESSIVE, AND SHEAR FAILURE DATA

(GRAPHITE/EPOXY)

SPECIMEN NO.		ULTIMATE STRENGTH (P.S.I.)
Longitudinal Tensile Strength Tests		
4A	0°	194,500
4B	0°	173,000
5A	0°	191,200
5B	0°	190,938
6A	0°	180,000
6B	0°	175,000
3A	0°	186,200
3B	0°	194,300
MEAN VALUE		185,630
Longitudinal Compressive Strength Tests		
C1	0°	123,140
C2	0°	114,600
C3	0°	132,400
C4	0°	138,200
MEAN VALUE		127,085
Transverse Tensile Test		
7A	90°	7,751
7B	90°	7,315
8A	90°	7,505
8B	90°	7,408
9A	90°	7,600
MEAN VALUE		7,515
Transverse Compressive Test		
10A	90°	31,670
10B	90°	35,010
11A	90°	35,030
11B	90°	33,500
MEAN VALUE		33,802

TABLE 2 (Cont'd)

SPECIMEN NO.	ULTIMATE STRENGTH (P.S.I.)
Shear Strength Tests	
T-1-1 90°	12,170
T-1-2 90°	11,790
T-2-1 90°	10,207
T-2-2 90°	10,940
T-3-1 90°	10,933
T-3-2 90°	11,006
MEAN VALUE	11,174

TABLE 3

SUMMARY OF AVERAGE FAILURE DATA

Material	No. of Tests	X (KSI)	X' (KSI)	Y (KSI)	Y' (KSI)	S=S' (KSI)
Glass-Epoxy	4	120.808 ± 9%				
	7		88.081 ± 5%			
	7			3.246 ± 8%		
	7				13.574 ± 10%	
	7					6.832 ± 7%
Graphite-Epoxy	8	185.630 ± 7%				
	4		127.085 ± 10%			
	5			7.515 ± 3%		
	4				33.802 ± 6%	
	6					11.174 ± 9%

NOTE % VARIATION SHOWN DENOTES MAXIMUM IN NUMBER OF SAMPLES TESTED.

TABLE 4

MATERIAL PROPERTIES (GLASS/EPOXY)

SPECIMEN NUMBER	E_{11} (10^6 P.S.I.)	E_{22} (10^6 P.S.I.)	G_{12} (10^6 P.S.I.)	ν_{12}	ν_{21}
Calculated Directly From Stress-Strain Curves					
2b 0°	4.74				
3b 0°	4.79				
Mean Value	4.765				
3a 90°		1.245			
5a 90°(I)		1.157			
5a 90°(II)		1.284			
6b 90°		1.157			
Mean Value		1.211			
2b 90°			0.431		
4a 90°(I)			0.408		
7a 90°			0.420		
Mean Value			0.420		
Calculated Using the Characterization Computer Program *					
1c 0°	4.945	1.170	0.4888	0.3043	0.0720
6b 0°	4.676	1.226	0.4645	0.2827	0.07412
2b ∓ 30°	5.107	1.426	0.4574	0.2676	0.07473
7b ∓ 30°	5.447	1.174	0.5216	0.4165	0.08978
4b ∓ 60°	5.081	1.645	0.4082	0.2230	0.07221
9b ∓ 60°	5.125	1.420	0.4733	0.2377	0.0659
5c 90°	4.669	1.248	0.4215	0.4074	0.1089
10b 90°	4.876	1.416	0.4844	0.4313	0.1252
Mean Values	4.991	1.341	0.465	0.3213	0.08536
Manufacturer's Values					
	5.7	1.4			

* 4 ply cylinders (-, +, +, -)

TABLE 3 ...

MATERIAL PROPERTIES (GRAPHITE/EPOXY)

SPECIMEN NUMBER		E_{11} (10^6 PSI)	E_{22} (10^6 PSI)	G_{12} (10^6 PSI)	ν_{12}	ν_{21}
Calculated Directly From Stress-Strain Curves						
5A	0	19.6				
4A	0	21.4				
6A	0	20.2				
6B	0	20.7				
MEAN VALUE		20.5				
7A	90		1.45			
7B	90		1.42			
9	90		1.39			
8A	90		1.35			
MEAN VALUE			1.403			
T-3-1	90			0.577		
T-1-2	90			0.598		
T-2-1	90			0.617		
T-2-2	90			0.583		
T-1-1	90			0.593		
MEAN VALUE				0.594		
Manufacturer's Values						
		21.9	1.29	---	0.26	0.017

TABLE 6

SUMMARY OF PRINCIPAL STRENGTH PARAMETERS

Material	F_1 $(KSI)^{-1}$	F_{11} $(KSI)^{-2}$	F_2 $(KSI)^{-1}$	F_{22} $(KSI)^{-2}$	F_6 $(KSI)^{-1}$	F_{66} $(KSI)^{-2}$
Glass/Epoxy	-3.076×10^{-3}	9.398×10^{-5}	2.344×10^{-1}	2.270×10^{-2}	0	2.142×10^{-2}
Graphite/Epoxy	-2.482×10^{-3}	4.239×10^{-5}	1.035×10^{-1}	3.936×10^{-3}	0	8.009×10^{-3}

TABLE 7

F_{12} TENSOR TESTS (GLASS/EPOXY)

SPECIMEN NUMBER		PREDICTED B_{12}	MEASURED B_{12}	ULTIMATE STRESS (KSI)	COMPUTED F_{12} $(KSI)^{-2}$	
10a	90°	- 8.00	- 8.69	σ_1 = 108.8	1.869×10^{-4}	
				σ_2 = -12.88		
10b	90°	-14.50	-15.49	σ_1 = 103.4	-6.690×10^{-4}	*
				σ_2 = - 6.392		
11a	90°	-13.80	-13.33	σ_1 = 100.0	-6.539×10^{-4}	
				σ_2 = - 6.911		
13b	90°	-13.90	-15.13	σ_1 = 105.4	-5.933×10^{-4}	
				σ_2 = - 6.669		

* Mean Value of $F_{12} = -6.387 \times 10^{-4}$ KSI^{-2}

TABLE 8

F_{12} TENSOR TESTS (GRAPHITE/EPOXY)

SPECIMEN NO.		PREDICTED B_{12}	MEASURED** B_{12}	ULTIMATE STRESS (KSI)	COMPUTED F_{12} $(KSI)^{-2}$
F-1	90°	-3	-3.5	σ_1 = 73.3	-4.563×10^{-4}
				σ_2 = -20.9	
F-2	90°	-3	-3.4	σ_1 = 85.1	-2.712×10^{-4}
				σ_2 = -24.1	
F-3	90°	-9.0	-8.8	σ_1 = 140.0	-2.686×10^{-4}
				σ_2 = -15.6	
F-4	90°	-9.2	-9.1	σ_1 = 155.0	-1.792×10^{-4}
				σ_2 = -17.5	
F-5	90°	-9.4	-9.3	σ_1 = 161.5	-1.609×10^{-4} *
				σ_2 = -17.4	
F-6	90°	-9.3	-9.2	σ_1 = 160.0	-1.623×10^{-4} *
				σ_2 = -17.6	

* Mean Value of $F_{12} = -1.616 \times 10^{-4}$ KSI^{-2}

**From "best" slope off load graph

TABLE 9

SUMMARY OF INTERACTION STRENGTH PARAMETERS FOR CUBIC MODEL

Material	F_{12} $(KSI)^{-2}$	F_{112} $(KSI)^{-3}$	F_{221} $(KSI)^{-3}$	F_{166} $(KSI)^{-3}$	F_{266} $(KSI)^{-3}$
Glass/Epoxy	-4.234×10^{-3}	1.588×10^{-5}	-1.129×10^{-4}	1.540×10^{-4}	-5.041×10^{-5}
Graphite/Epoxy	-4.424×10^{-4}	5.170×10^{-7}	-5.985×10^{-6}	-4.054×10^{-6}	-2.268×10^{-4}

TABLE 10

GEOMETRY* OF TUBES USED IN PRESSURE TESTS

(GLASS/EPOXY)

TUBE DESIGNATION	$\bar{R}$ (IN)	$\bar{t}$ (IN)
6a 0	1.017	.0400
6b 0	1.017	.0406
6c 0	1.017	.0407
7a $\overline{+}$ 30°	1.018	.0397
7b $\overline{+}$ 30°	1.018	.0408
7c $\overline{+}$ 30	1.018	.0405
8a $\overline{+}$ 45	1.021	.0406
8b $\overline{+}$ 45	1.021	.0408
8c $\overline{+}$ 45	1.020	.0397
9a $\overline{+}$ 60°	1.021	.0401
9b $\overline{+}$ 60°	1.021	.0410
9c $\overline{+}$ 60°	1.021	.0404
10a 90°	1.021	.0410
10b 90°	1.021	.0400
10c 90°	1.021	.0404

* 4 Ply Cylinders $(-\theta, +\theta, +\theta, -\theta)$

TABLE 11

GEOMETRY OF TUBES USED IN PRESSURE TESTS

(Graphite/Epoxy)

Tube Designation	$\bar{R}$ (in)	$\bar{t}$ (in)
1(a) 0°	2.010	.020
1(b) 0°	2.005	.020
2(a) $\mp$ 30°	2.010	.021
3(a) $\mp$ 45°	2.005	.021
3(b) $\mp$ 45°	2.010	.021
4(a) $\mp$ 50°	2.005	.020
5(a) $\mp$ 55°	2.013	.021
5(b) $\mp$ 55°	2.011	.021
5(c) $\mp$ 55°	2.010	.021
6(a) $\mp$ 60°	2.013	.021
6(b) $\mp$ 60°	2.010	.020
6(c) $\mp$ 60°	2.012	.021
7(a) $\mp$ 75°	2.013	.021
7(b) $\mp$ 75°	2.010	.021
8(a) 90°	2.012	.021
8(b) 90°	2.010	.021

TABLE 12

PRESSURE STRENGTH TEST DATA

(Glass/Epoxy)

Specimen Number		Measured Failure Pressure (psi)
6a 0°		131.0
6b 0°		135.0
6c 0°		108.0
Mean Value	124.7	
7a ∓ 30°		241.0
7b ∓ 30°		260.0
7c ∓ 30°		240.0
Mean Value	247.0	
8a ∓ 45°		557.5
8b ∓ 45°		582.0
8c ∓ 45°		630.0
Mean Value	589.8	
9a ∓ 60°		675.0
9b ∓ 60°		643.0
9c ∓ 60°		665.0
Mean Value	661.0	
10a 90°		250.0
10b 90°		242.0
10c 90°		289.0
Mean Value	260.3	

TABLE 13

PRESSURE STRENGTH TEST DATA

(Graphite/Epoxy)

Specimen Number		Measured Failure Pressure (P.S.I.)
1(a) 0°		170
1(b) 0°		185
Mean Value	177.5	
2(a) ∓ 30°		350
3(a) ∓ 45°		1550
3(b) ∓ 45°		1500
Mean Value	1525	
4(a) ∓ 50°		2365
5(a) ∓ 55°		2340
5(b) ∓ 55°		2175
5(c) ∓ 55°		2290
Mean Value	2268	
6(a) ∓ 60°		1610
6(b) ∓ 60°		1555
6(c) ∓ 60°		1530
Mean Value	1565	
7(a) ∓ 75°		460
7(b) ∓ 75°		510
Mean Value	485	
8(a) 90°		333
8(b) 90°		295
Mean Value	314	

TABLE 14

ELASTIC CONSTANTS AND TRANSVERSE BURST STRENGTH FOR SCOTCHPLY (1002) TUBES AT VARIOUS TEST TEMPERATURES

TEST TEMPERATURE	TUBE DESIGNATION	E_{11}/β (psi)	E_{22}/β (psi)	E_{11} (psi)	E_{22} (psi)	ν_{12}	ν_{21}	σ_2 burst (psi) (Mode 1)
- 80°F	24b 90°	6.23×10^6	1.59×10^6	5.86×10^6	1.50×10^6	0.482	0.123	4346
- 75°F	23c 90°							4399
- 45°F	23b 90°	6.43×10^6	1.76×10^6	6.32×10^6	1.73×10^6	0.250	0.068	4186
- 20°F	23a 90°	5.76×10^6	1.39×10^6	5.04×10^6	1.22×10^6	0.721	0.173	4110
- 20°F	22b 90°	5.99×10^6	1.51×10^6	5.80×10^6	1.46×10^6	0.356	0.089	4200
- 20°F	22c 90°							4224
70°F	12c 90°							3411
70°F	13c 90°	5.86×10^6	1.32×10^6	5.61×10^6	1.26×10^6	0.437	0.098	3369
70°F	11c 90°	6.01×10^6	1.29×10^6	5.66×10^6	1.22×10^6	0.520	0.112	3545
158°F	19b 90°	6.40×10^6	1.18×10^6	6.11×10^6	1.13×10^6	0.495	0.092	3216
158°F	16a 90°	6.35×10^6	1.15×10^6	6.07×10^6	1.10×10^6	0.495	0.090	2876
200°F	19a 90°	6.08×10^6	0.98×10^6	5.78×10^6	0.93×10^6	0.552	0.089	2300
200°F	14a 90°							2450
250°F	14b 90°	6.30×10^6	0.57×10^6	5.87×10^6	0.53×10^6	0.875	0.079	1405
250°F	14c 90°	6.08×10^6	0.66×10^6	5.91×10^6	0.65×10^6	0.511	0.056	1280
250°F	15a 90°							1325

$\beta = (1 - \nu_{12}\nu_{21})$, $\sigma_2 = p\bar{R}/2\bar{t}$, $\bar{R} = 1.015"$, $\bar{t} = 0.030"$

TABLE 15

TEMPERATURE VARIATION RESULTS

Specimen Designation	Temperature at Failure (°F)	Maximum Tensile Stress Y (PSI)	Modulus E_{22} (PSIx10^{-6})
I - 3	-149	6362	2.87
F - 3	- 92	6174	
F - 3 (REPOT)	- 74	7880	
G - 2	- 65	8234	2.10 *
G - 3	- 41	6499	1.98 *
H - 1	- 40	7555	1.87
C - 1	75	7751	1.45
C - 2	75	7215	1.45
H - 2	145	7894	1.22
H - 3	195	5924	1.32
I - 2	198	5312	1.05
I - 1	226	4391	.898

$\theta = 90°$, $\bar{R} \approx 1.0"$, $\bar{t} \approx 0.015"$

* These two specimens were loaded slower than the rest. The temperature increased slightly during testing. The modulus was measured at -68°F for G - 2 and -43°F for G - 3.

Error in maximum stress and modulus was 3.5 and 4.5 percent respectively.

Error in temperature was five degrees Fahrenheit except for those specimens tested at room temperature, whose error in temperature was negligible.

TABLE 16

SUMMARY OF GRAPHITE/EPOXY PERFORMANCE IN VACUUM*

Specimen No.	Time in Vacuum (hrs)	Failure Stress Y (PSI)	Matrix Modulus (E_{22}) (10^6 PSI)
1	0	-	1.46
	18	-	1.65
	87	4610	1.60
2	1.5	-	1.62
	3	-	1.62
	20	-	1.58
	54	-	1.58
	70	-	1.58
	146	9528	1.58
3	0	-	1.41
	1	-	1.41
	18	-	1.41
	100	-	1.54
	140	-	1.54
	214	8914	1.54
4a	48	2766	-
4b	0	8560	-
5a	24	8837	-
5b	0	9452	-
6a	70	9682	-
6b	96	10527	-
7a	48	9375	-
7b	72	9759	-

* Pressure was ~2 x 10^{-7} torr; $\bar{R}$ = 1.0"; $\bar{t}$ = 0.030", θ = 90°

TABLE 17

ELASTIC CONSTANTS AND TRANSVERSE BURST STRENGTH FOR SCOTCHPLY (1002) TUBES HAVING DIFFERENT LENGTHS OF POST-CURE

LENGTH OF POST-CURE	TUBE DESIG-NATION	E_{11}/β (psi)	E_{22}/β (psi)	E_{11} (psi)	E_{22} (psi)	ν_{12}	ν_{21}	σ_2 (psi) (Mode 1)
0 HRS.	18a 90°	5.896×10^6	1.307×10^6	5.591×10^6	1.239×10^6	0.4832	0.1071	3058
0 HRS.	18b 90°	6.049×10^6	1.417×10^6	5.670×10^6	1.328×10^6	0.5176	0.1212	2948
0 HRS.	18c 90°							3329
7 HRS.	21a 90°							3523
7 HRS.	21b 90°	6.054×10^6	1.329×10^6	5.599×10^6	1.229×10^6	0.5852	0.1285	3490
7 HRS.	21c 90°	5.855×10^6	1.260×10^6	5.543×10^6	1.193×10^6	0.4974	0.1071	3279
16.75 HRS.	11c 90°	6.013×10^6	1.297×10^6	5.663×10^6	1.222×10^6	0.5199	0.1122	3545
16.75 HRS.	12c 90°							3411
16.75 HRS.	13c 90°	5.865×10^6	1.319×10^6	5.612×10^6	1.262×10^6	0.4374	0.0984	3369
24 HRS.	20a 90°	5.978×10^6	1.283×10^6	5.743×10^6	1.233×10^6	0.4280	0.0982	3653
24 HRS.	20b 90°	5.908×10^6	1.273×10^6	5.426×10^6	1.169×10^6	0.6152	0.1326	3972
24 HRS.	20c 90°							3903

$\beta = (1 - \nu_{12}\nu_{21})$, $\sigma = p\bar{R}/2\bar{t}$, $\bar{R} = 1.016"$, $\bar{t} = 0.030"$

TABLE 18

VARYING POST-CURE COOL DOWN RATE RESULTS

Specimen Designation	Cool Down Rate (Nominal) (F°/hr)		Maximum Tensile Stress (PSI)	Modulus E_{22} ($PSIx10^6$)
C - 1	-27	Normal Cool Down Rate	7751	1.45
C - 2	-27		6679	1.45
D - 1	-100		6703	1.50
D - 2	-100		7505	1.35
E - 1	-343		6990	1.37
E - 2	-343		6574	1.46

$\theta = 90°$, $\bar{R} \approx 1.0"$, $\bar{t} \approx 0.015"$

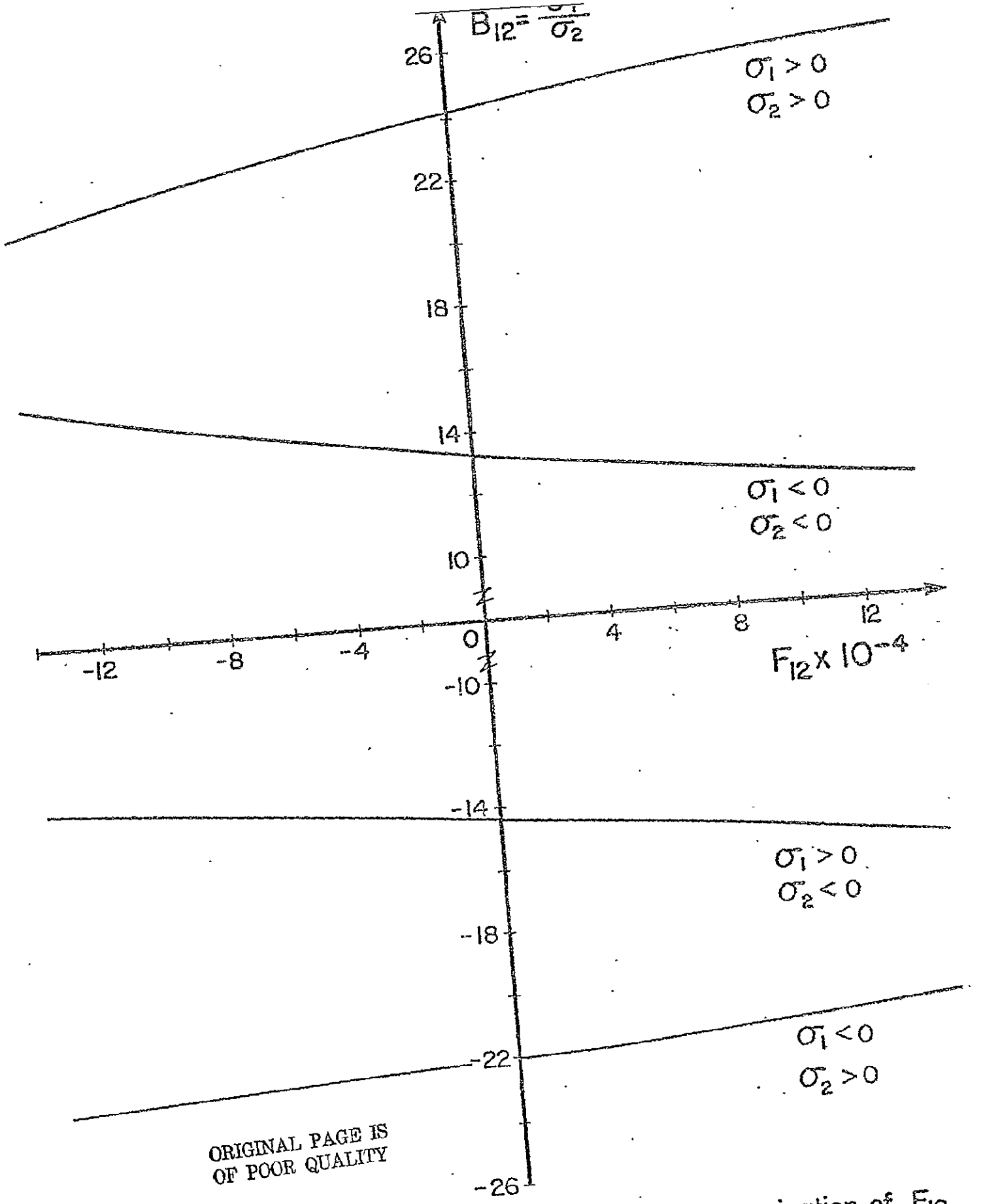

Fig. 1 Optimum Biaxial Stress Ratio, B_{12}, for the Determination of F_{12} (Glass/Epoxy)

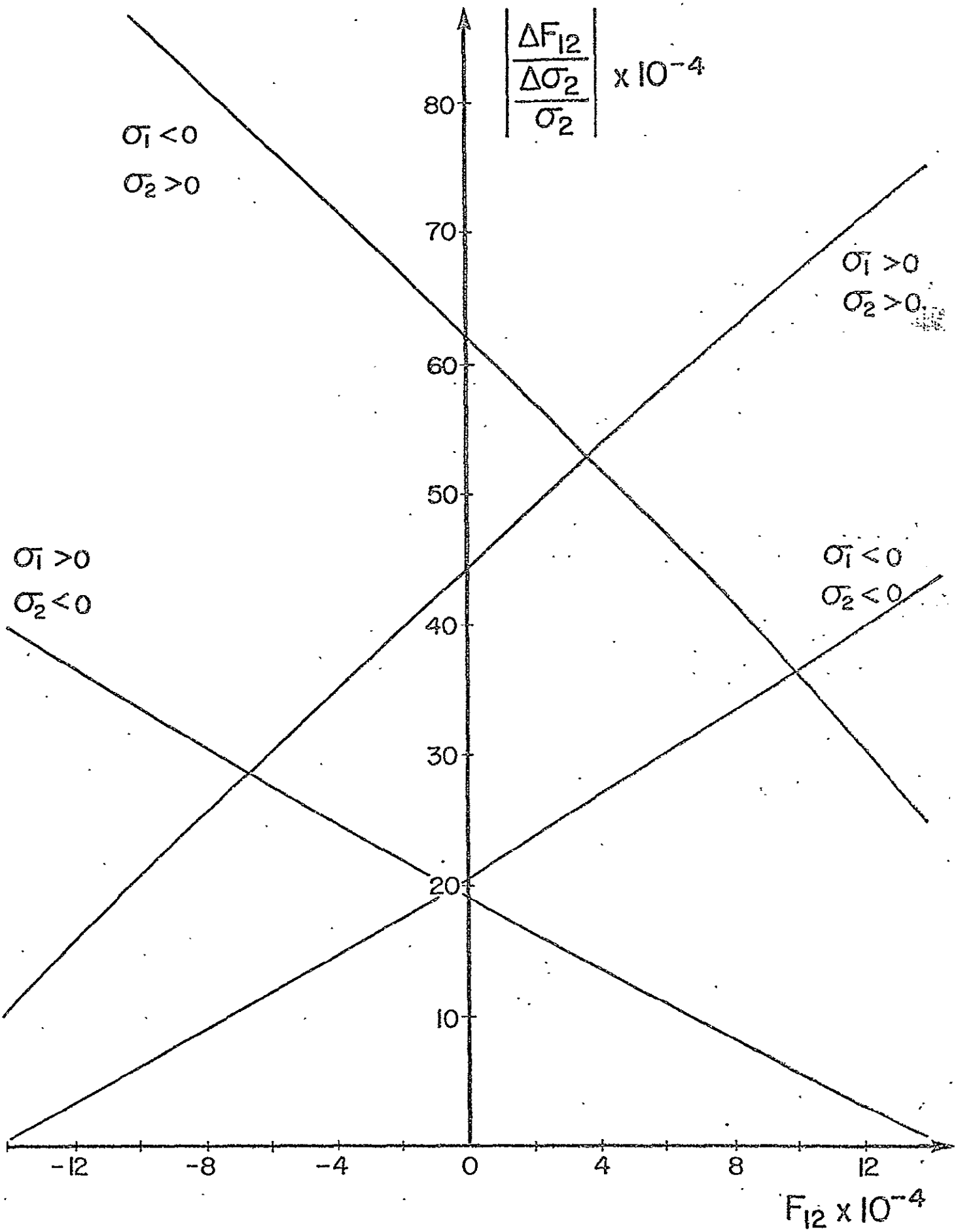

Fig. 2 Attainable Resolution of F_{12} for Optimal Ratios, $B_{12} = \frac{\sigma_1}{\sigma_2}$
(Glass/Epoxy)

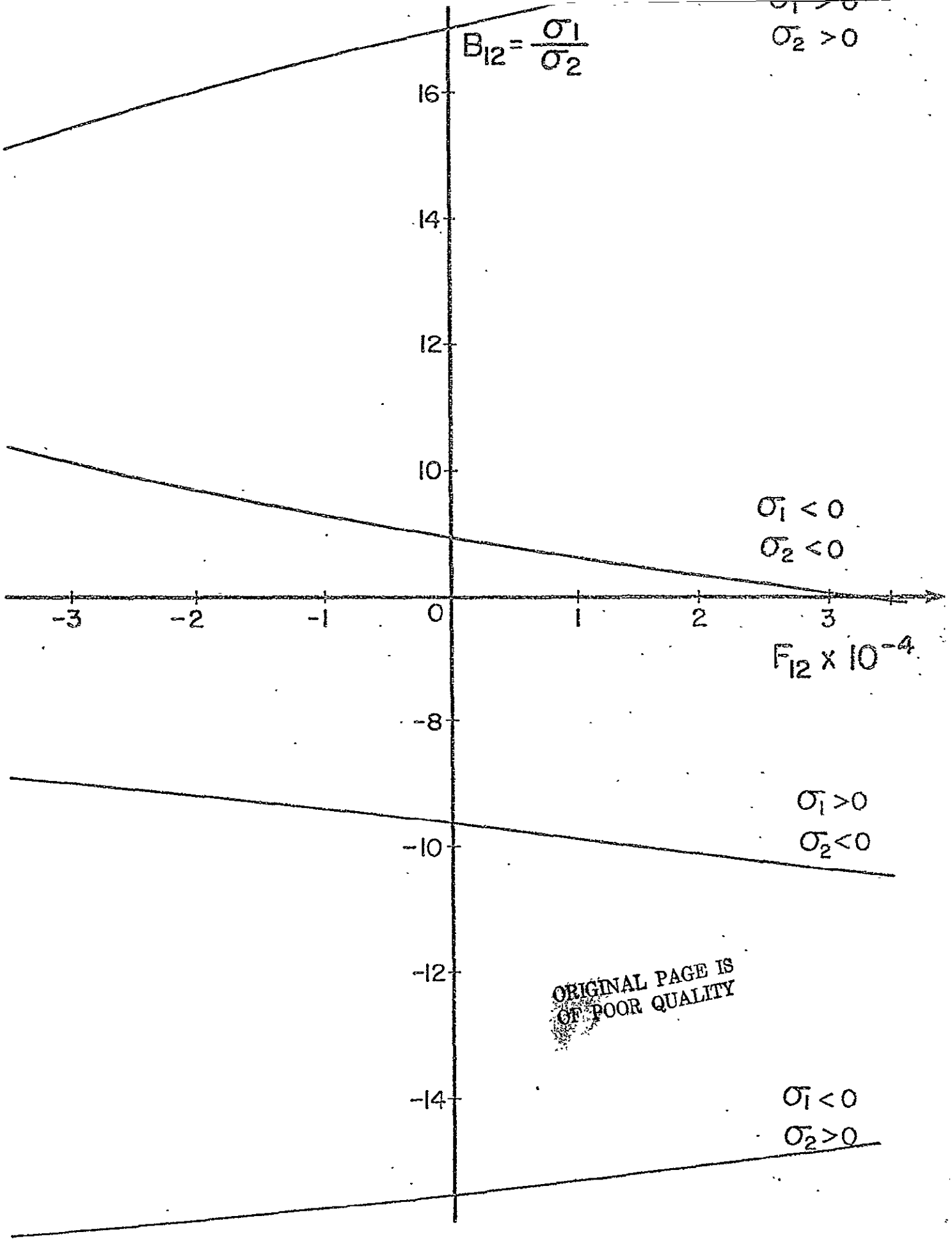

Fig. 3 Optimum Biaxial Stress Ratio, B_{12}, for Determination of F_{12} (Graphite/Epoxy)

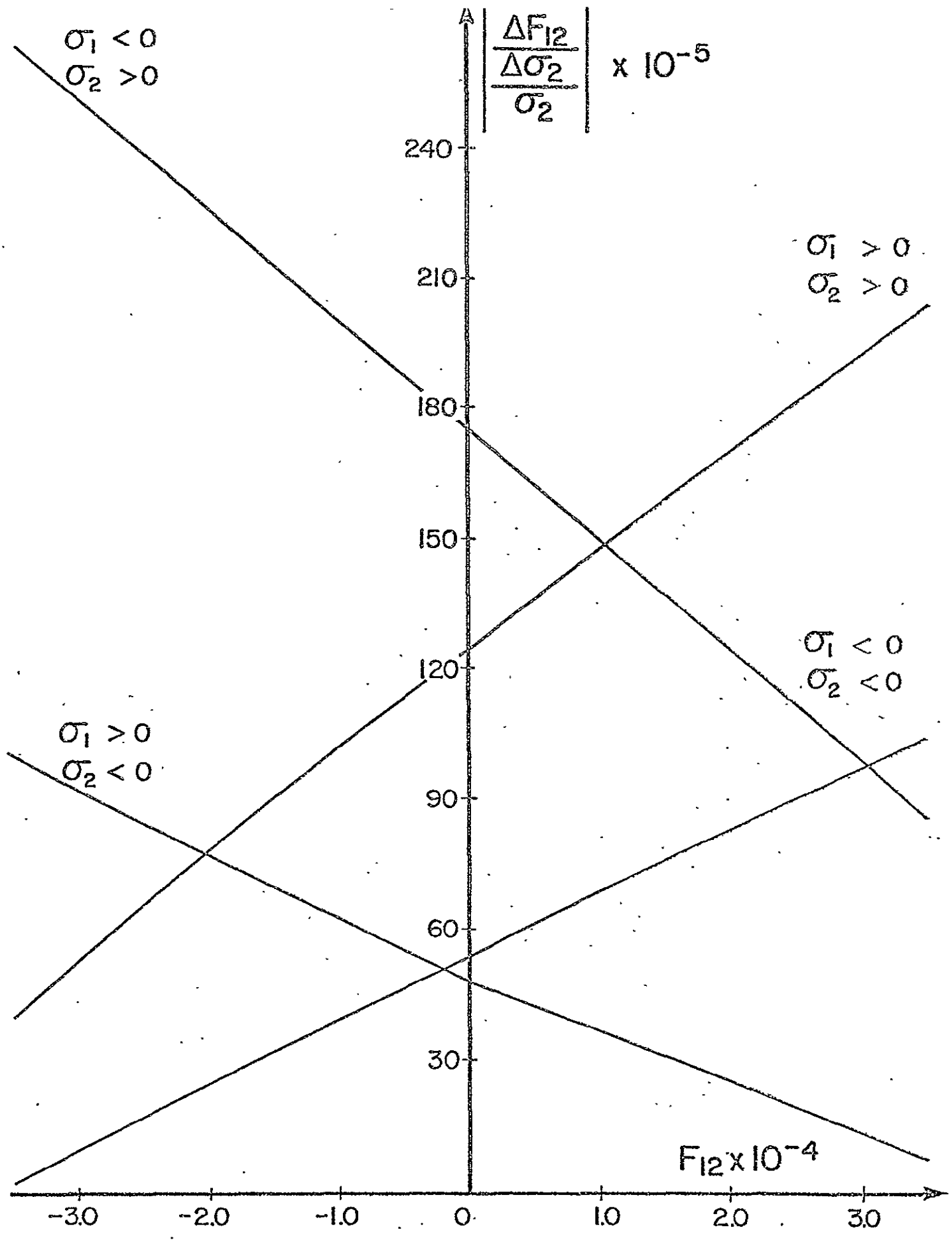

Fig. 4 Attainable Resolution of F_{12}, for Optimal Ratios, $B_{12} = \frac{\sigma_1}{\sigma_2}$
(Graphite/Epoxy)

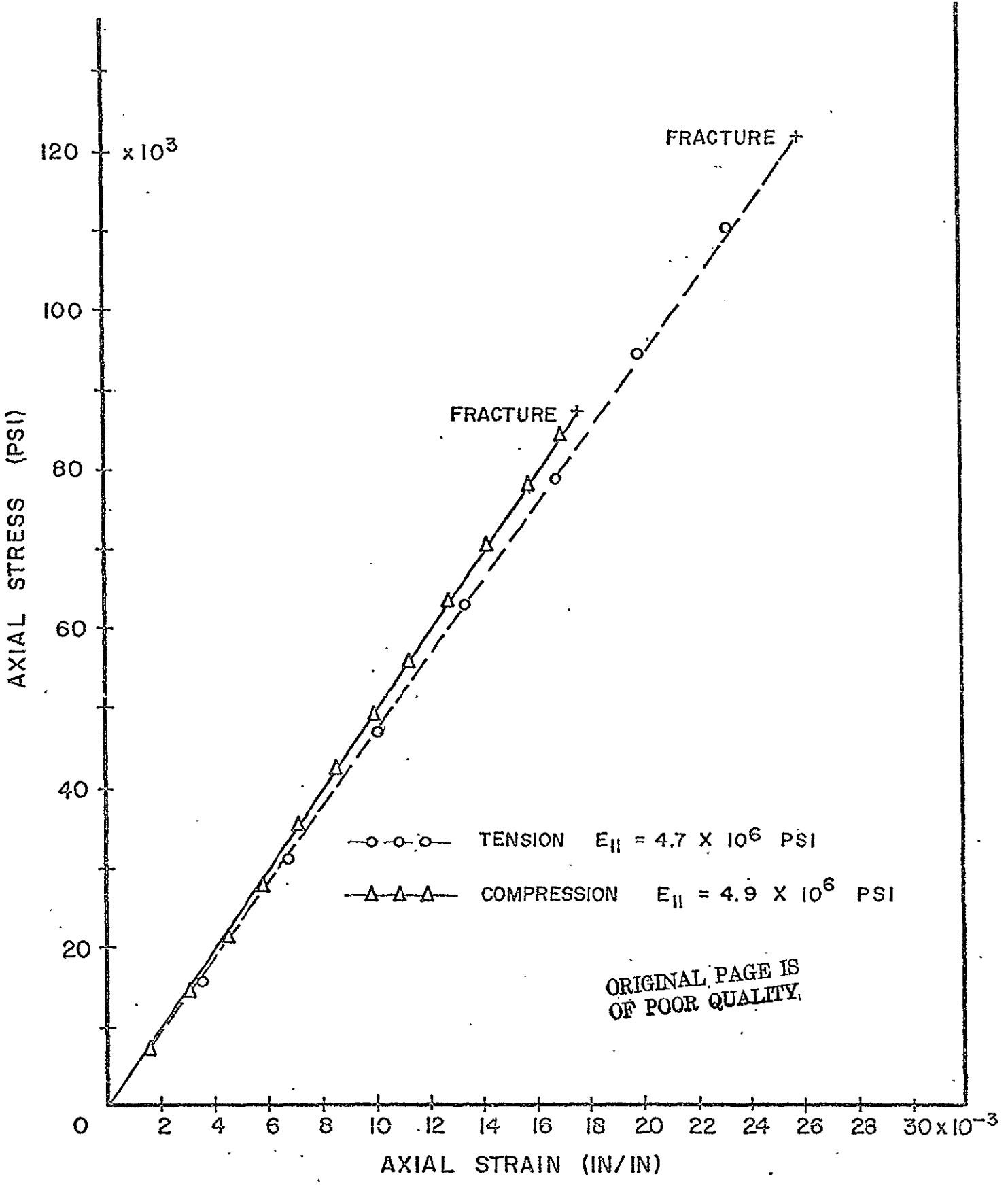

FIG. 5 STRESS – STRAIN CURVES FOR SCOTCHPLY (1002) LOADED PARALLEL TO FIBER DIRECTION

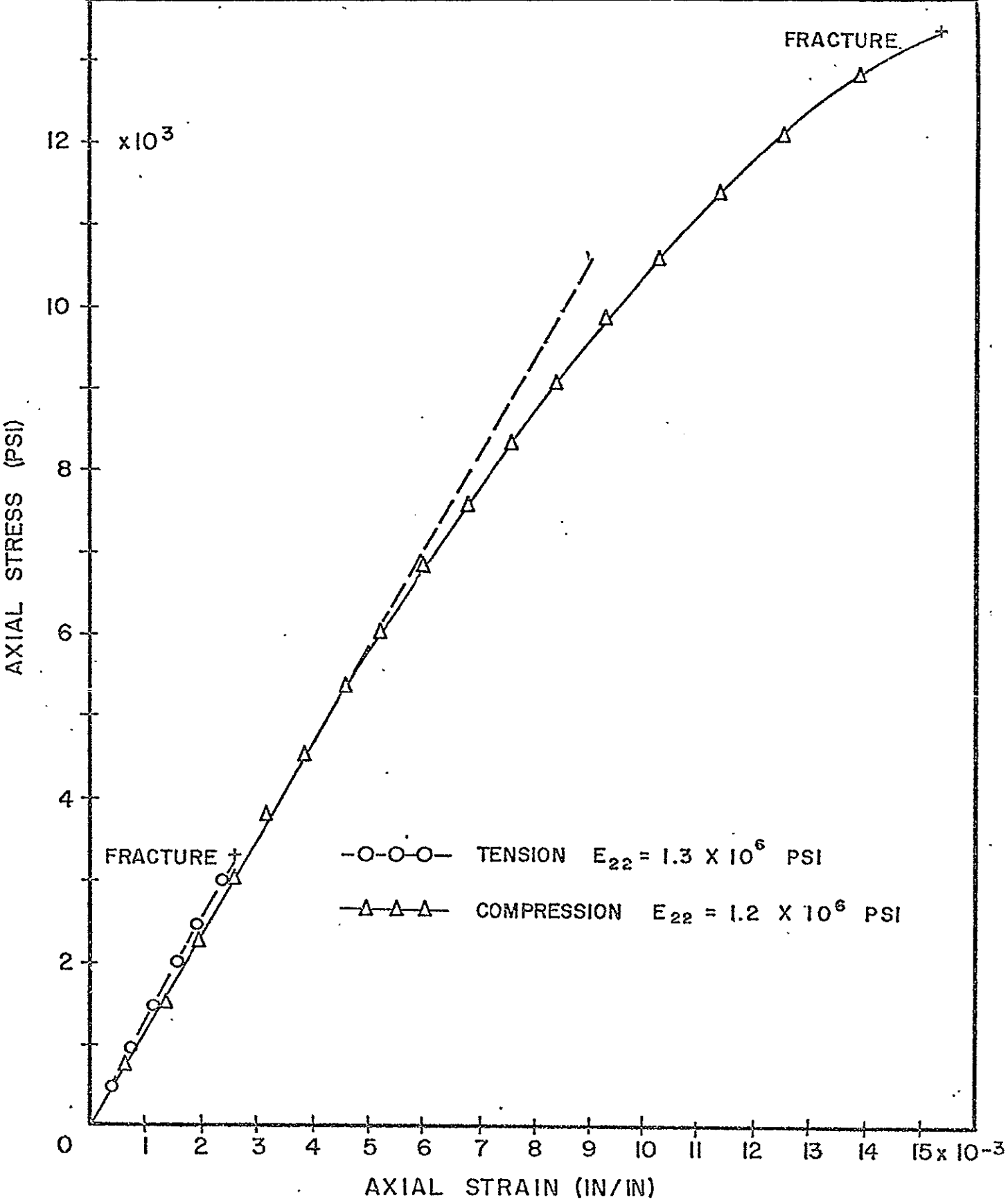

FIG. 6 STRESS-STRAIN CURVES FOR SCOTCHPLY (1002) LOADED PERPENDICULAR TO FIBER DIRECTION

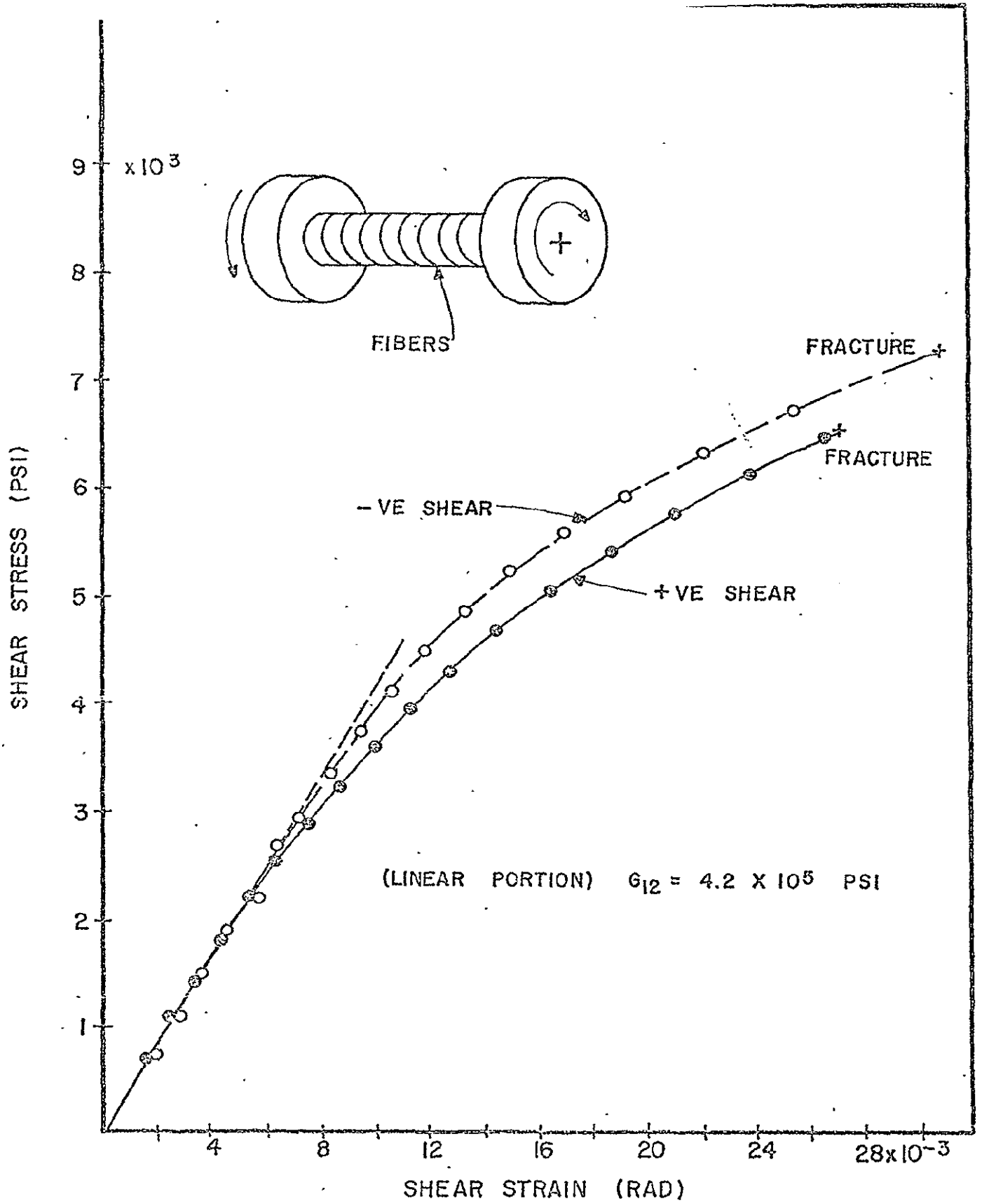

FIG. 7 STRESS-STRAIN CURVES FOR SCOTCHPLY (1002) IN PURE SHEAR

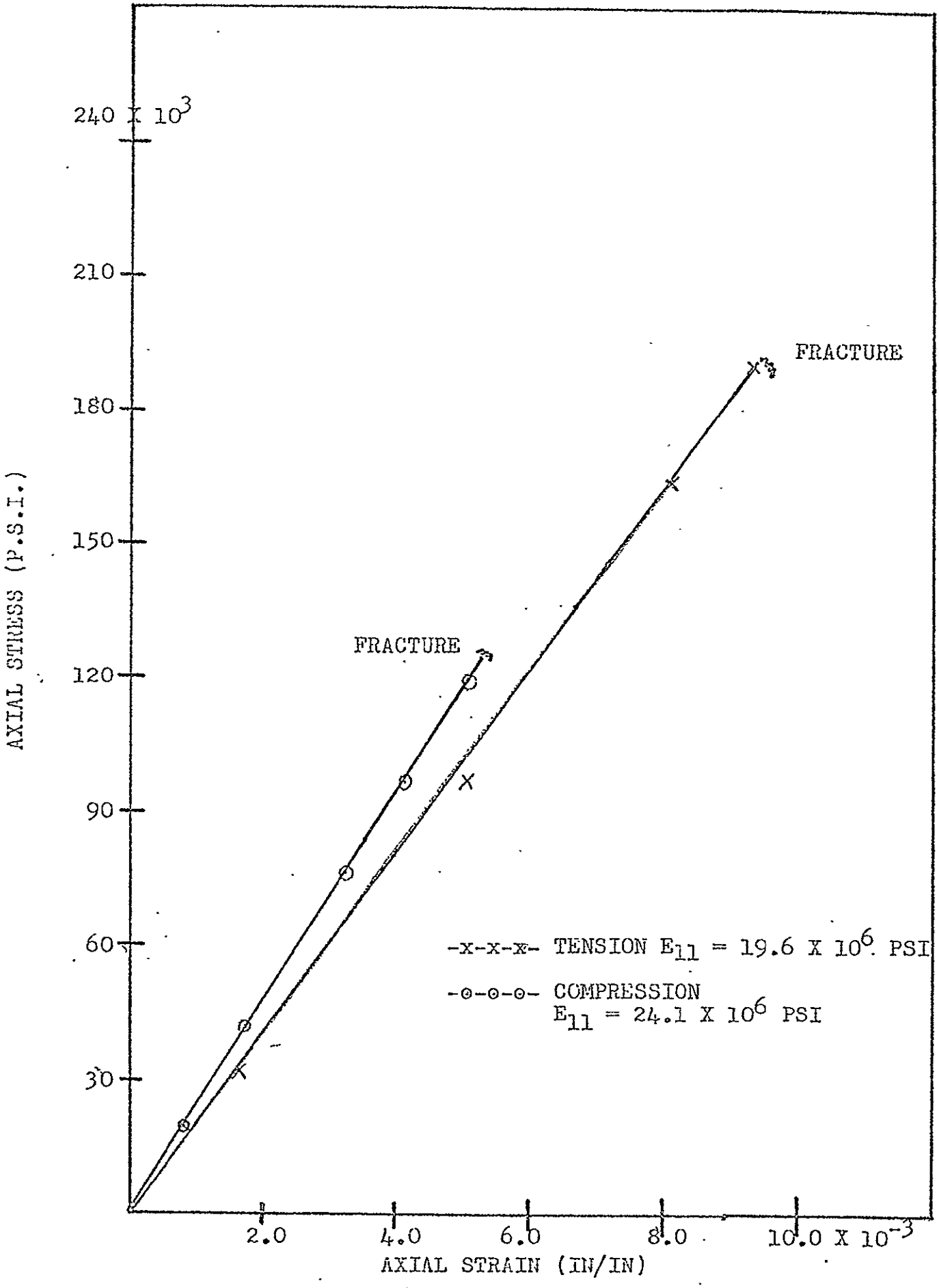

FIG. 8 STRESS STRAIN CURVES FOR GRAPHITE-EPOXY COMPOSITE (SP-288T300) LOADED PARALLEL TO FIBER DIRECTION

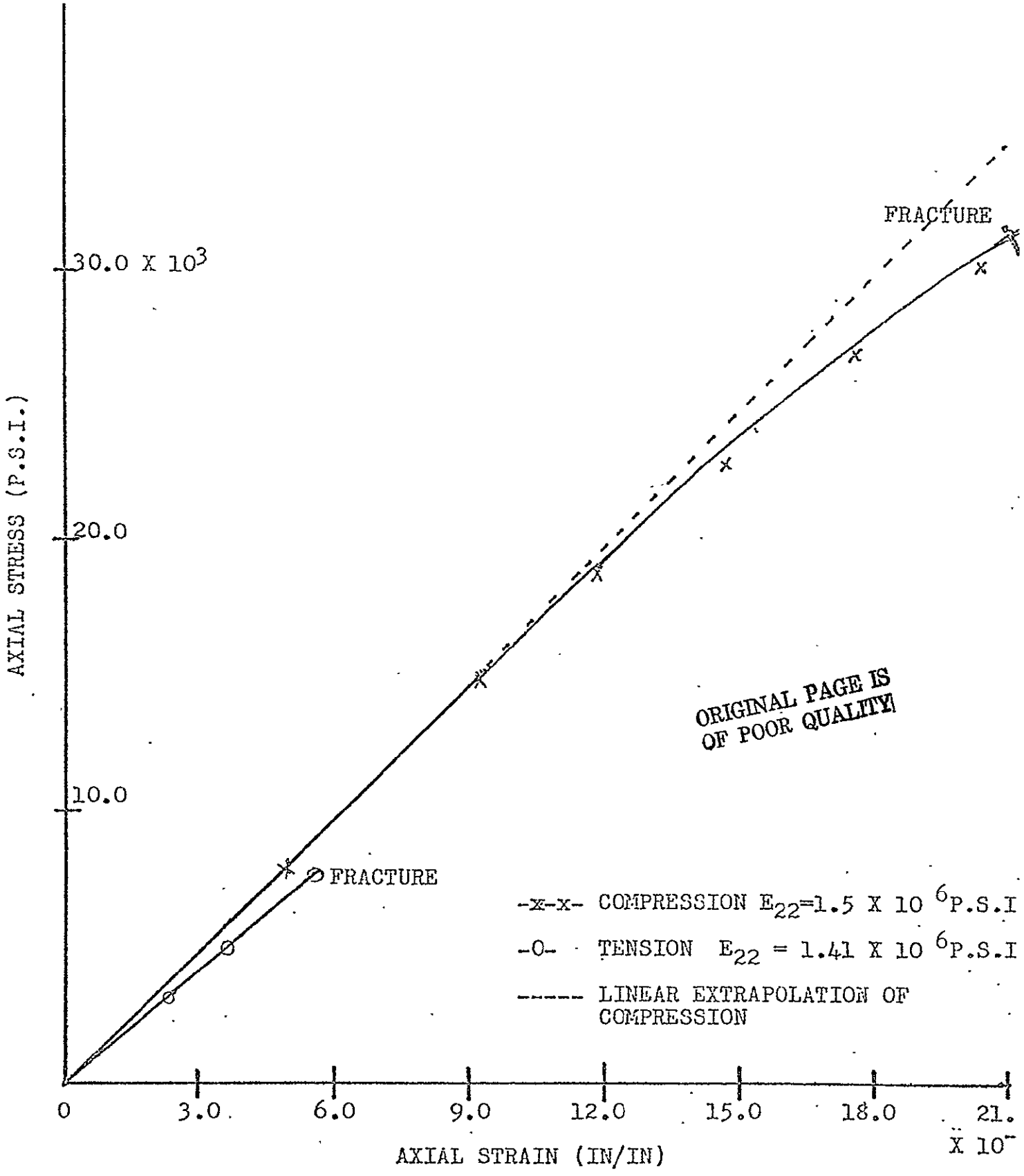

FIG. 9 STRESS-STRAIN CURVES FOR GRAPHITE-EPOXY COMPOSITE (SP-288T300) LOADED PERPENDICULAR TO FIBER DIRECTION

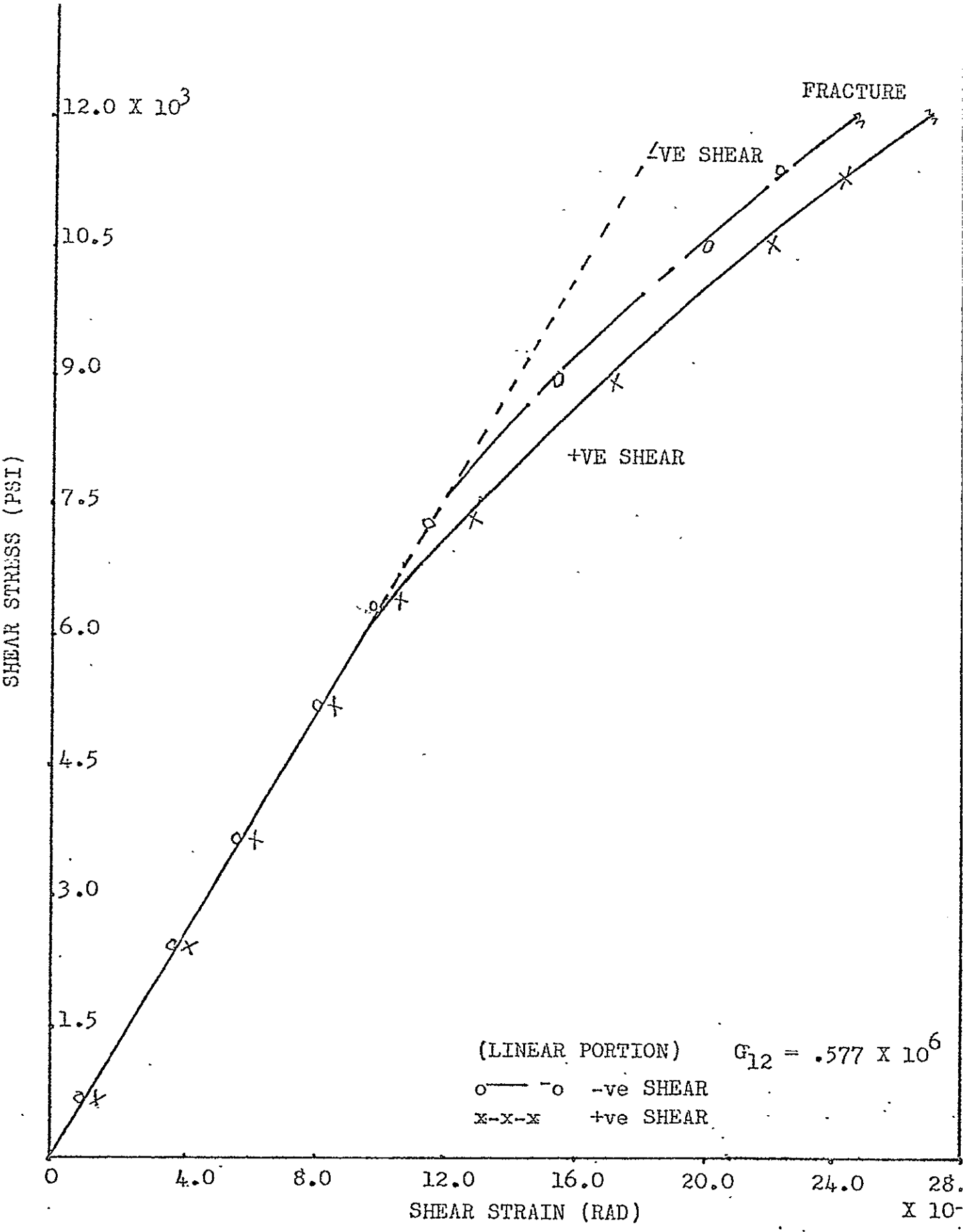

FIG. 10 STRESS-STRAIN CURVES FOR GRAPHITE-EPOXY (SP-288T300) IN PURE SHEAR

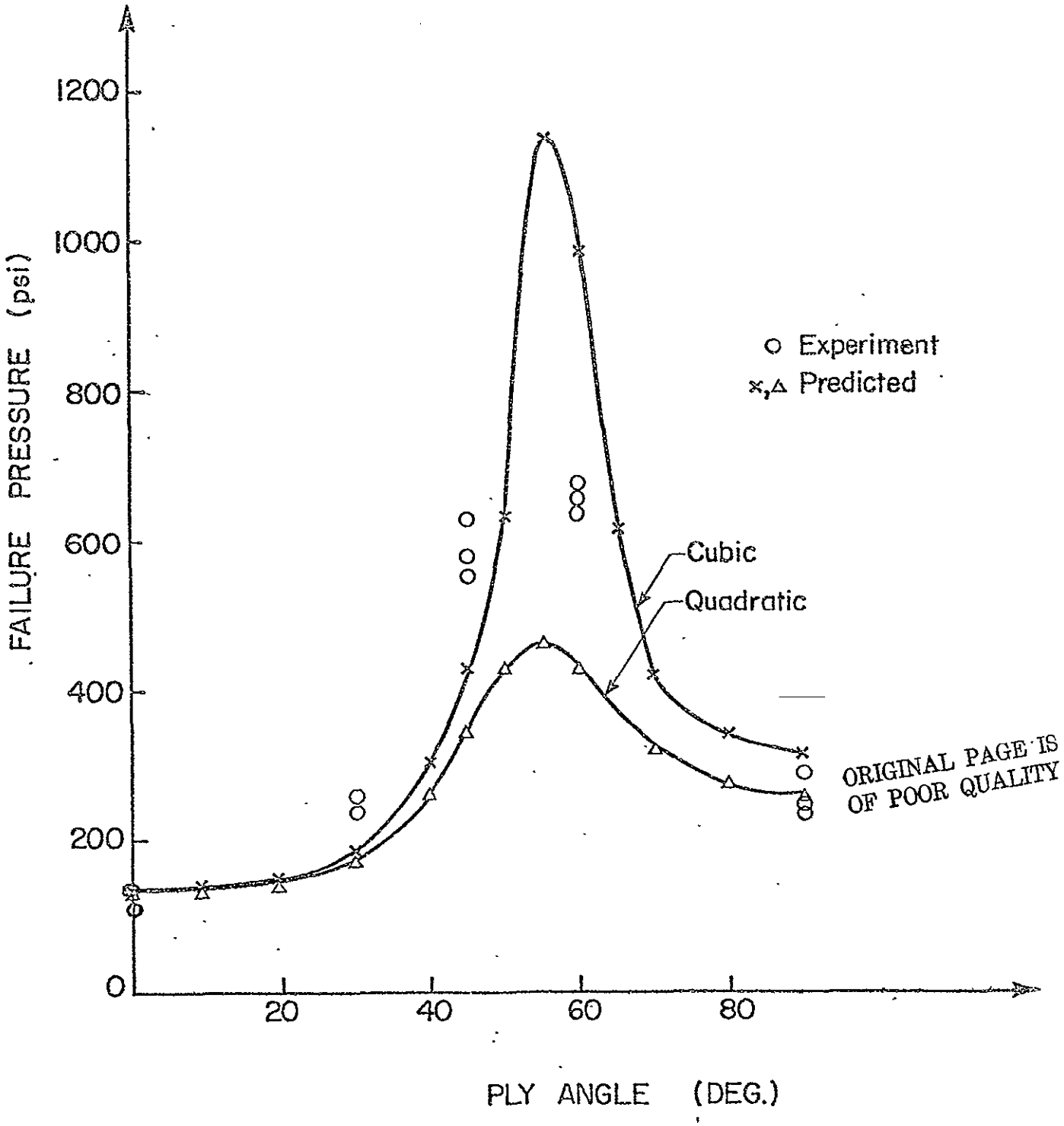

Fig. 11 Failure of Symmetric Laminated Tubes Under Pressure.
(Glass/Epoxy)

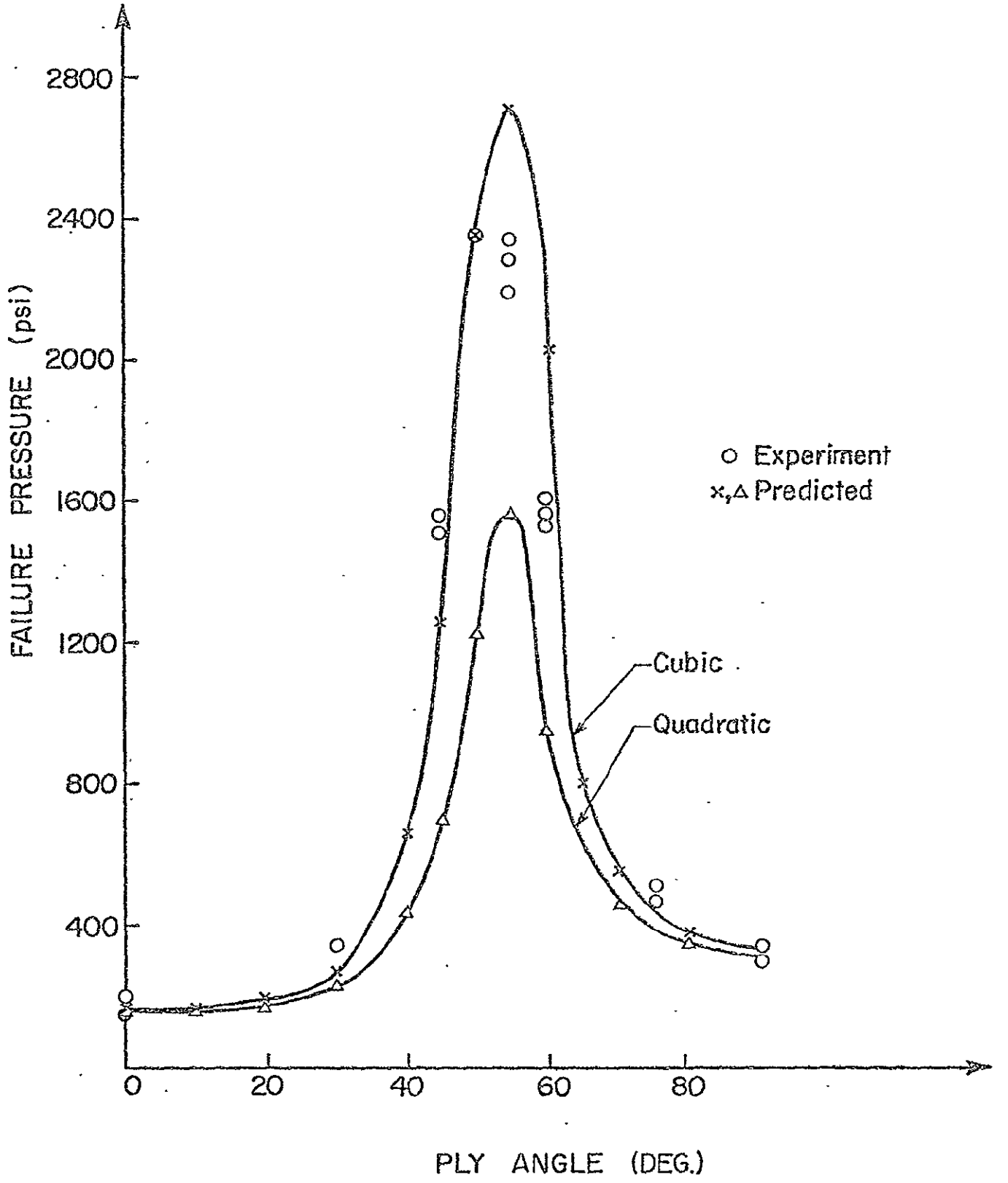

Fig. 12 Failure of Symmetric Laminated Tubes Under Pressure.
(Graphite / Epoxy)

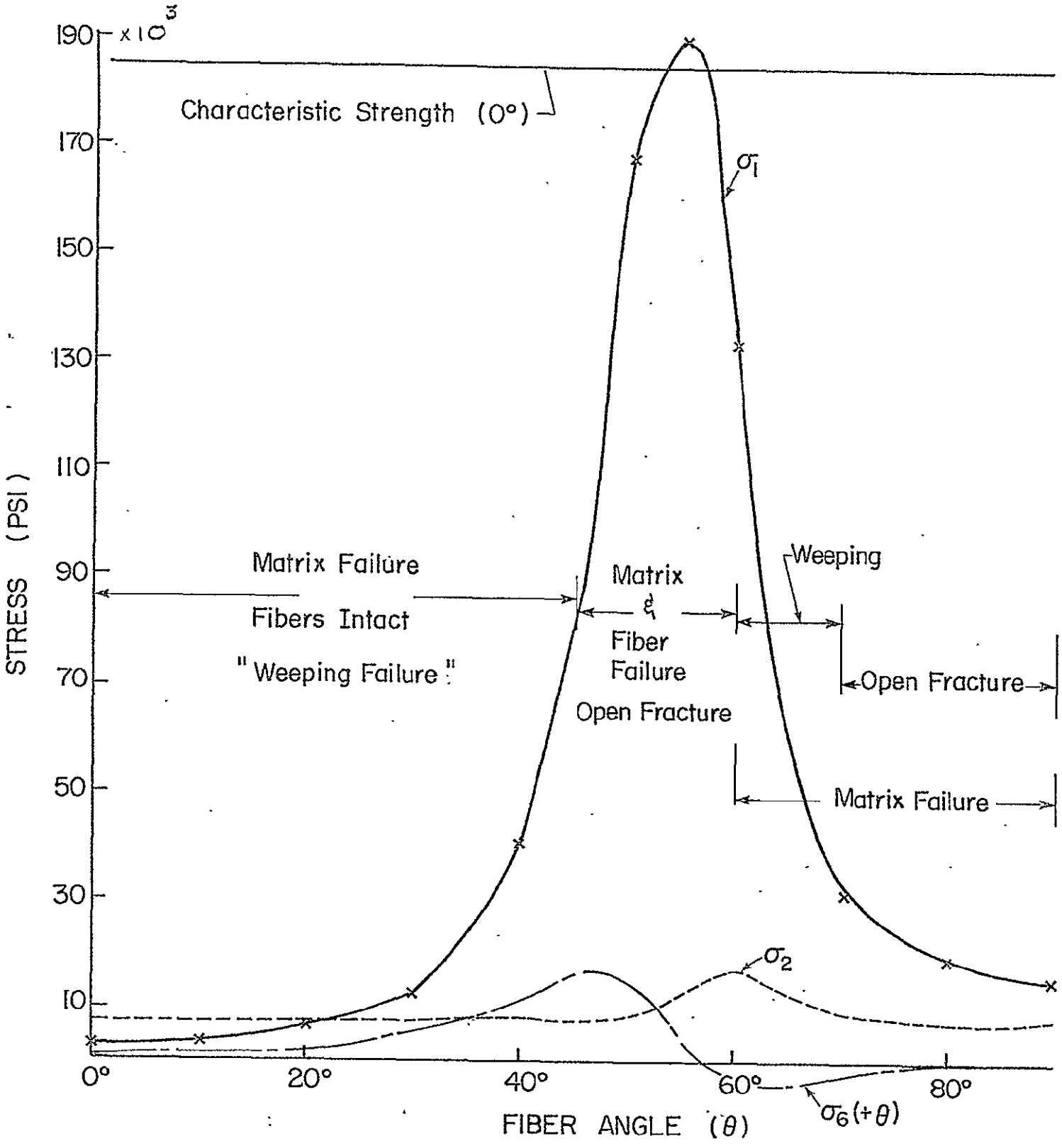

Fig. 13 Variation in Predicted (Cubic) Principal Failure Stress with Fiber Orientation.

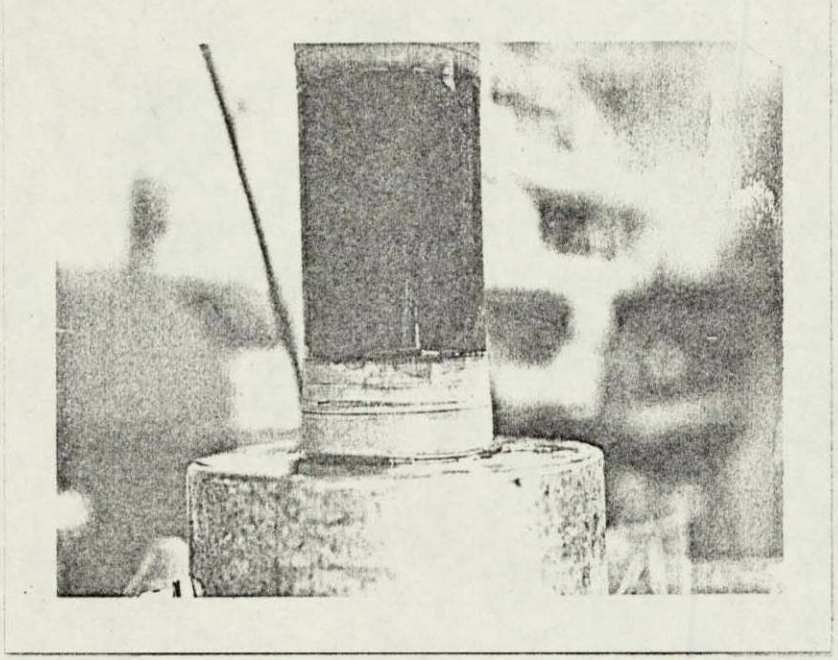

$\theta = 0°$

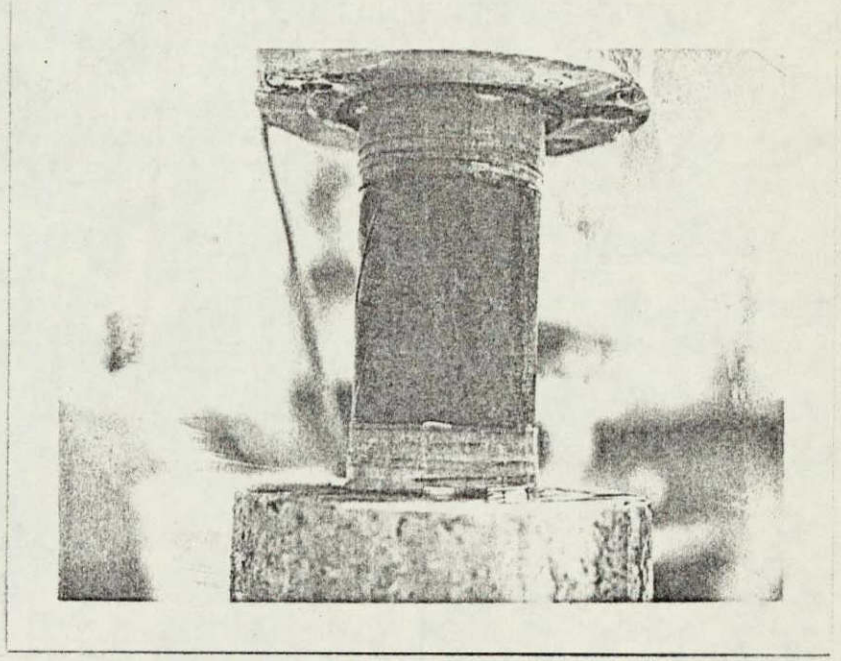

$\theta = \mp 30°$

Fig. 14 "Weeping" Failure Modes of Tubes Subjected~Internal Pressure.

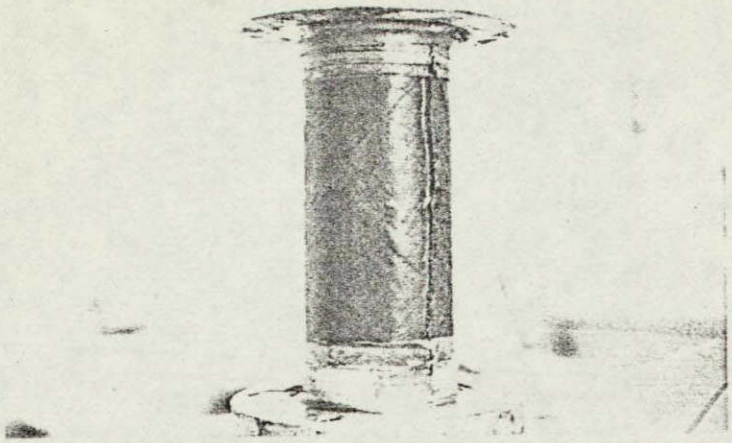

$\theta = \mp 45°$

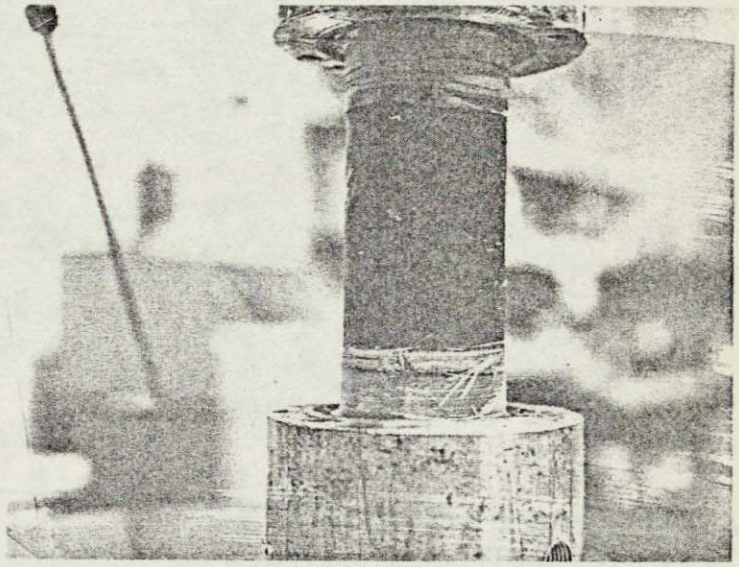

$\theta = \mp 50°$

$\theta = \mp 55°$

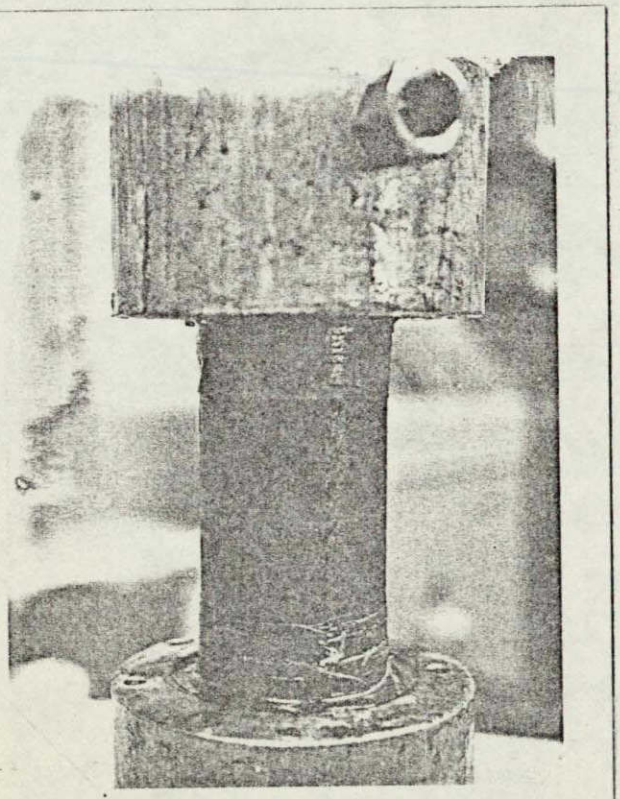

Fig. 15 Failure of Matrix and Fibers in Open Fracture Mode.

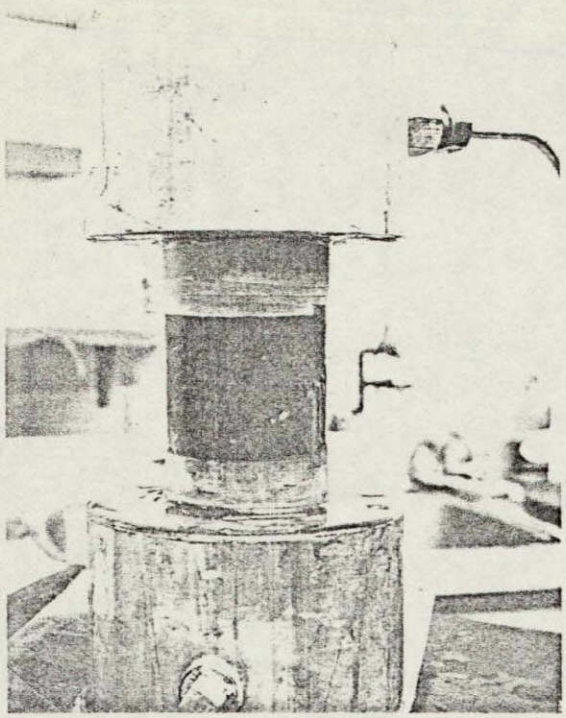

$\theta = \mp 60°$

Fig. 16 Transition Failure (Weeping) Mode Due to Matrix Failure

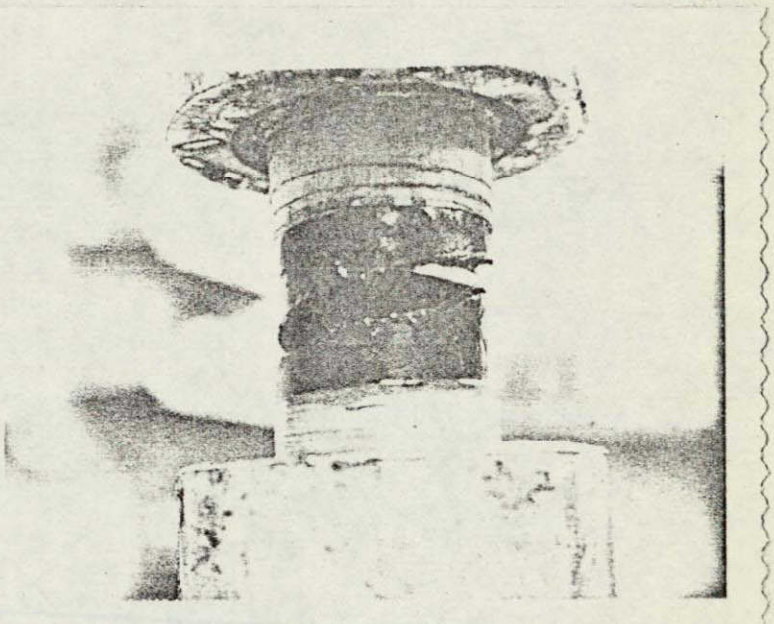

$\theta = \mp 75°$

$\theta = 90°$

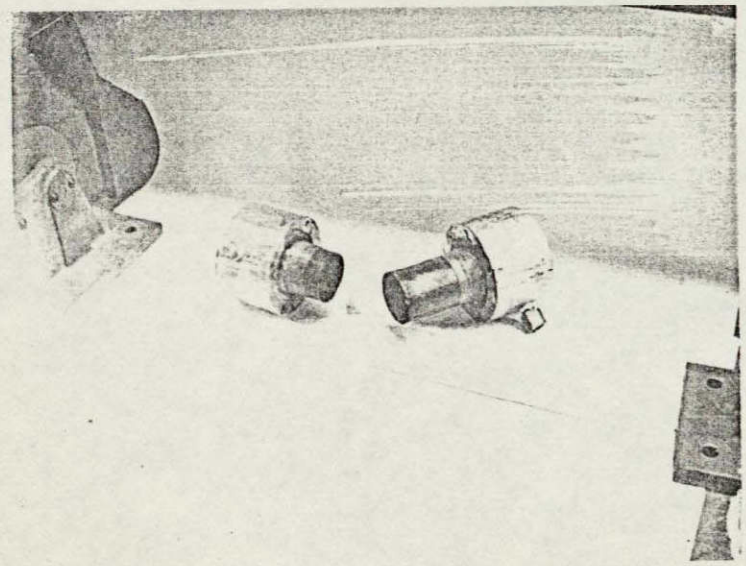

Fig. 17 Failure of Matrix in Open Fracture Mode.

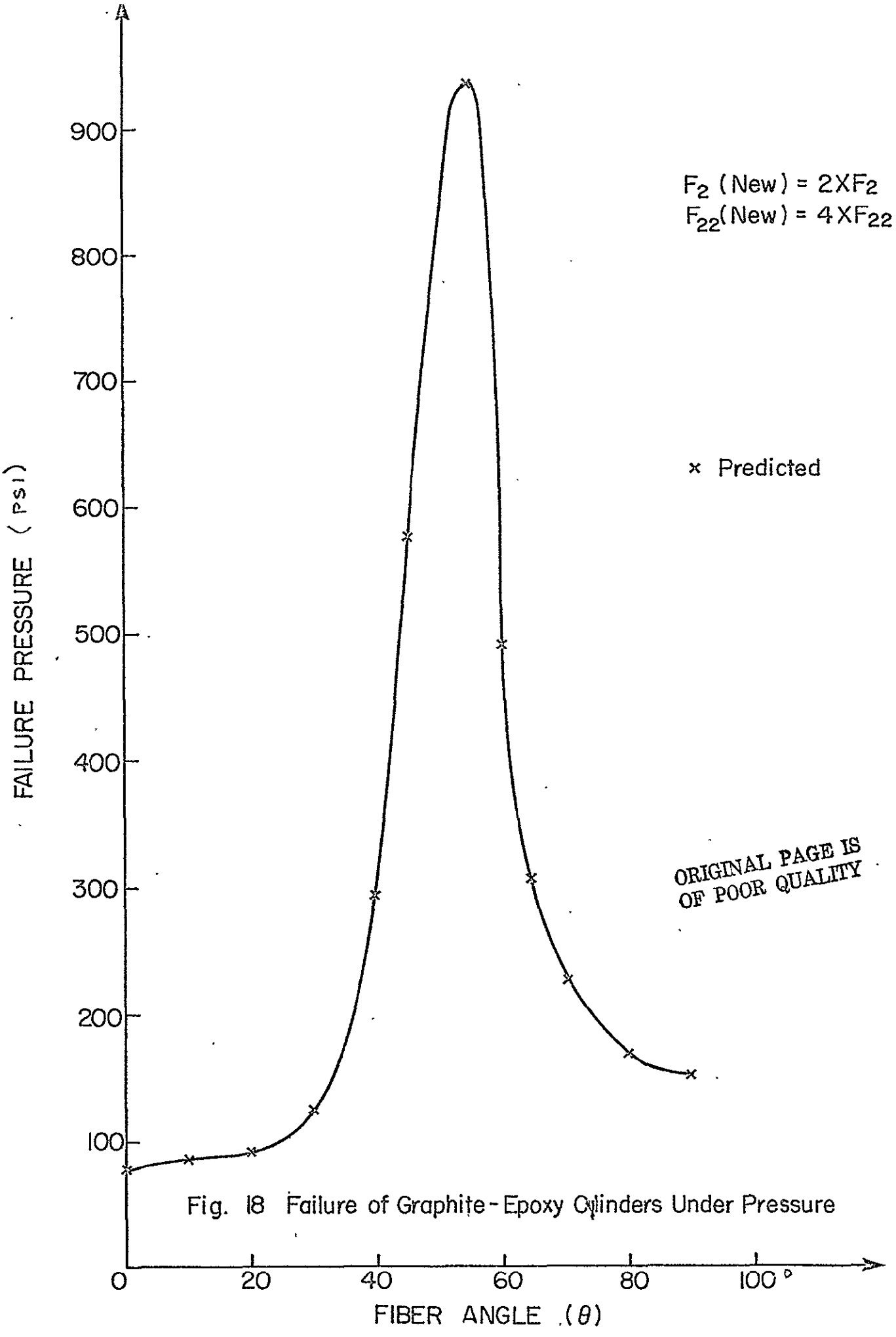

Fig. 18 Failure of Graphite-Epoxy Cylinders Under Pressure

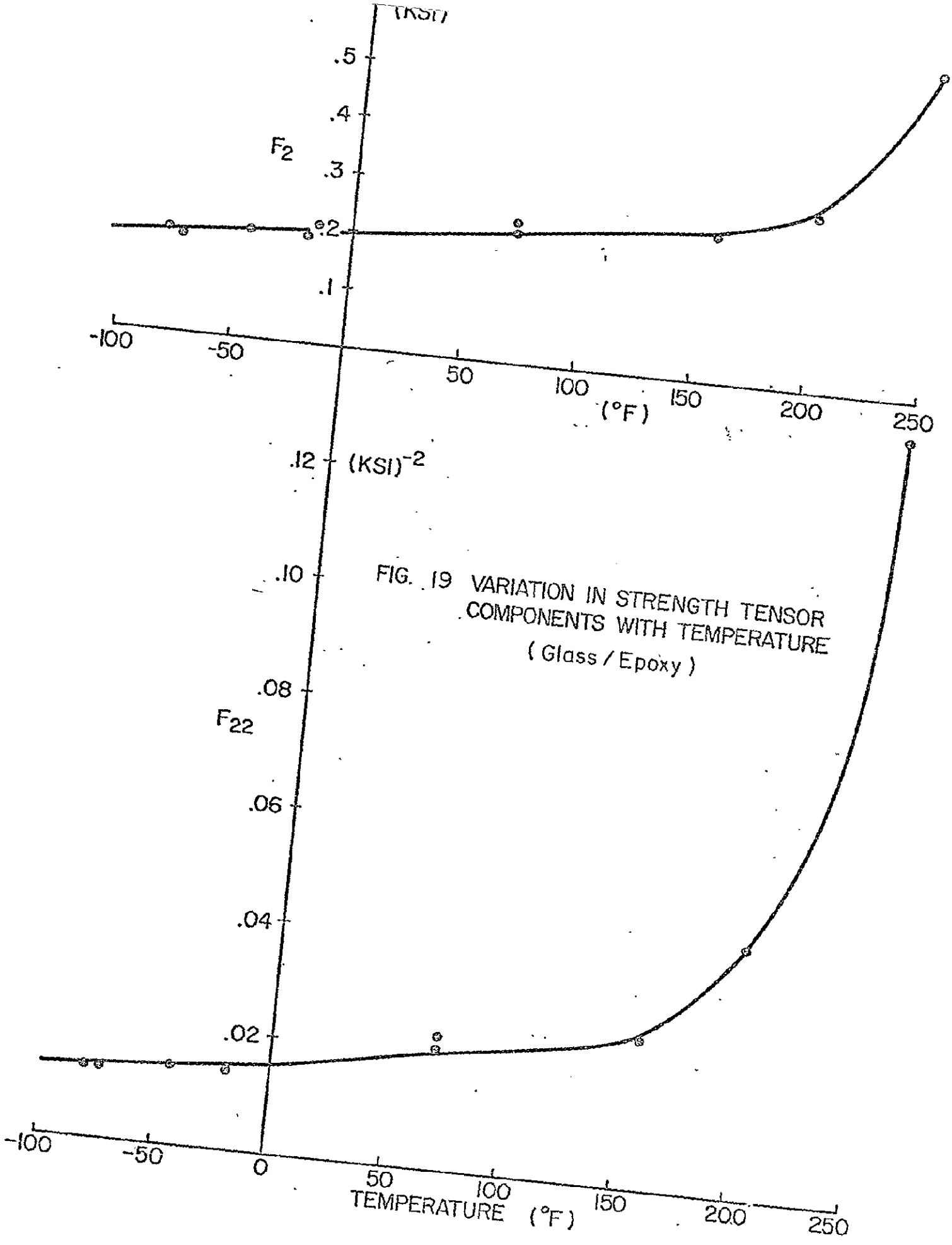

FIG. 19 VARIATION IN STRENGTH TENSOR COMPONENTS WITH TEMPERATURE
(Glass / Epoxy)

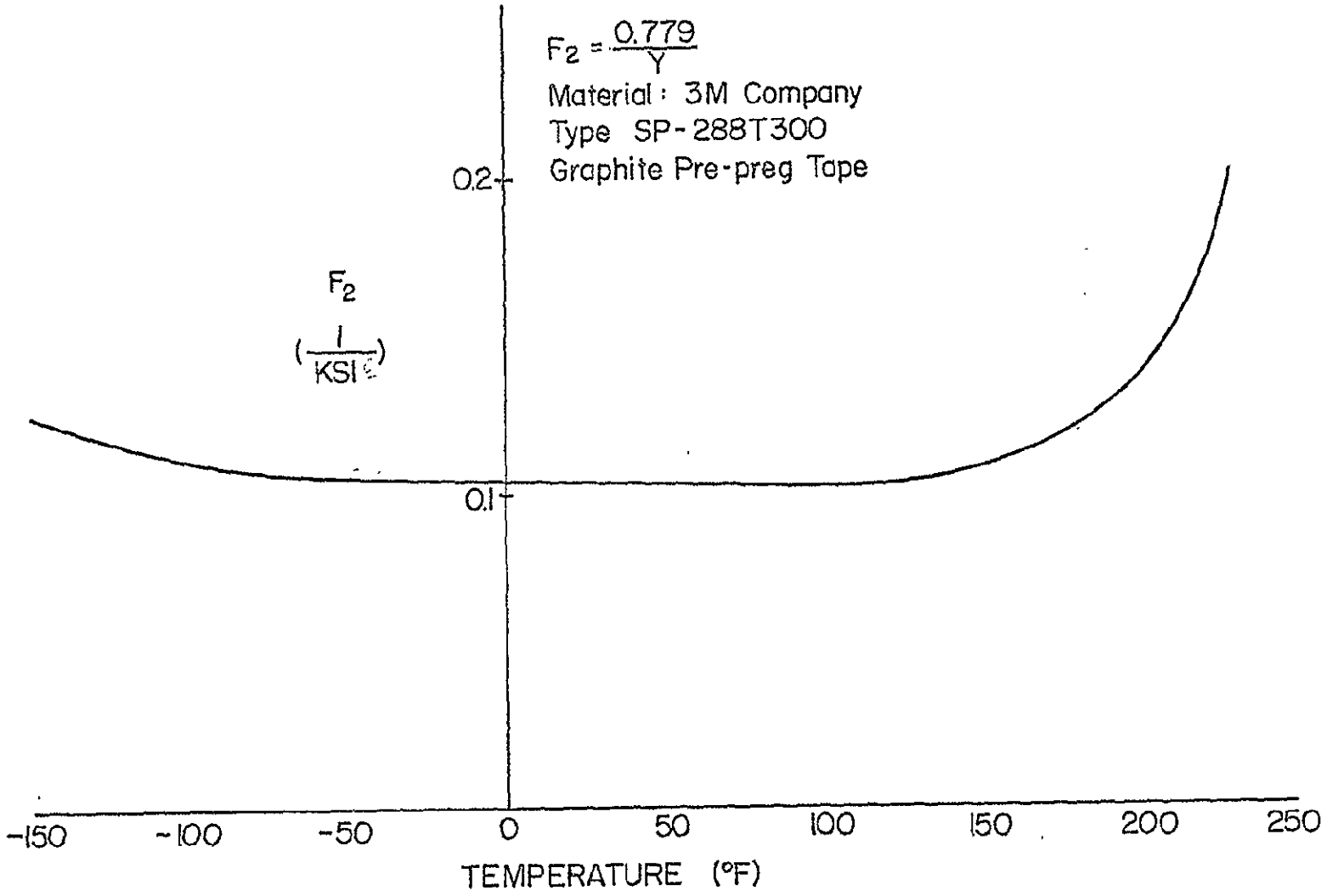

FIG. 20

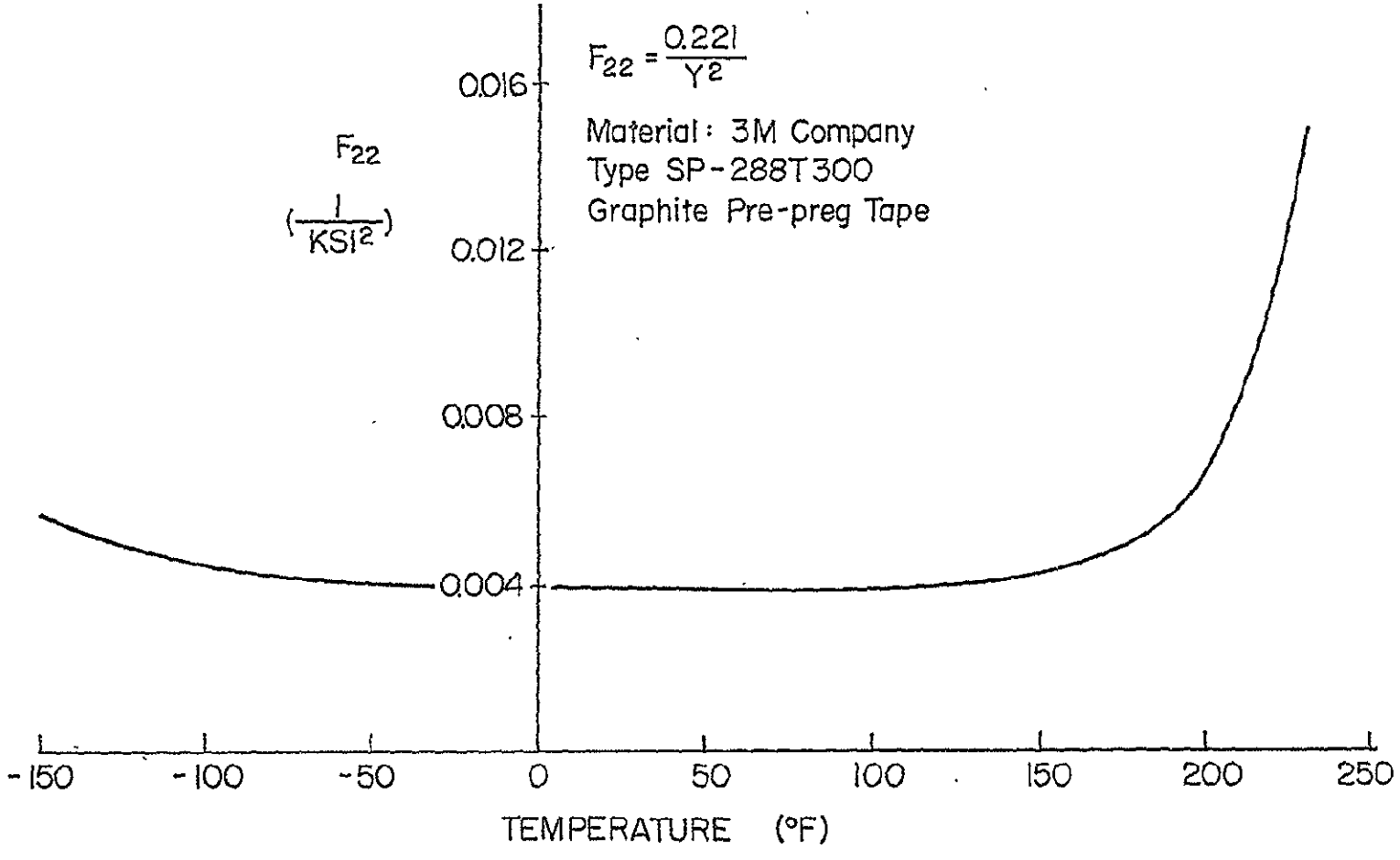
$F_{22} = \frac{0.221}{Y^2}$
Material: 3M Company
Type SP-288T300
Graphite Pre-preg Tape
F_{22}
$(\frac{1}{KSI^2})$
0.016
0.012
0.008
0.004
-150
-100
-50
0
50
100
150
200
250
TEMPERATURE (°F)

FIG. 21

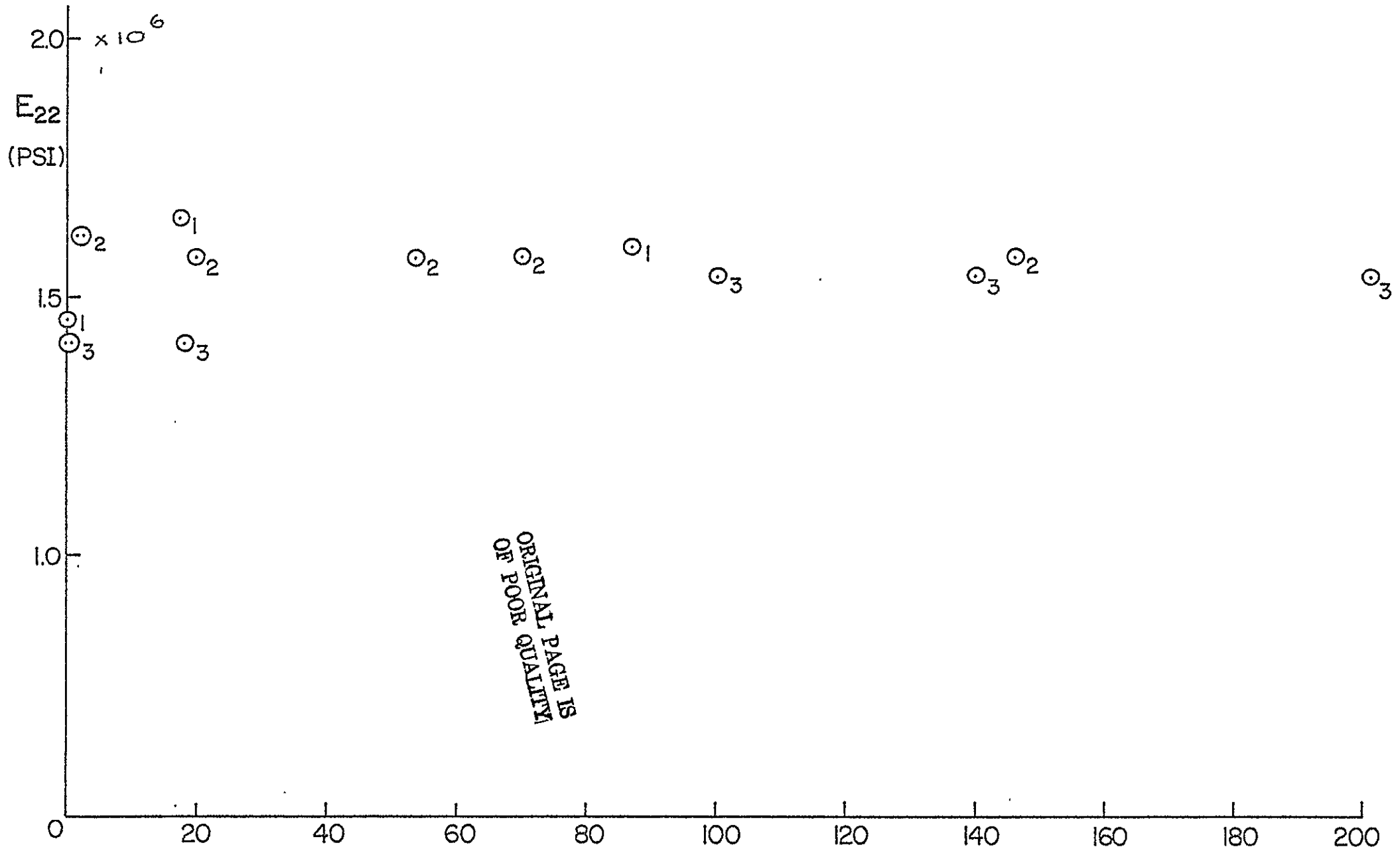

FIG. 22 E_{22} (Matrix) Modulus Variation.

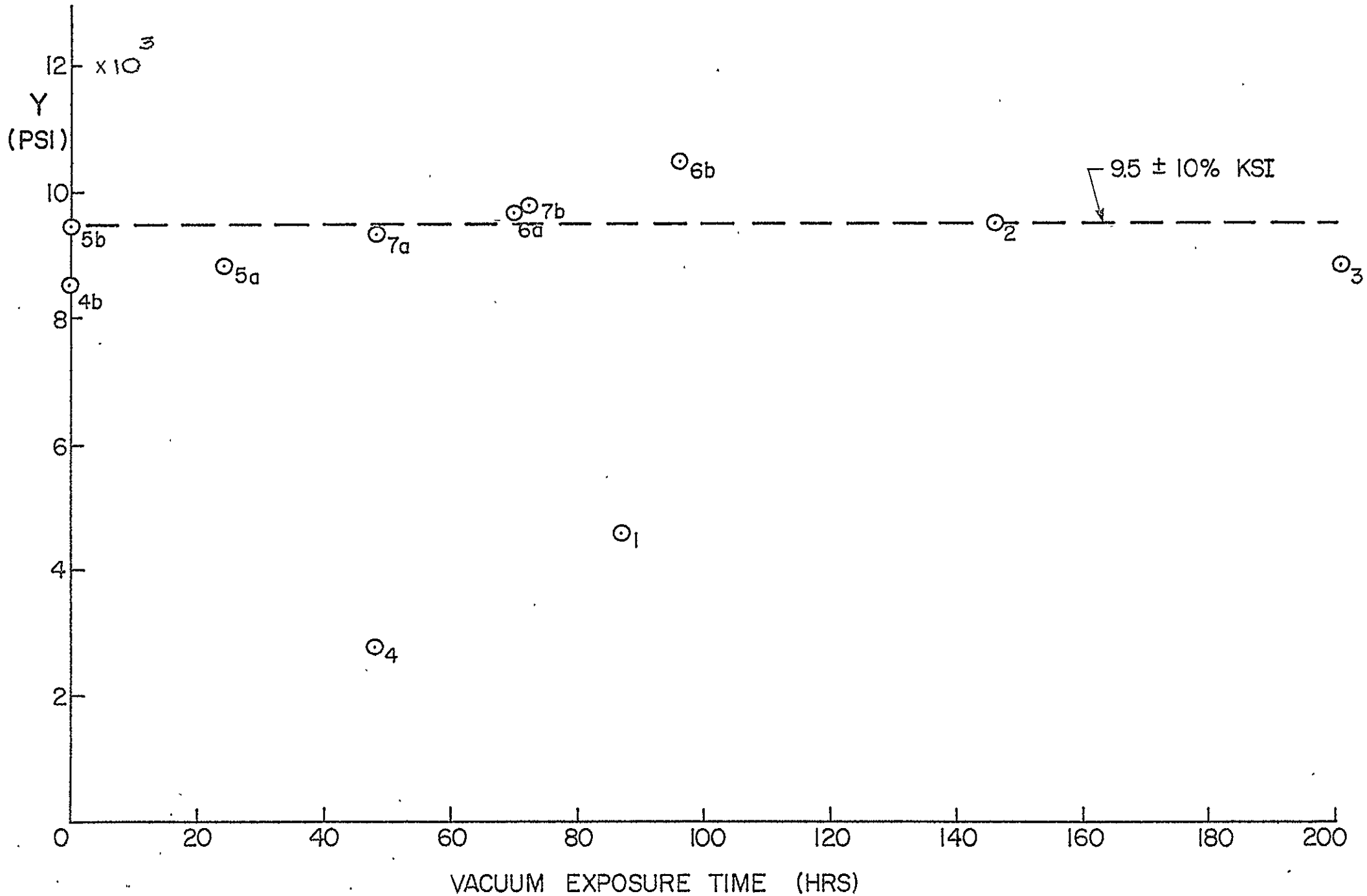

Fig. 23 Y (Matrix) Tensile Failure Stress Variation.

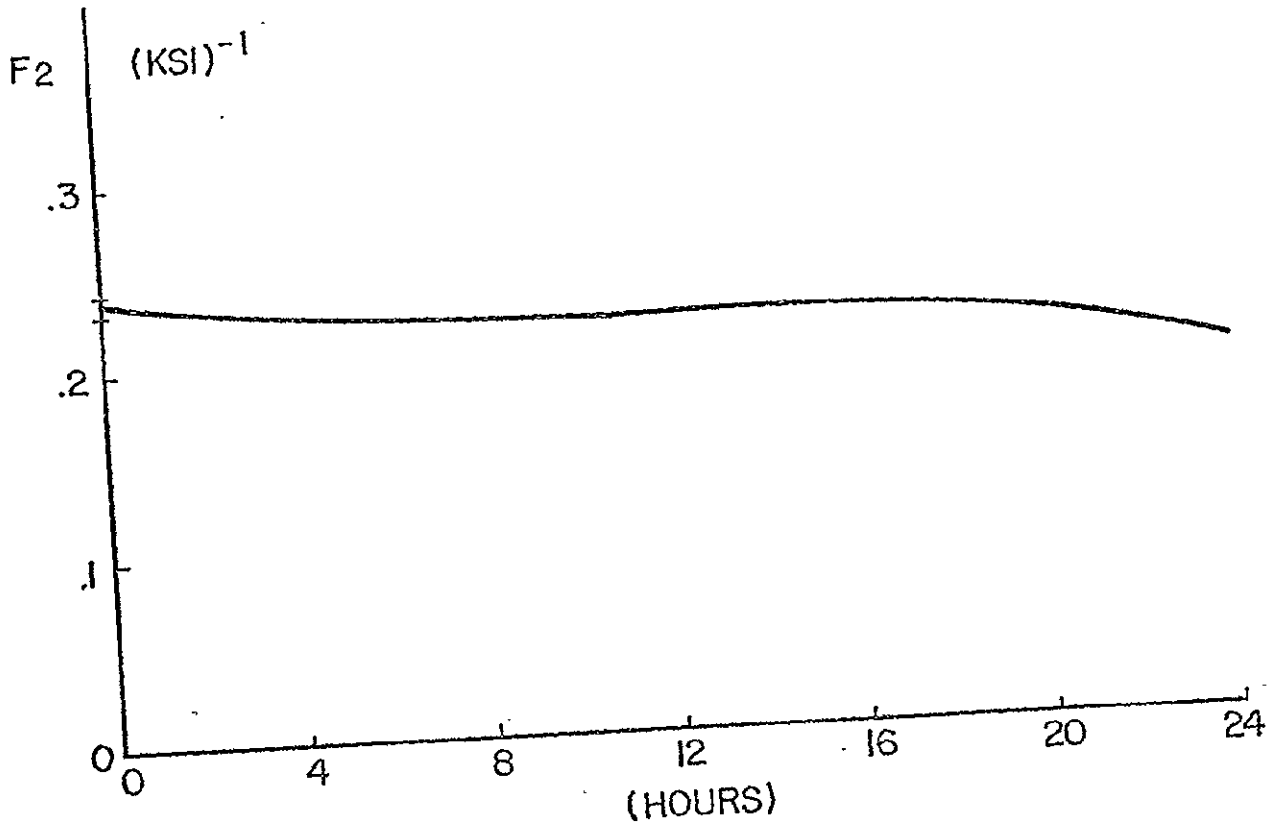

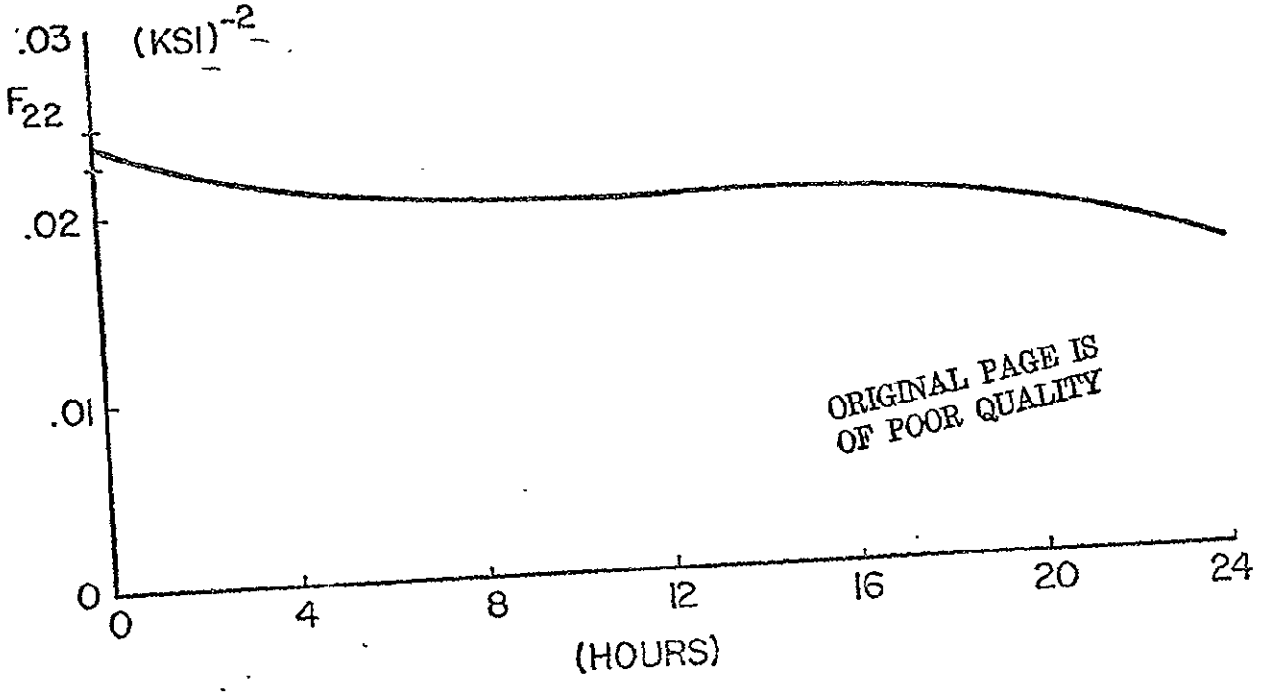

FIG. 24 THE VARIATION IN STRENGTH TENSOR COMPONENT WITH POST-CURE TIME
(Glass / Epoxy)

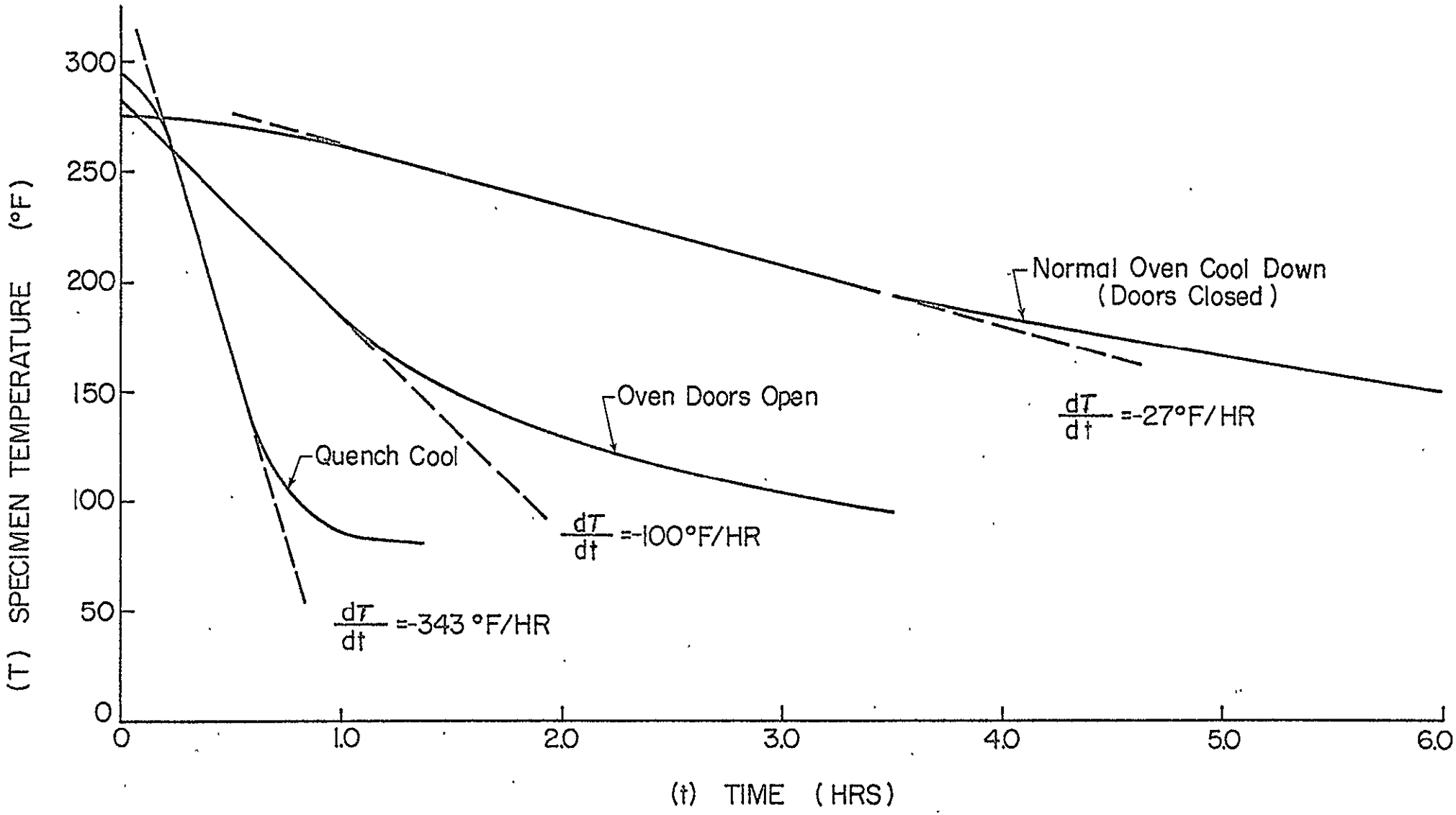

Fig. 25 Varying Rates of Post-Cure Cool Down for Graphite-Epoxy Specimens in Autoclave.

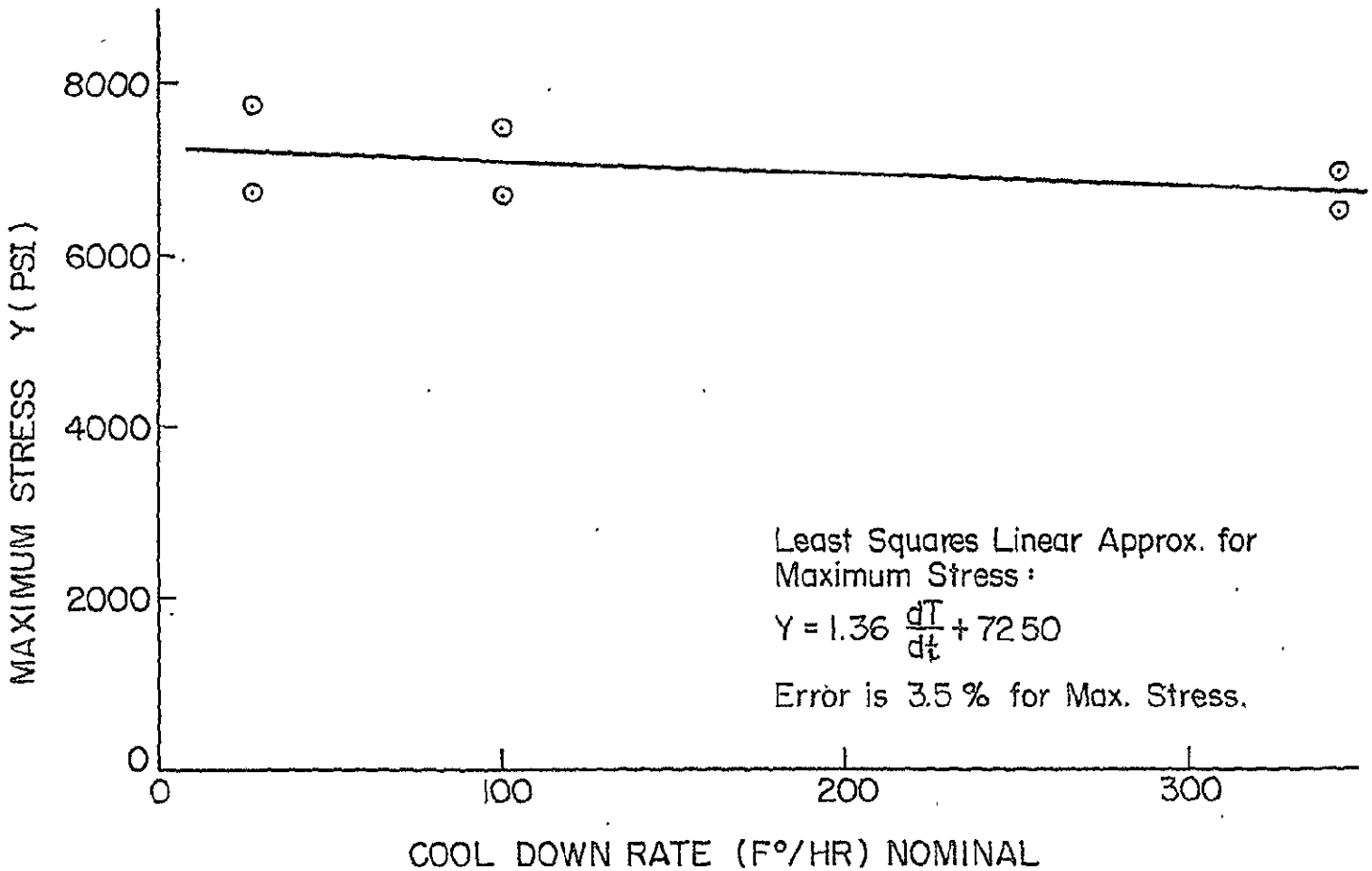

FIG. 26

APPENDIX A

FABRICATION OF SPECIMENS

Most of the experimental test articles used in this study were circular cylindrical tubes fabricated in a belt-wrapper machine as shown in Fig. A.1. This particular apparatus applies constant pressure around approximately 340° of a mandrel through the use of a silicone coated fiberglass belt under tension. The mandrel is positioned on the loose silicone/fiberglass belt between two rollers. One of these rollers can be moved forward in a groove and tightened down so that there is a gap of about 1.5 inches between the two rollers (Fig. A.2). One of the lower rollers is mounted at both ends on air cylinders and these cylinders are connected through a pressure regulator to an air supply. When the air cylinders are pressurized, the lower roller is pushed forward so that tension is applied to the belt. This causes the mandrel to be pressed up against the two upper rollers and the belt applies pressure around the mandrel. There is a reversible, variable speed motor connected to one of the lower rollers. When the motor is engaged, the roller rotates causing the belt to move, which, in turn, causes the mandrel to rotate. In this way, the prepreg tape can be wrapped tightly onto the mandrel.

In order to wrap a particular fiber angle on the mandrel and to avoid overlapping or gaps at the seams of the material, the pre-impregnated (pre-preg) tape must be cut very accurately to the desired width. The following procedure is used to determine the length and width of the tape required to fabricate a specimen having any fiber angle, θ.

Figure A.3 shows the dimensions of the finished specimen and of the tape required to make that specimen. In this figure, D

is the outside diameter of the mandrel, L is the required length of the test specimen, C is the outside circumference of the mandrel, W is the width of the pre-preg tape, ℓ is the length of the pre-preg tape and θ is the fiber angle. The dimensions of the pre-preg tape are calculated using the following relations:

$$C = \pi D, \quad W = \pi D \sin\Phi, \quad \text{and} \quad \ell = L/\cos\theta$$

where $\Phi = 90 - \theta$ degrees. When performing these calculations for additional laminae other than the first, the value of D must be increased by twice the thickness of the pre-preg tape each time.

The two pre-preg materials used in this study were obtained from 3M and are denoted by "Scotchply" type 1002 (glass/epoxy) and type SP-288T300 (graphite/epoxy). Note that in all cases, the manufacturer's curing specifications were followed except where deliberate deviations were imposed in post-cure times and cool down rates.

Once all of the plies are wrapped onto the mandrel, a porous teflon coated fiberglass cloth is wrapped around the tube again using the belt wrapper to ensure a wrinkle-free application. The specimen is then removed from the belt-wrapper and bagged in Vac-Pak type E3760 film and sealed with a vacuum bag sealant. Canvas strips are placed along the bag seam and around the ends of the mandrel, inside the vacuum bag, to allow a vacuum over the entire tube (Fig. A.4). Using a vacuum pump, a vacuum of ~ 29 inches of Hg is established and maintained in the bag around the specimen.

For some materials, such as graphite/epoxy, external pressure curing is required. This necessitated the development of a portable pressure chamber to set in the oven, as depicted in Fig. A.5. Details of the vacuum bagged specimen mounted in the high pressure cylinder are shown schematically in Figs A.6,7.

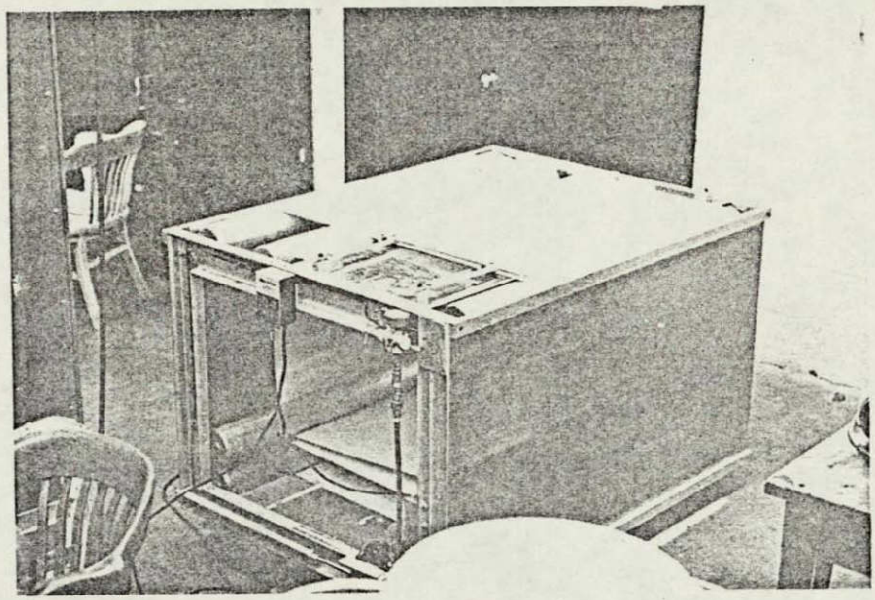

FIG. A.1 BELT-WRAPPING MACHINE

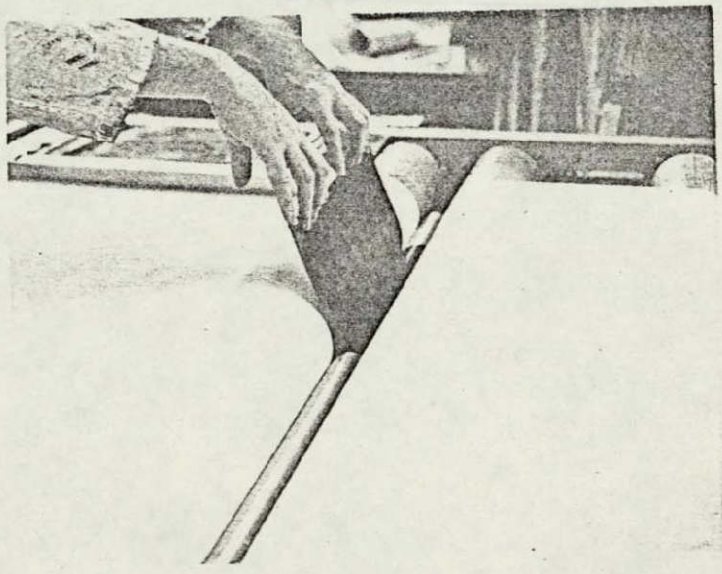

FIG. A.2a WRAPPING A LAYER OF GRAPHITE-EPOXY TAPE ONTO THE ALUMINUM MANDREL

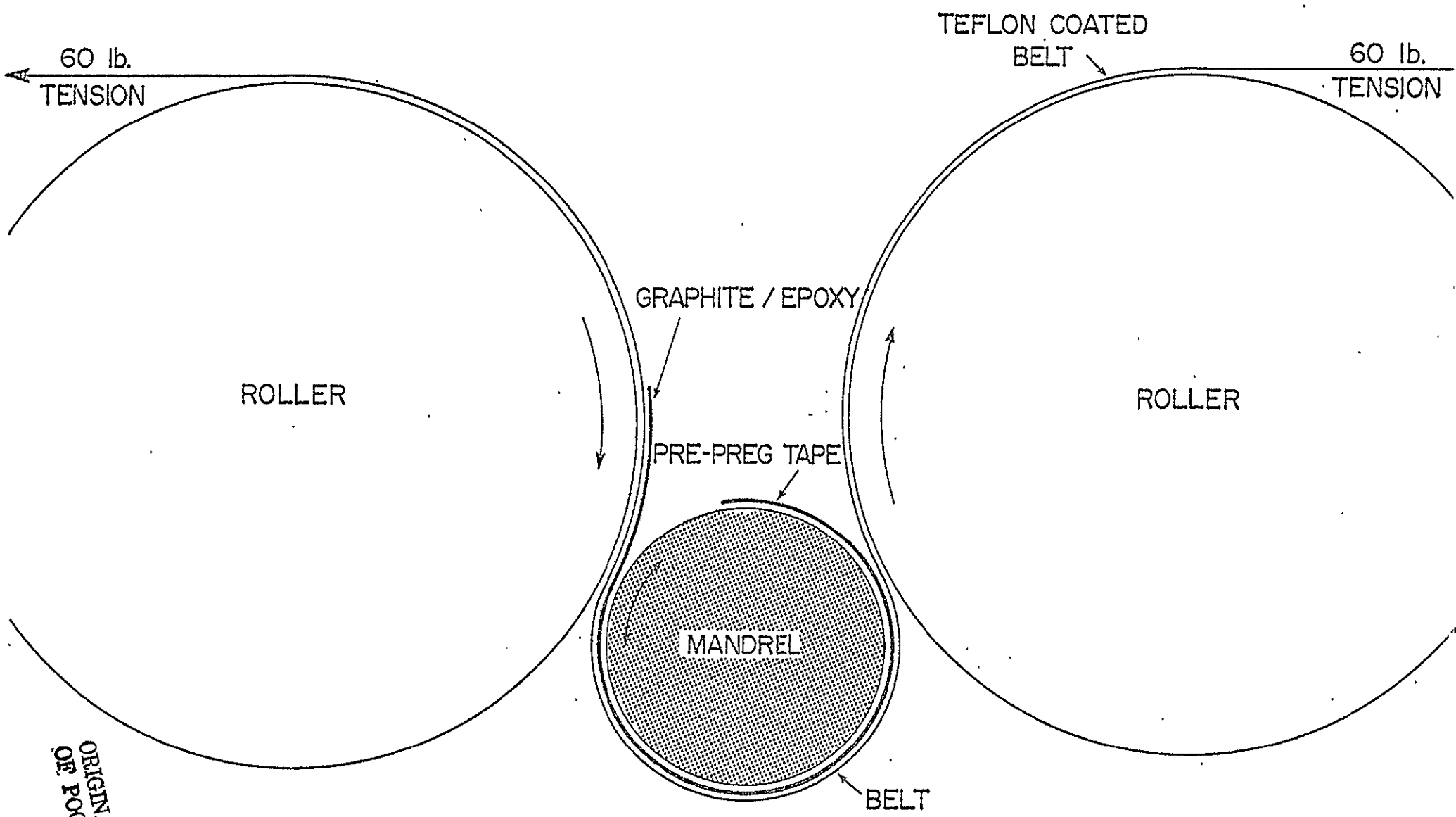

FIG. A.2(b) BELT WRAPPER

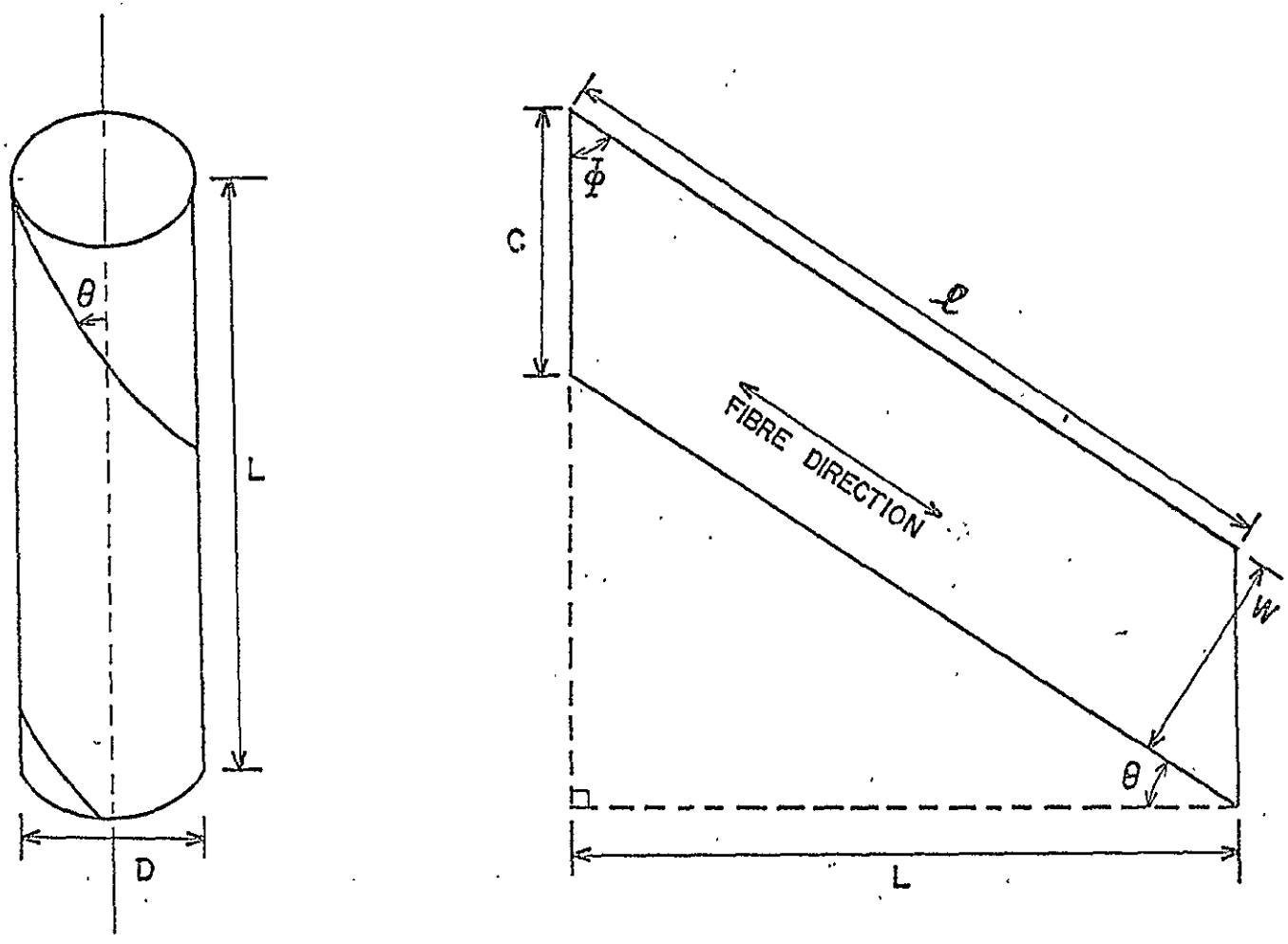

FIG. A.3 LAMINA GEOMETRY

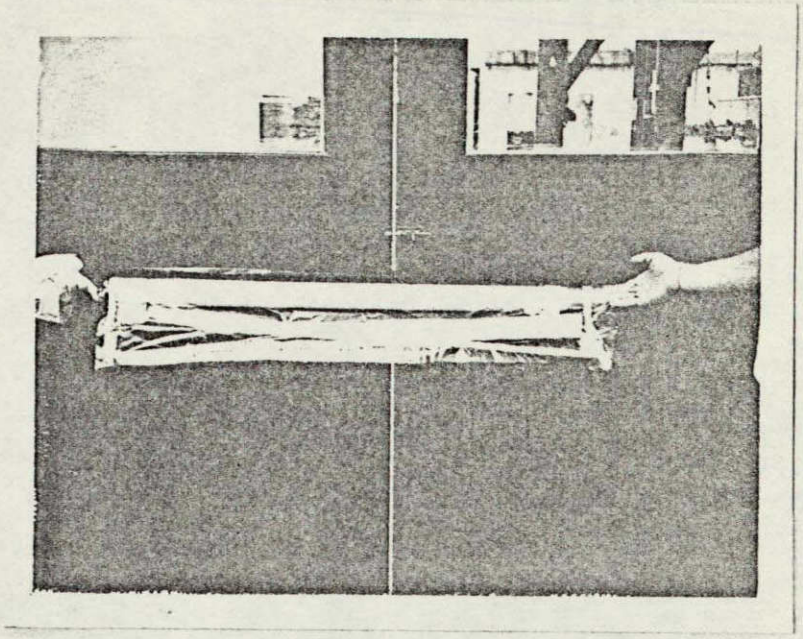

FIG. A.4 VACUUM BAGGED SPECIMEN

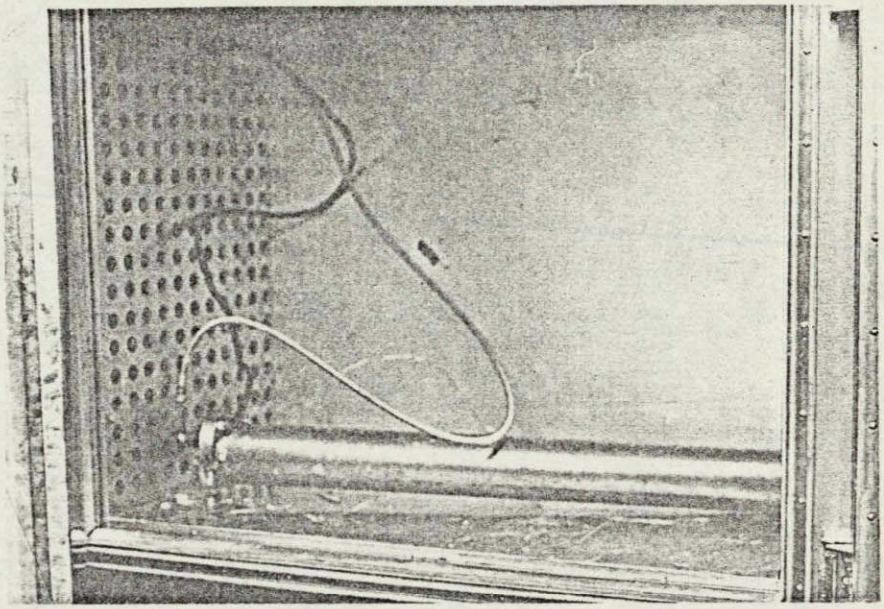

FIG. A.5 PRESSURE VESSEL IN OVEN READY FOR CURE CYCLE TO BEGIN

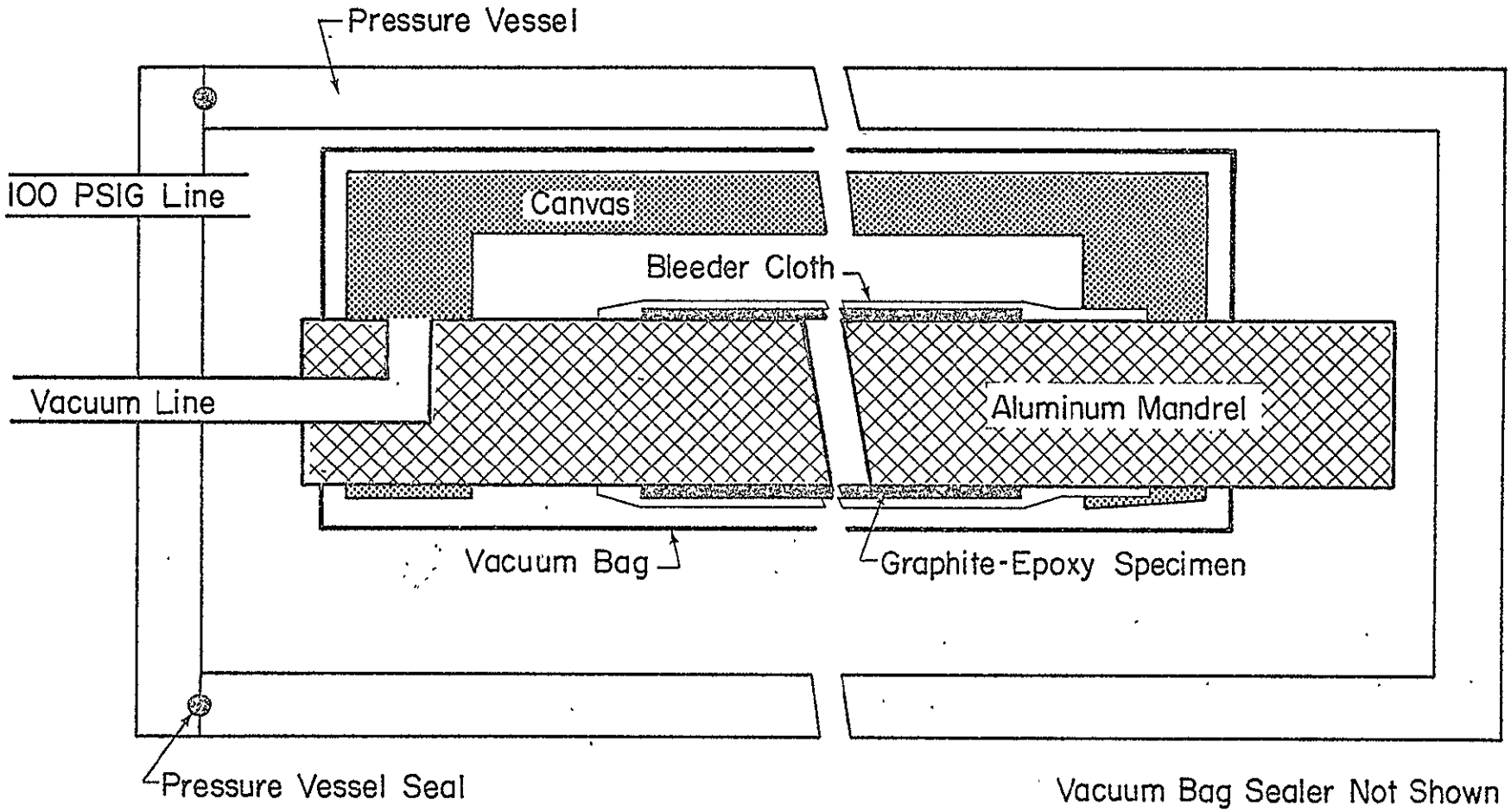

FIG. A.6 SPECIMEN INSIDE PRESSURE VESSEL (NOT DRAWN TO SCALE)

MANUFACTURE OF THREE TUBES AT A TIME

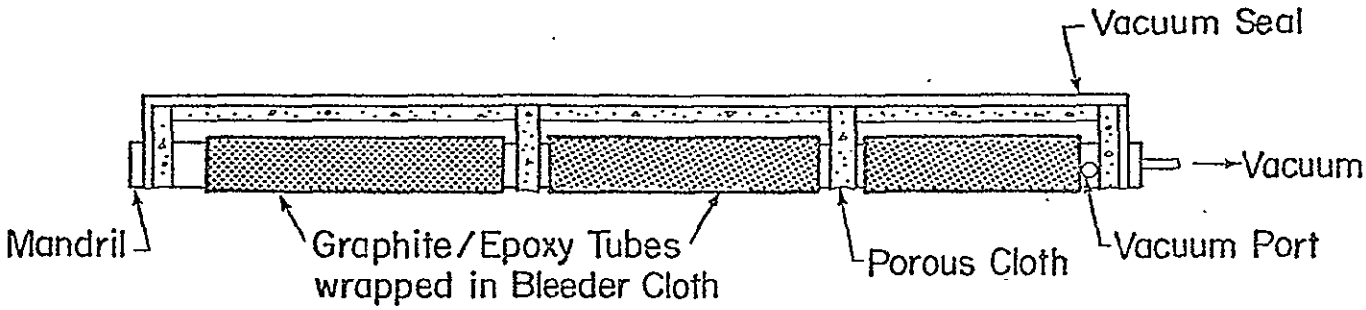

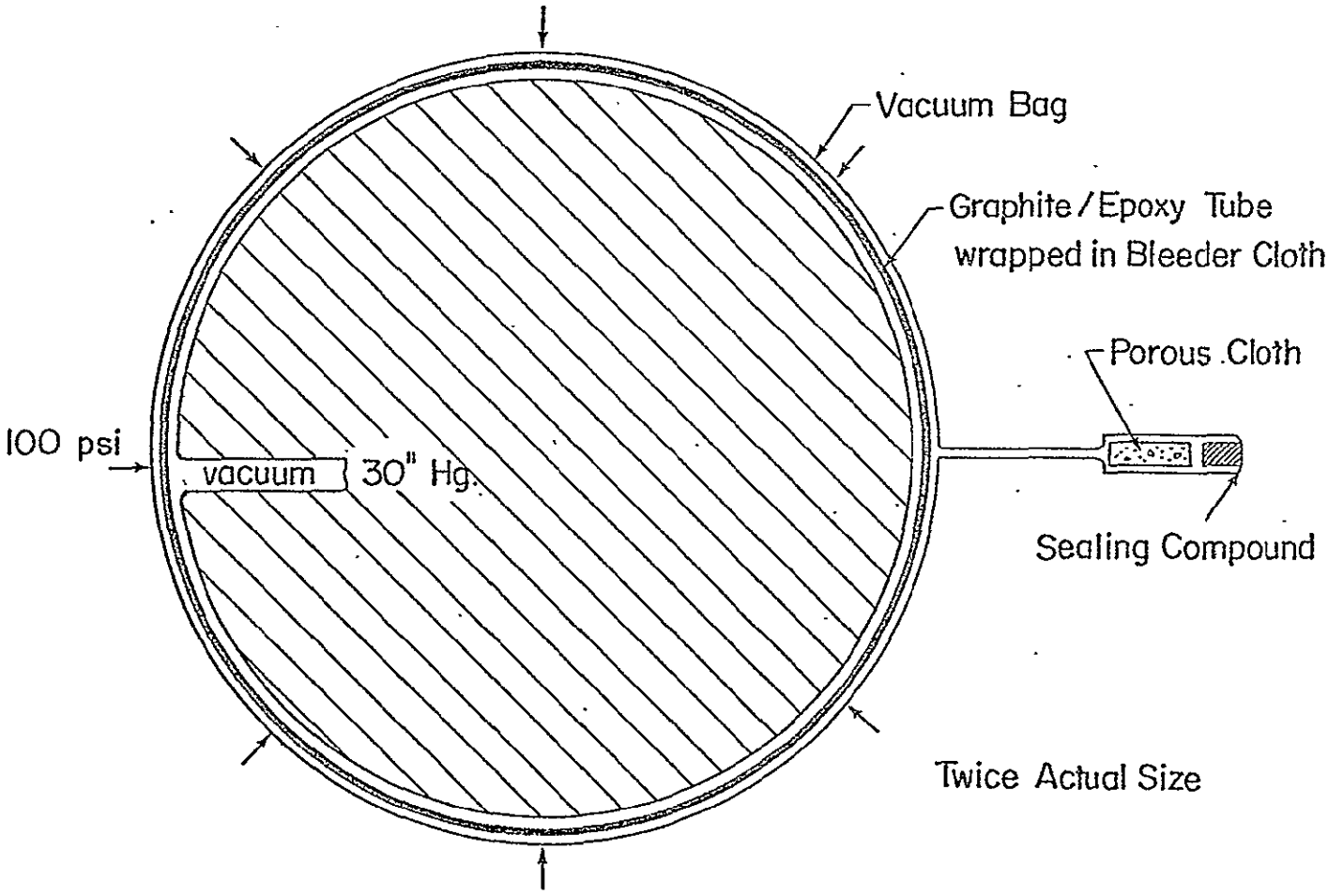

FIG. A7 TUBE FORMING SCHEMATIC

APPENDIX B

TEST METHODS

GENERAL PREPARATION OF SPECIMENS

After removal of the tubes from the autoclave, they are cut to the desired length by sliding them over a cutting mandrel mounted on a lathe (Fig. B.1). Using a slow lathe speed, the tube is turned and an air operated abrasive cutting disc, mounted in the tool post, is used to make a square cut. The tube ends are sanded smooth and thickness measurements are taken at eight positions equally spaced around the circumference at both ends and in the middle section in order to obtain an average tube wall thickness. The specimens are then readied for testing by reinforcing the ends with stepped down layers of fine mesh fiberglass cloth and epoxy and potting them in end plates, made of a suitable material, to a depth of one inch with a room temperature curing epoxy. Several specimens were strain gauged with 350 ohm, 0.5 inch foil gauges to provide stress-strain data up to failure (see Fig. B.2).

It should be noted that our original design for the end fittings (Fig. B.3) was used throughout the program, except for the vacuum tests. In this case, a superior end clamping device utilizing universal gimbals was employed, as shown in Fig. B.4.

Test Apparatus

To determine the orthotropic stiffness and strength parameters in the fiber and matrix directions, requiring only uniaxial load conditions, a four-screw, electrically driven Tinius-Olson tension/compression machine was used. In addition, a strain gauge conditioning unit, X-Y plotter and other associated electronic equipment were necessary to record load, strain response and specimen

temperature, as shown in Figs. B.5-B.7. Note that the graphite/epoxy thermal studies were performed in this apparatus while the glass/epoxy thermal studies were conducted in a temperature chamber using internal pressure loading (see Ref. 9 for details).

For shear measurements, a simple frame apparatus was used to torsionally load the cylinders by means of hydraulically driven pistons (see Fig. B.8).

For the biaxial load tests, a combination of axial compression and internal pressure was required. The actual test set-up is shown in Fig. B.9 with a schematic illustration of the equipment provided in Fig. B.10. As shown, an air-operated hydraulic oil pump was used to maintain the reservoir at a pressure of approximately 6,000 psi. The specimens were pressurized from this reservoir by adjusting a flow valve while monitoring the internal pressure by means of a pressure transducer downstream from the valve. The specimens were mounted in the Tinius Olsen machine which provided the axial compressive load. This load was converted to a voltage by means of a potentiometer mounted in the testing machine. By knowing the pressure transducer's calibration in psi/volt and the testing machine's calibration in lb/volt, the required pressure versus axial compressive load curve can be plotted for a particular biaxial stress ratio B_{12}. This curve was recorded on an X-Y plotter having internal pressure and axial compressive load as inputs. The valve was opened just enough to allow a slow, steady increase in pressure in the tube, while the amount of axial load applied by the testing machine was controlled manually to ensure that the loading followed the pre-calculated load curve up to failure. In this way, a constant biaxial stress ratio was maintained throughout the test. Typical output for the glass specimen is given in Fig. B.11.

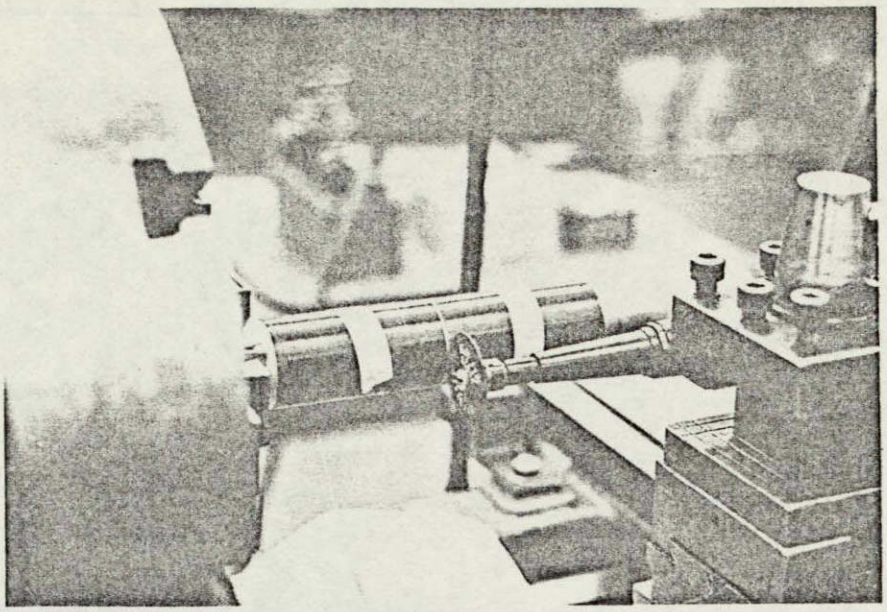

FIG. B.1 GRAPHITE-EPOXY TUBE BEING CUT

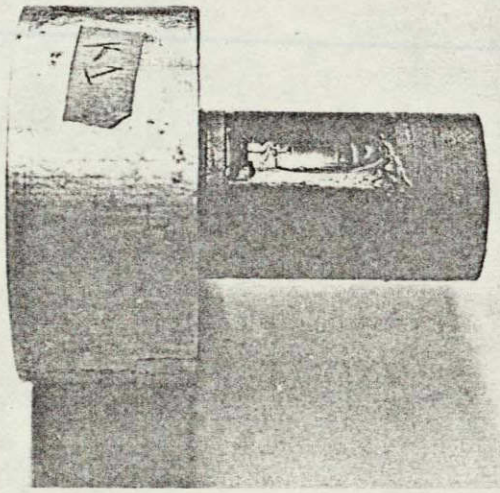

FIG. B.2 FIBERGLASS REINFORCEMENT APPLIED TO END OF SPECIMEN

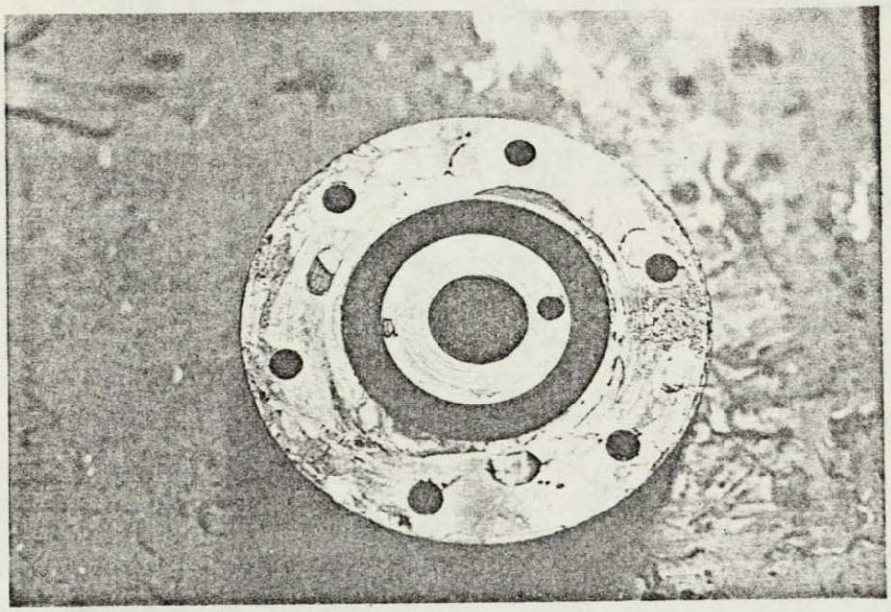

FIG. B.3 END FITTING READY FOR POTTING

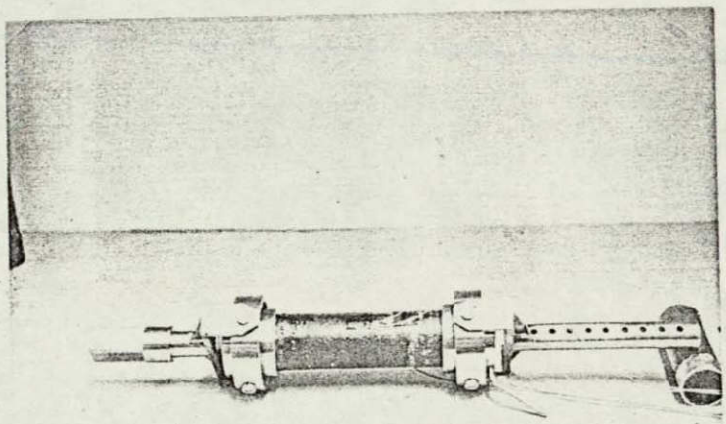

FIG. B.4

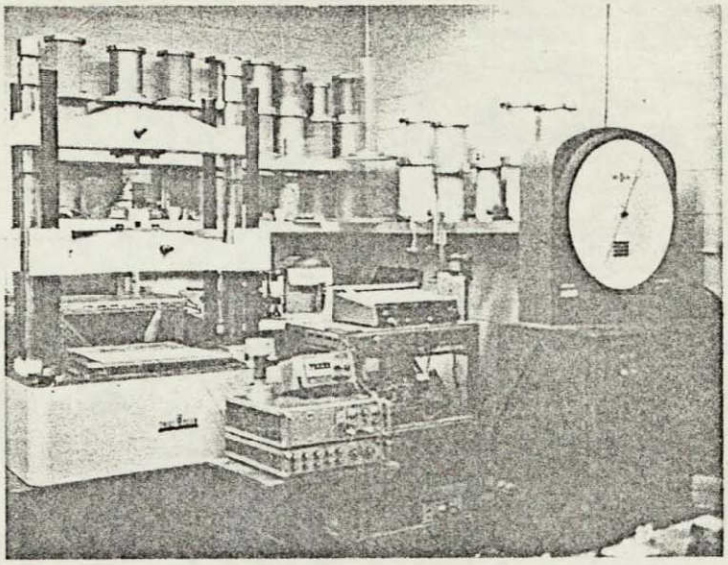

FIG. B.5 TEST SET UP FOR ROOM TEMPERATURE TESTS

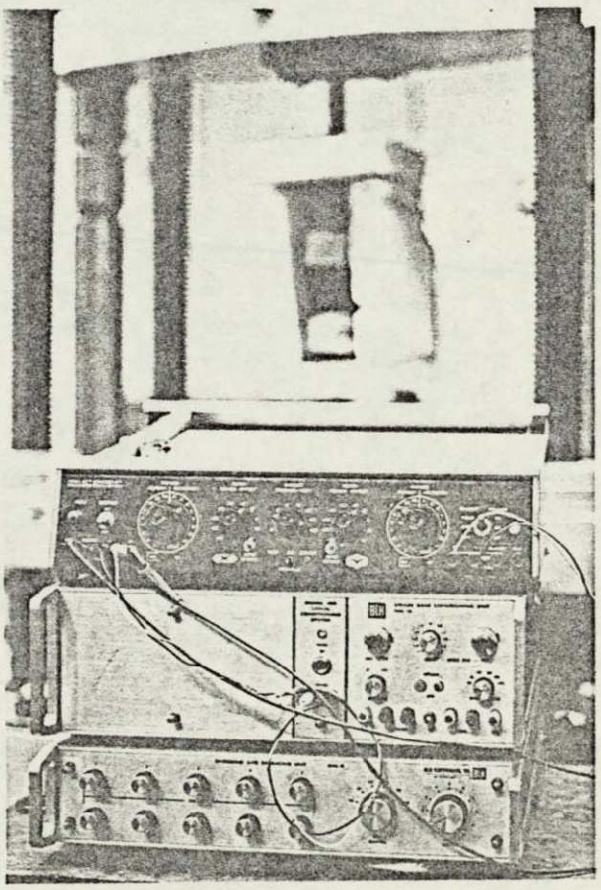

FIG. B.6

STRAIN GAUGE CONDITIONING UNIT AND X-Y RECORDER

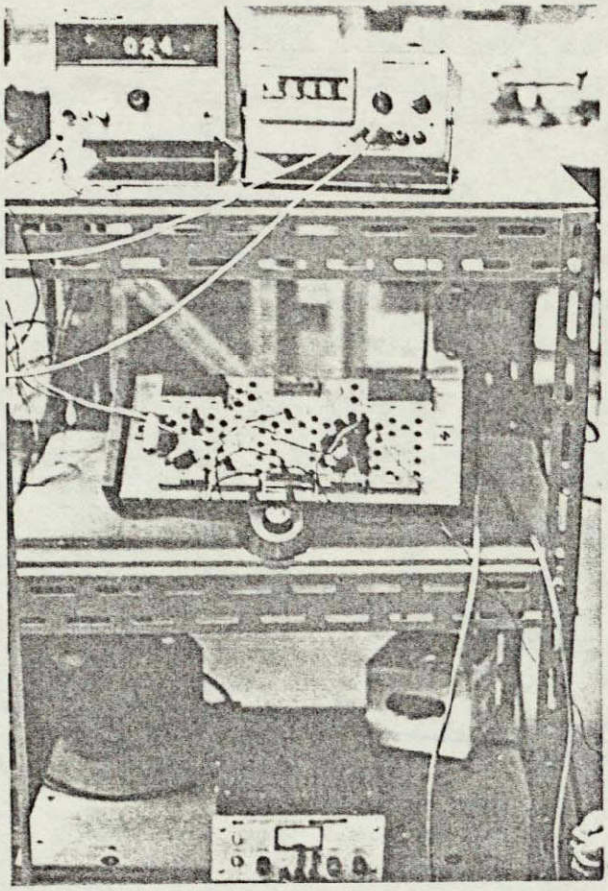

TEMPERATURE AND STRAIN
DISPLAY ON VOLTMETERS

OPERATIONAL AMPLIFIER

POWER SUPPLY

FIG. B.7 SET UP FOR LOAD SIGNAL

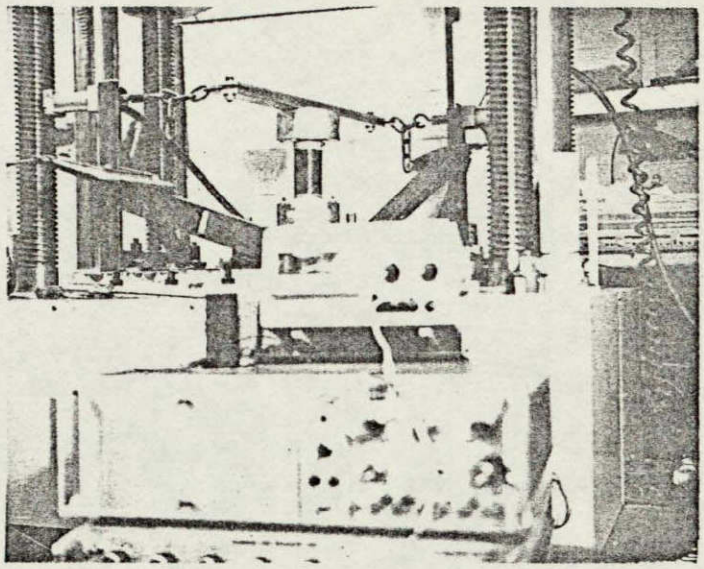

FIG. B.8

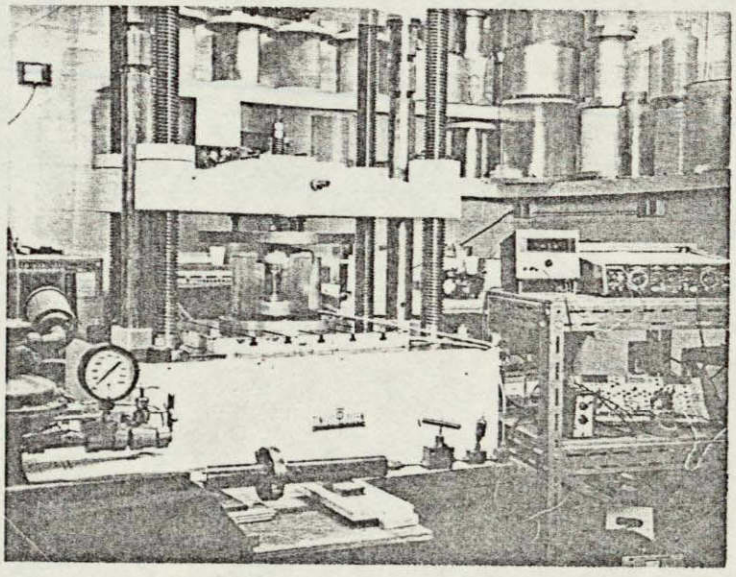

FIG. B.9

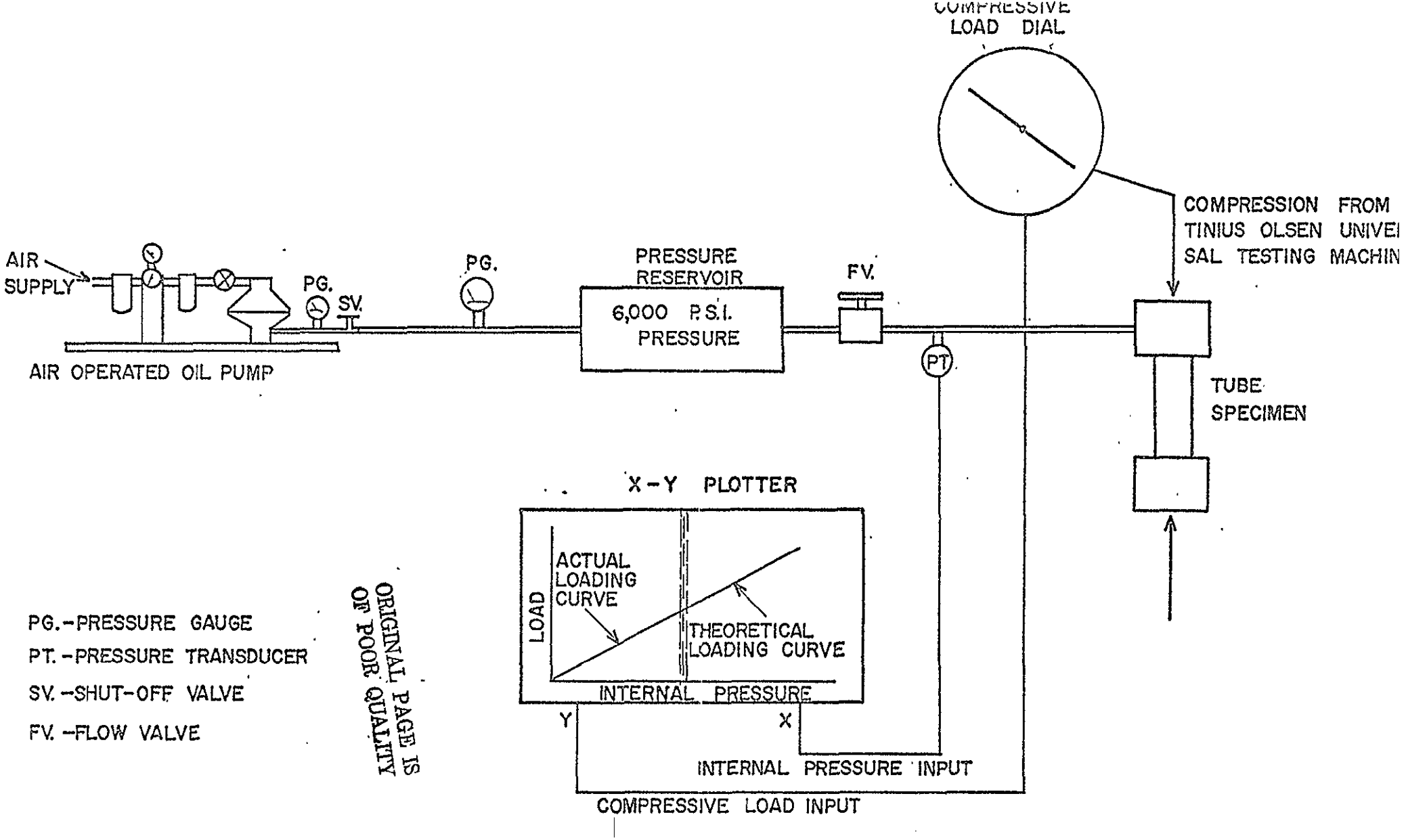

FIG. B.10 SCHEMATIC DIAGRAM OF THE TEST SET-UP FOR THE DETERMINATION OF THE F_{12} INTERACTION TENSOR

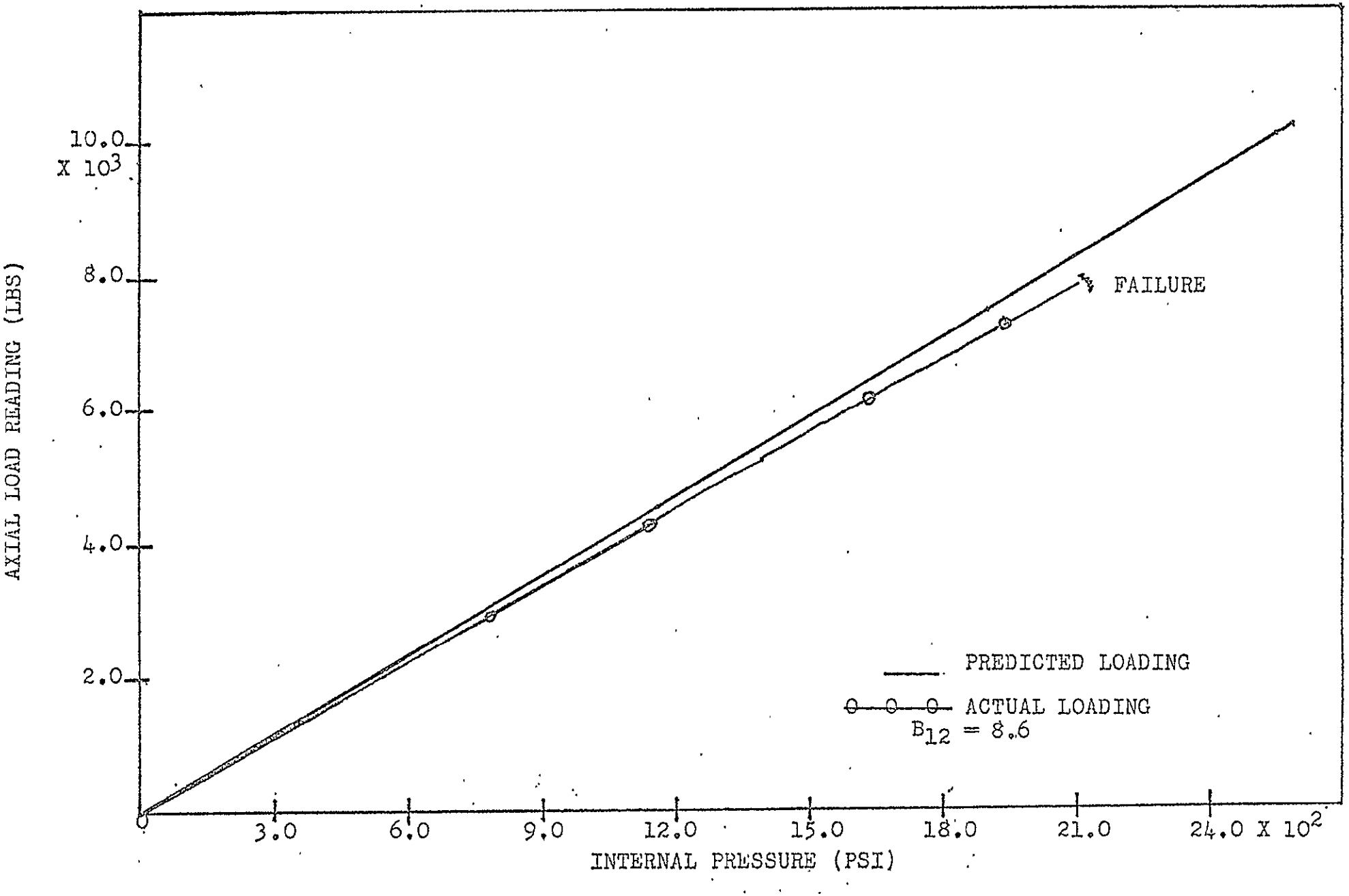

FIG. B.11 LOADING FOR F_{12} TEST (TUBE A-2)

APPENDIX C

VACUUM TEST FACILITY WITH IN-SITU LOADING

Introduction - The Need for Such a System

The central parameter in a space environment is an extremely high vacuum of infinite pumping capacity. Pressures of approximately 10^{-12} torr and lower are encountered at orbital altitudes. The effect of this vacuum on materials is the loss of adsorbed and absorbed gases as well as sublimation or evaporation of the more volatile constituents of the material itself. This is particularly true of many organic/polymeric materials which are used as matrix or bonding agents in composite materials. Most commercial polymers are mixtures of basic polymeric material and various additives such as solvents, catalysts, anti-oxidants, manufacturing aids, etc. These additives usually distill out of the base polymer mixture to form significant portions of the weight loss and the remaining polymer frequently will have properties significantly different than the "advertised product". Elevated temperature accelerates the process by increasing molecular mobility.

Maintaining a working vacuum of 10^{-12} torr is extremely difficult, however, the same outgassing effect is obtained at somewhat higher, more easily obtained pressures. The effect of a perfect vacuum (0 torr) is that each molecule leaving an exposed surface never returns. In this case, the molecular loss rate is a function only of the nature of the material (i.e., vapor pressure and molecular weight) and absolute temperature. This effect is closely approached when the mean-free-path is sufficiently large in comparison to system dimensions. In actual practice, this can be achieved at pressures as

high as 10^{-4} and 10^{-5} torr (mean-free-path for air .5 to 5 meters). A system maximum operating pressure of 10^{-5} torr is therefore considered sufficient for the proposed simulation. At this pressure, radiation is by far the dominant thermal energy transfer mechanism so heating/cooling effects similar to those encountered in space can be achieved.

A primary requirement in the evaluation of polymer matrix composites for space applications is an assessment of their behaviour in hard vacuum. Since the topic of interest in this project concerns the composite strength and stiffness, it is therefore necessary to develop a space simulator facility capable of mechanically loading the materials while they are subject to the vacuum (and thermal + radiation) environment. It is felt that unless these in-situ tests are conducted, it is possible to obtain erroneous results that are not indicative of the material response while it is actually operating under space conditions.

Facility Description

The space simulator facility with an in-situ loading capability which has been designed* and constructed at UTIAS is shown in Fig. C.1. The high vacuum system is composed of several major components for pumping, valving, pressure measurement, baking, trapping and piping. The individual specifications and limitations of these components are the subject of this section. Of great significance is the manner in which these components are joined together and operated to form the total system. Refer to Fig. C.2 for the system schematic.

* I wish to acknowledge that we could not have developed this facility without the use of a vacuum chamber and design guidance supplied by Prof. J. B. French (Associate Director, UTIAS) and his colleague, Dr. N. M. Reid.

1. The Main Chamber is cylindrical in shape measuring 51 centimeters in diameter by 117 centimeters long. It is constructed of 300 series stainless steel with semi-smooth unpolished interior walls. Several ports and feedthroughs of various sizes are available for use around the chamber. Main loading access is provided through a hinged, full diameter door at one end of the cylinder (see Fig. C.1).

2. The Roughing Pump is a rotary, oil sealed displacement type pump (Welch "Duo-Seal" model 1402B). This pump has an initial optimum capacity for air of 100 liters/min. or 1.67 liters/sec. and an advertised base pressure of 10^{-4} torr, however, a working pressure of 10^{-3} torr is more realistic. This one mechanical pump provides both system roughing and diffusion pump backing.

3. The Diffusion Pump is a four stage, progressive compression jet pump using low vapor pressure oil as a working fluid. It is an Edwards Model F-903, having a pumping capacity of 2300 liters/sec. and an ultimate pressure of about 10^{-9} torr.

4. Valves - The proper placement of high vacuum valves in a system can greatly increase its versatility and prevent contamination in the event of a component failure. This system has four valves, two automatic and two manual (see Fig. C.2). Automatic electric valves which close when power is lost are positioned at the mechanical pump inlet and at the diffusion pump outlet. These valves seal the system and prevent repressurization through the mechanical pump in the event electrical power is lost. Such back flow would contaminate the system with oil. A manual gate valve allows isolation of the chamber from the pumping stack which facilitates access to the chamber without shutting down the pumps or warming the cold trap. A manual bypass valve connects the mechanical pump directly to the chamber for re-evacuation so the gate valve can be re-opened and

operation resumed.

5. Traps - A high conductance, liquid nitrogen cooled, cryogenic trap is located above the diffusion pump. The purpose of this trap is to condense backstreaming oil from the diffusion pump keeping contamination from the chamber. The trap also acts, to some extent, as a cryopump for condensables coming from the chamber, especially water vapor. An activated alumina trap is used in the backing line of the improved system (Fig. C.2) to prevent backstreaming of oil from the mechanical pump.

6. Pressure Measurement - Two thermistor-type, Pirani gauges are used to measure pressures from ambient to 10^{-3} torr. One gauge is located near the main chamber in the roughing line to monitor the upper range of pressure during pump-down. The other is located at the diffusion pump outlet to monitor backing pressure. This type of gauge measures pressure indirectly by the thermal conductivity of the gas surrounding the thermistor bead and is limited by the decreasing ofpressure-dependent conductance, compared to radiation, as the dominant heat transfer mechanism below 10^{-3} torr.

Main chamber pressure below 10^{-3} torr is monitored by a Bayard-Alpert hot-cathode ionization gauge. This gauge actually measures gas molecular density between an electron source (heated filament in this case) and an electron collector (grid). Gas molecules struck by electrons are ionized and attracted to a collector wire maintained at ground potential. The electron emission current is carefully controlled so that the current in the collector circuit is only a function of gas molecular density (pressure). As pressure is reduced, fewer electrons collide with a gas molecule so they directly bombard the grid, producing soft x-ray photons. These x-rays release photo-electrons from surfaces within the gauge which

in sufficient numbers cause a current in the collector circuit which overpowers the ion current. The Bayard-Alpert gauge has been designed to minimize this effect, however a pressure of about 10^{-10} torr is the practical lower limit due to photoemission current.

7. Baking - The chamber is surrounded by heating elements of 4500 watts power. Power to the elements is cycled during baking to hold the chamber walls at 200°C. Baking accelerates the desorption of gases from the chamber walls resulting in lower pressures at the end of the bake process.

8. Control System - Electrical power is channeled to the pumps and valves by three switches and two relays. The diffusion pump requires three things: 1. 220 volts for the oil heater; 2. water for cooling; and 3. backing vacuum provided by the backing pump. The control system is set up so that if either the diffusion pump overheats or 110 volt power to the backing pump is lost, the 220 volt power will be automatically cut off. This simple system is intended to allow safe unattended overnight operation. The only service the system requires is refill of the cryotrap with LN_2 every day.

System Response

A comparison between the predicted and actual measured response of the vacuum system in terms of pressure drop as a function of time is shown in Figs. C.3 and C.4. Note that only the "empty" configuration is reported since the presence of a test sample affects the behaviour due to outgassing. However, it was found that these curves did not change appreciably and after about two hours, an operating pressure of $\sim 2 \times 10^{-7}$ torr was achieved (Fig. C.5).

In-Situ Loading

As noted earlier, a loading fixture was mounted on the one closure plate of the vacuum chamber. If one examines Fig. C.1(b), a graphite/epoxy test cylinder can be seen attached to this fixture by means of universal gimbals fastened to the specimen's end caps, as shown in Fig. C.6. Loading was applied to the sample while it was in the vacuum chamber by means of externally positioned hydraulic pressure pistons which can be seen in Fig. C.7. Actual load transmission from outside the chamber was accomplished utilizing stainless steel, leak-proof flexible bellows. Also shown in Fig. C.7a are measurements being taken of the specimen temperature and axial strain while in vacuum during loading up to failure.

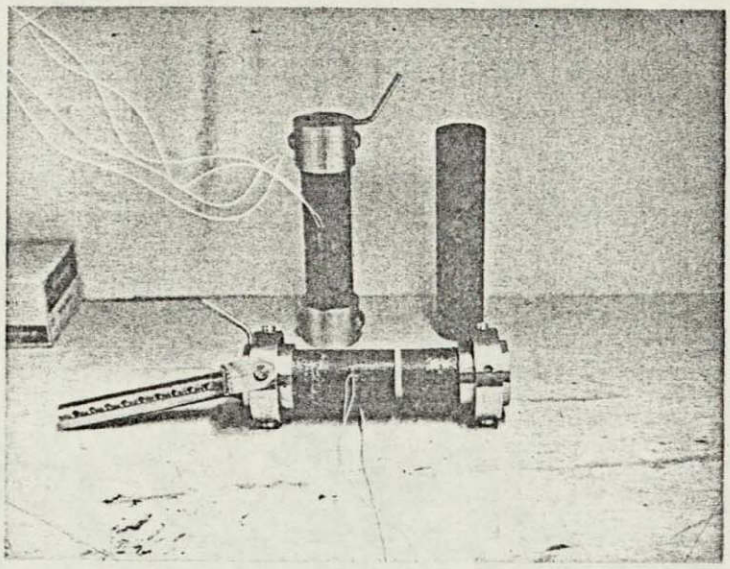

FIG. C.6

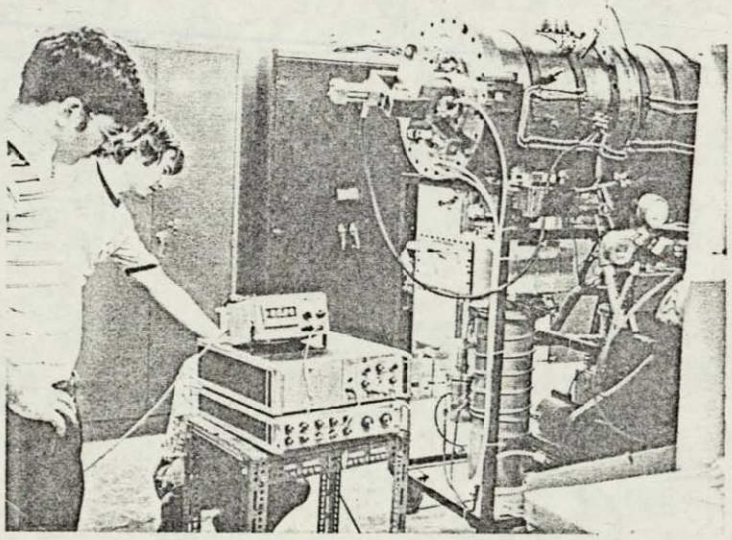

FIG. C.7(a)

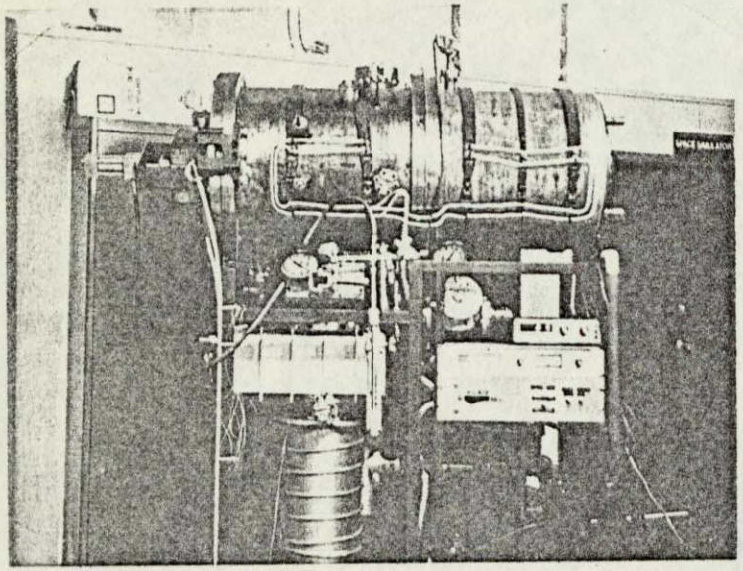

(a) Thermal Vacuum Test Facility.

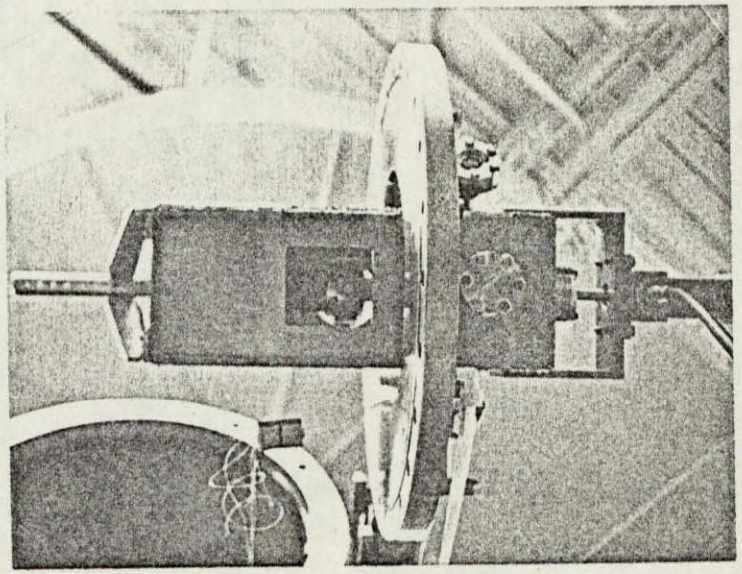

(b) Hinged Chamber Door with Load Fixture Attached.

FIG. C.I

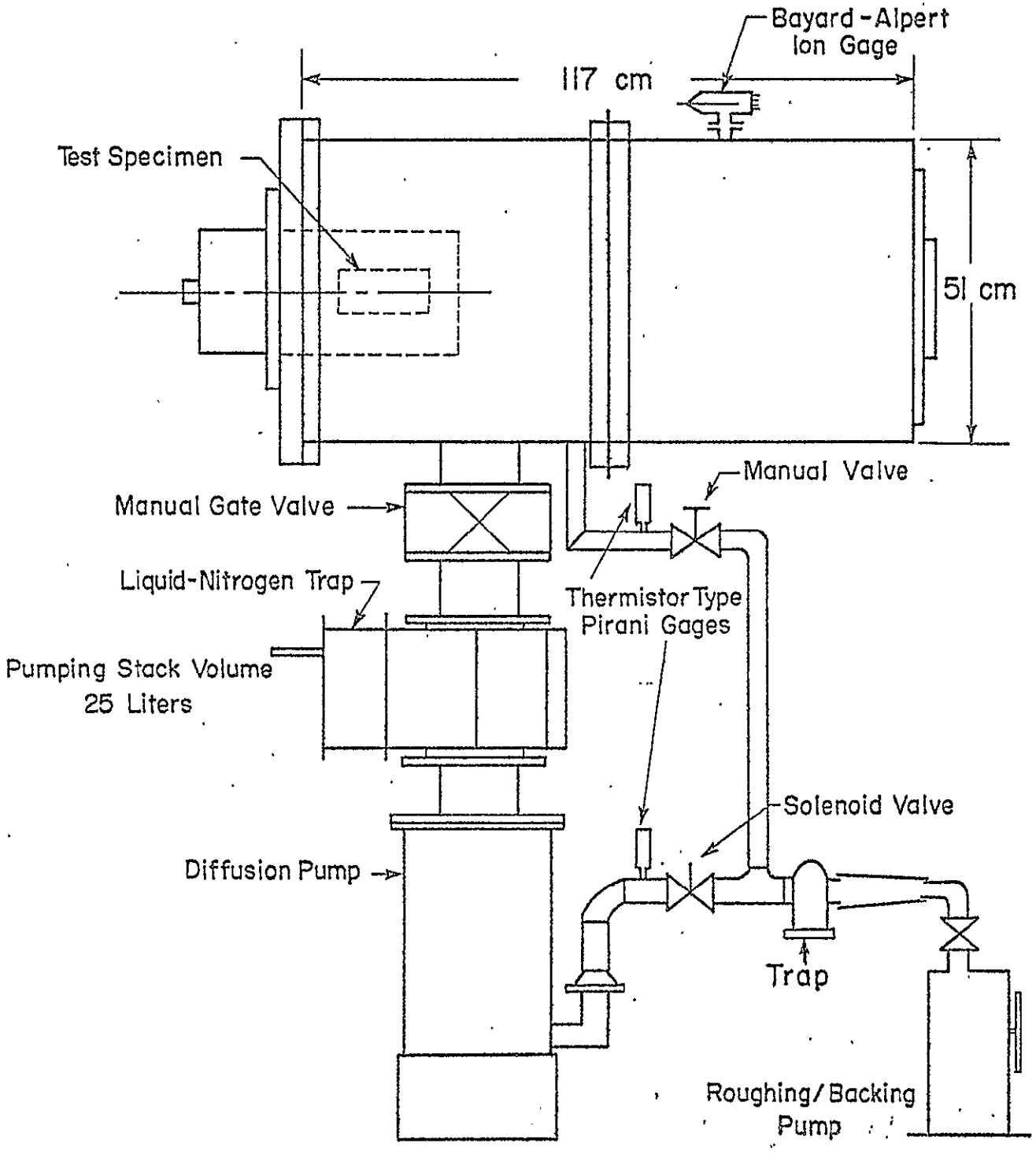

Total Volume = 250 liters
Total Surface Area = 2.50×10^4 cm
Note: Includes all Chamber Extremities.

FIG.C2 SYSTEM SCHEMATIC

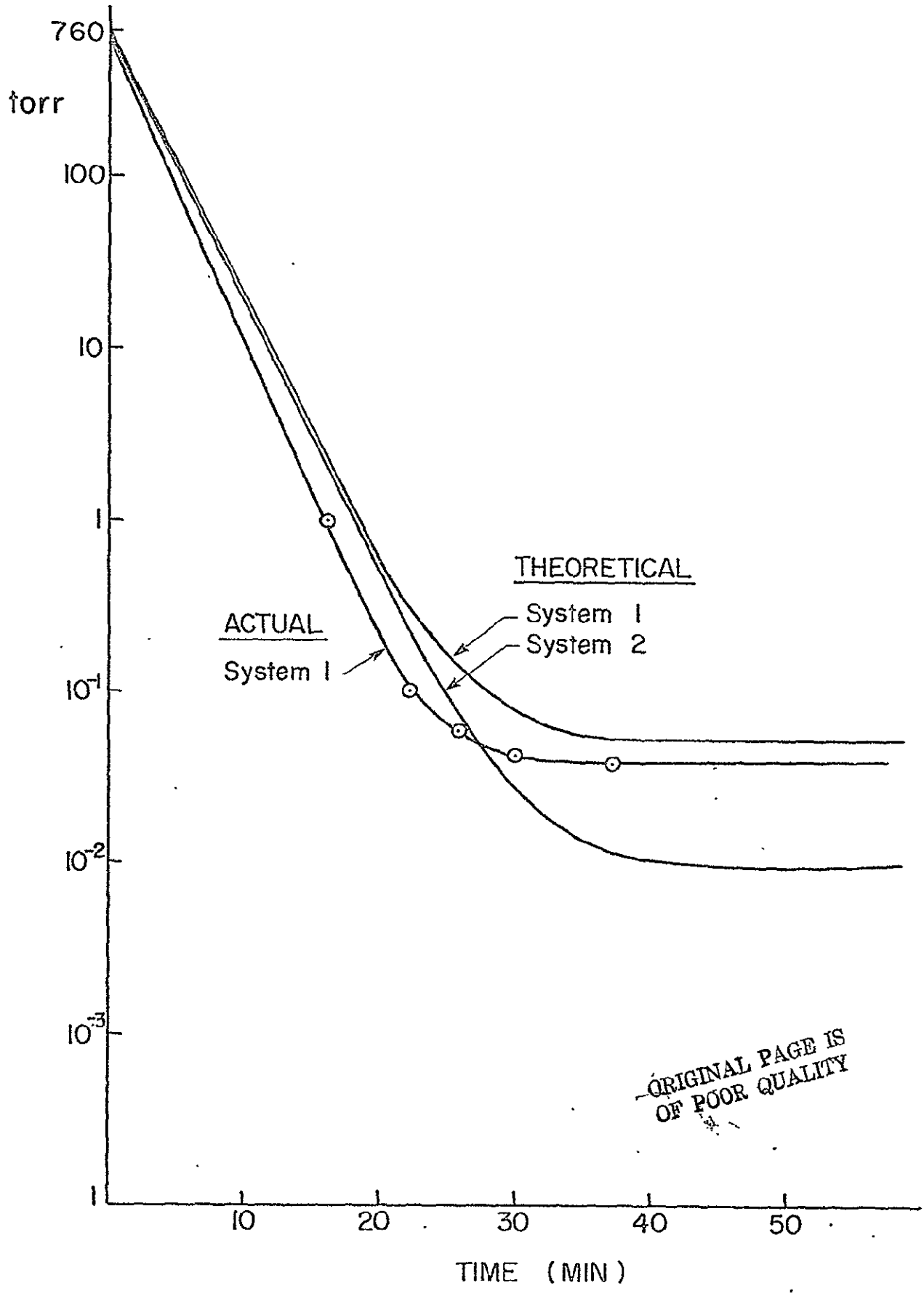

Fig. C.3 PRESSURE DROP in CHAMBER due to MECHANICAL ROUGHING PUMP

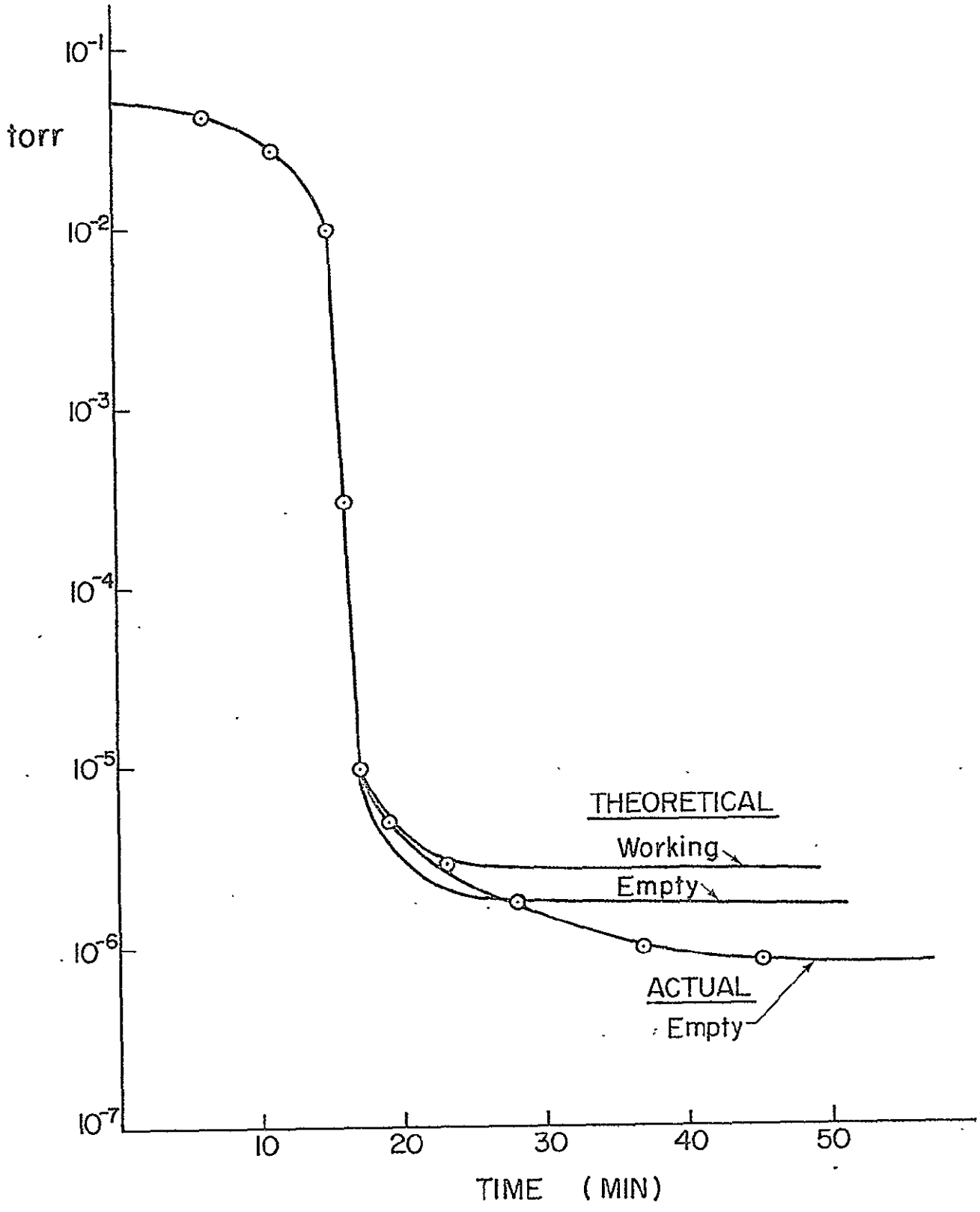

Fig. C.4 PRESSURE DROP in CHAMBER due to DIFFUSION PUMP

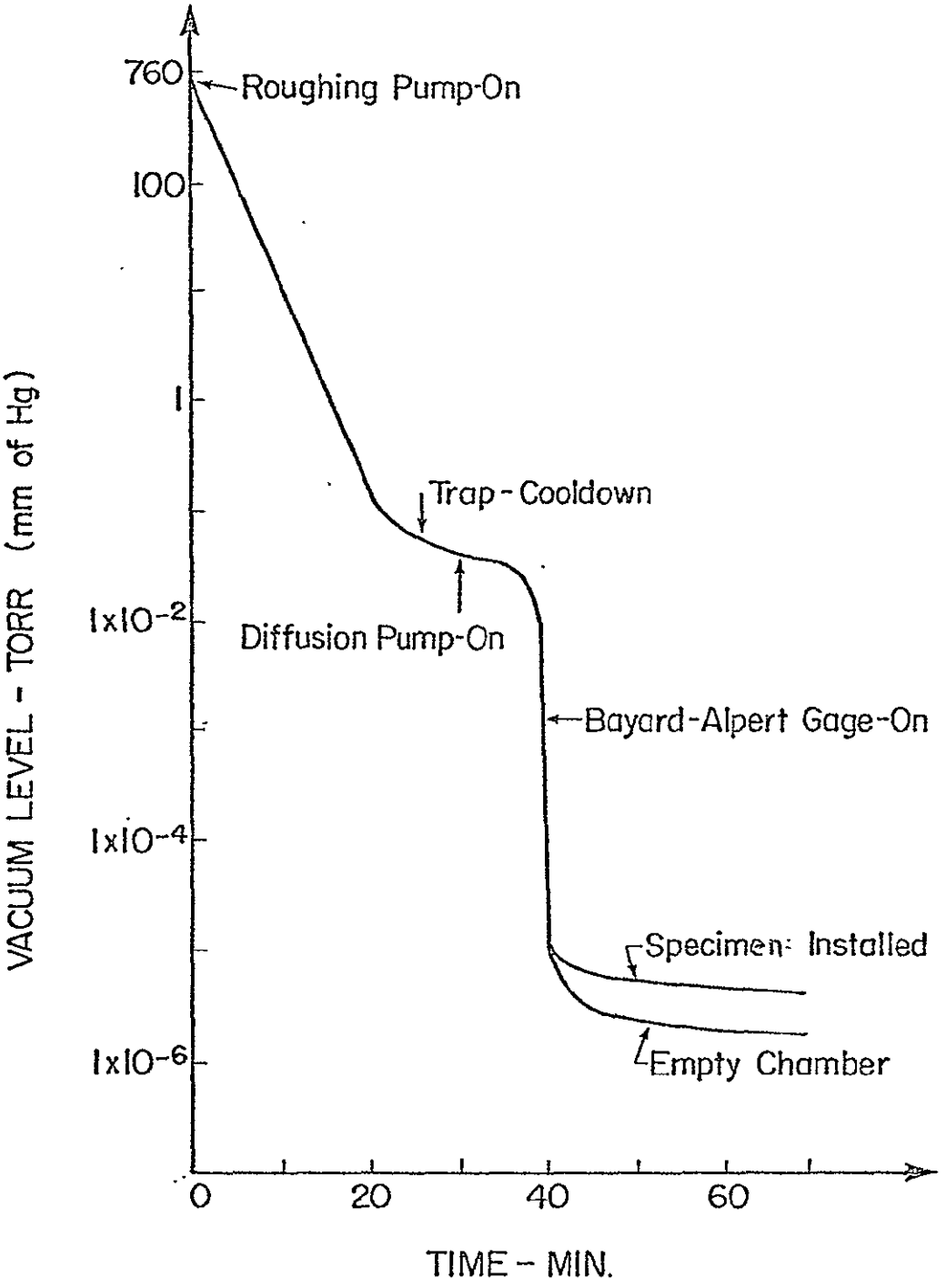

FIG. C.5 Chamber Pumpdown Profile